Ionic Homeostasis at the Perisynaptic Cradle

PhD Thesis, January 2019

PhD Student: Kevin Breslin.

Supervisors: Prof. Liam McDaid, Dr. Jim Harkin,
Dr. John Wade and Dr. KongFatt Wong-Lin

Presented as a requirement for the degree of PhD in the
School of Computing and Intelligent Systems
Faculty of Computing and Engineering
University of Ulster, Magee Campus
Date: 14th January 2019

"I confirm that the word count of this thesis is less than 100,000 words"

Contents

List of Tables:

Tables of Variables

List of Figures:

Chapter 2:

Chapter 3

Chapter 4:

Chapter 5:

Chapter 6:

Tables of Variables

Table 1: Astrocyte Morphology. (Potassium Experiment)

Parameter	Value	Unit	Description	Ref
Lengths:				
d_{IPS}	300×10^{-9}	m	Perisynaptic internal diameter	[1]
d_{EPS}	500×10^{-9}	m	Perisynaptic external diameter	[1]
r_{IPS}	150×10^{-9}	m	Perisynaptic internal radius	[1]
r_{EPS}	250×10^{-9}	m	Perisynaptic external radius	[1]
l_{PS}	300×10^{-9}	m	Perisynaptic length	[1]
d_P	100×10^{-9}	m	Process diameter	[2]
r_P	50×10^{-9}	m	Process radius	[2]
l_P	25×10^{-6}	m	Process length	[2]
d_{Syn}	270×10^{-9}	m	Synapse diameter	[2]
r_{Syn}	135×10^{-9}	m	Synapse radius	[2]
l_{syn}	$300x\ 10^{-9}$	m	Synapse length	[2]
Areas:				
CSA_{PS}	7.068×10^{-14}	m^2	Perisynaptic cross sectional area = πr_{IPS}^2	[3]
SA_{PS}	2.8274×10^{-13}	m^2	Perisynaptic surface area = $2\pi r_{IPS} l_{PS}$	[3]
CSA_P	7.854×10^{-15}	m^2	Process cross sectional area = πr_P^2	[3]
SA_P	7.854×10^{-12}	m^2	Process surface area = $2\pi r_P l_P$	[3]
CSA_{Syn}	2.8628×10^{-14}	m^2	Synapse cross sectional area = πr_P^2	[3]
SA_{Syn}	1.2723×10^{-13}	m^2	Synapse surface area = $2\pi r_P l_P$	[3]
$SA_{PsEC\text{-}GECS}$	$1.5715 \times 10\text{-}^{14}$	m^2	Surface area between PsECS and GECS = $l_{PS} * (d_{IPS} - d_{Syn}) + (CSA_{PS} - CSA_{Syn})$	[3]
Volumes:				
Vol_{PS}	3.7699×10^{-17}	L	Perisynaptic volume = $1000\pi l_{PS}(r_{EPS}^2 - r_{IPS}^2)$	[3]
Vol_P	1.9635×10^{-16}	L	Process volume = $1000\pi r_P^2 l_P$	[3]
Vol_{Syn}	8.5883×10^{-16}	L	Synapse volume = $1000\pi r_P^2 l_P$	[3]
Vol_{PsECS}	2.0145×10^{-18}	L	Perisynaptic ECS volume	[3]

Table 2: Astrocyte Morphology. (Calcium Experiment)

Parameter	Value	Units	Description	Ref
Lengths:	(as Table 1)			
Areas:				
CSA_{PS}	3.5343×10^{-14}	m^2	Perisynaptic cross sectional area	[4]
SA_{PS}	1.4137×10^{-13}	m^2	Perisynaptic surface area	[4]
CSA_{P}	7.854×10^{-15}	m^2	Process cross sectional area	[4]
SA_{P}	7.854×10^{-12}	m^2	Process surface area	[4]
CSA_{Syn}	2.8628×10^{-14}	m^2	Synapse cross sectional area	[4]
SA_{Syn}	1.2723×10^{-13}	m^2	Synapse surface area	[4]
$SA_{PsECS-GECS}$	1.5715×10^{-14}	m^2	Surface area between PsECS and GECS	[4]
Volumes:				
Vol_{PS}	1.8850×10^{-17}	L	Perisynaptic volume	[4]
Vol_{P}	1.9635×10^{-16}	L	Process volume	[4]
Vol_{Syn}	8.5883×10^{-16}	L	Synapse volume	[4]
Vol_{PsECS}	2.0145×10^{-18}	L	Perisynaptic ECS volume	[4]

Table 3: Astrocyte Model Variables. (Potassium Experiment)

Variable	Initial Value	Units	Description	Ref
V_A	-0.09	V	Astrocyte Membrane potential	[3]
$[K^+]_{PsC}$	0.1	M	K^+ concentration in the perisynaptic cradle	[5]
$[Na^+]_{PsC}$	0.015	M	Na^+ concentration in the perisynaptic cradle	[5]
$[K^+]_{PsECS}$	0.003	M	Perisynaptic extracellular K^+ concentration	[5]
$[Glu]_{ECS}$	1×10^{-6}	M	Perisynaptic extracellular Glutamate concentration	[3]

Table 4: Astrocyte Model Variables. (Calcium Experiment)

Variable	Initial Value	Units	Description	Ref
VA	-0.09	V	Astrocyte Membrane potential	[4]
$[K^+]_{PsC}$	0.1	M	K^+ concentration in the perisynaptic cradle	[5]
$[K^+]_{PsECS}$	0.004	M	Perisynaptic extracellular K^+ concentration	[4]
$[Na^+]_{PsECs}$	0.135	M	Perisynaptic extracellular Na^+ concentration	[4]
$[Glu]_{ECS}$	25×10^{-9}	M	Perisynaptic extracellular Glutamate concentration	[4]

Table 5: Astrocyte Model Parameters. (Potassium Experiment)

Parameter	Value	Units	Description	Ref
V_m	-0.09	V	Astrocyte resting membrane potential	
φ_w	0.267	eV	Well activation energy	[6]
k_B	1.38×10^{-23}	J/K	Boltzmann constant	
R	8.31	J/mol/K	Gas constant	
T	310	K	Temperature	
F	96485	C/mol	Faraday constant	
Q	1.6022×10^{-19}	C	Coulomb	
C_m	0.01	F/m^2	Membrane capacitance	[5]
g_{Kir}	144	S/m^2	K_{ir} channel conductance	[3]
g_K	16.9131	S/m^2	K^+ background transport conductance	[3]
g_{Na}	0.4293	S/m^2	Na^+ background transport conductance	[3]
K_K	0.018	S/m	K^+ Poole-Frenkel channel constant	[3]
K_{Na}	0.018	S/m	Na^+ Poole-Frenkel channel constant	[3]
$PNKA_{max}$	0.1×10^{-5}	mol/m^2	Maximum NKA-ATPase Pump Rate	[5]
K_{Nai}	1.5×10^{-3}	M	Na^+ threshold for NKA-ATPase	[3]
K_{KE}	10×10^{-3}	M	K^+ threshold for NKA-ATPase	[3]
z_K	1		K^+ Valency	
z_{Na}	1		Na^+ Valency	
z_{Glu}	-1		Glu Valency	
$[Glu]_{PsECS}$	1.5×10^{-3}	M	Glu concentration in the perisynaptic cradle	[3]
$[H^+]_{PsC}$	60×10^{-9}	M	H^+ Concentration in the perisynaptic cradle	[3]
$[K^+]_{AS}$	0.1	M	K^+ Concentration in the astrocyte soma	[3]
$[Na^+]_{AS}$	0.015	M	Na^+ Concentration in the astrocyte soma	[5]
$[H^+]_{PsECS}$	40×10^{-9}	M	Perisynaptic extracellular H^+ concentration	[3]
$[Na^+]_{PsECS}$	0.145	M	Perisynaptic extracellular Na^+ concentration	[5]
$[K^+]_{GECS}$	0.003	M	Perisynaptic global ECS K^+ concentration	[5]
$[Na^+]_{GECS}$	0.145	M	Perisynaptic global ECS Na^+ concentration	[5]
ε_0	8.85×10^{-12}	F/m	Vacuum permittivity	[3]
ε_r	0.82	F/m	Relative permittivity of brain tissue	[3]
g_{ECS}	3.3	S/m^2	Perisynaptic ECS leak conductance	[3]
α_{EAAT}	0.0032	A/m^2	Glutamate transport fitting parameter	[3]
β_{EAAT}	28.8	mV^{-1}	Glutamate transport fitting parameter	[3]
r_g	5×10^{-7}	M^{-1}	Slope of glutamate uptake	[3]
s_g	9×10^{-6}	M	Threshold for glutamate uptake	[3]

Table 6: Astrocyte Model Parameters. (Calcium Experiment)

Parameter	Value	Units	Description	Ref
g_K	17.9364	S/m^2	K^+ background transport conductance	[4]
g_{Na}	0.9761	S/m^2	Na^+ background transport conductance	[4]
z_{Ca}	2		Calcium Valency	[4]
$[Ca^{2+}]_{PsECS}$	1.5×10^{-3}	M	Perisynaptic extracellular Ca^{2+} concentration	[4]
$[K^+]_{GECS}$	0.004	M	Perisynaptic global ECS K^+ concentration	[4]
$[Na^+]_{GECS}$	0.135	M	Perisynaptic global ECS Na^+ concentration	[4]
$[Ca^{2+}]_{GECS}$	1.5×10^{-3}	M	Perisynaptic global ECS Ca^{2+} concentration	[4]
$[Ca^{2+}]_{PsC}$	100×10^{-9}	M	Ca^{2+} concentration in the perisynaptic cradle	[4]
$[Ca^{2+}]_{PsECS}$	1.5×10^{-3}	M	Perisynaptic extracellular Ca^{2+} concentration	[4]

Table 7: Neuron Model Parameters. (Potassium Experiment)

Parameter	Value	Unit	Description	**Ref**
$\mathbf{g_{KNeu}}$	360	S/m^2	Maximum K^+ channel conductance	[3]
$\mathbf{g_{NaNeu}}$	1200	S/m^2	Maximum Na^+ channel conductance	[3]
$\mathbf{g_{LNeu}}$	3	S/m^2	Maximum leak channel conductance	[3]
$\mathbf{E_{KNeu}}$	-0.12	V	K^+ channel reversal potential	[3]
$\mathbf{E_{NaNeu}}$	0.115	V	Na^+ channel reversal potential	[3]
$\mathbf{E_{LNeu}}$	0.010613	V	Leak channel reversal potential	[3]
$\mathbf{P_{NaKmaxNeu}}$	-6.8017×10^{-9}	mol/m^2	Maximum NaK-ATPase Pump Rate	[3]
$\mathbf{K_{NaiNeu}}$	1.5×10^{-3}	M	Na^+ threshold for NaK-ATPase	[3]
$\mathbf{K_{KENeu}}$	10×10^{-3}	M	K^+ threshold for NaK-ATPase	[3]
$\mathbf{[Na^+]_{Syn}}$	0.015	M	Na^+ concentration in the synapse	[3]

Table 8: Neuron NKA Parameters. (Calcium Experiment)

Parameter	**Value**	**Units**	**Description**	**Ref**
$\mathbf{P_{NKAmaxNeu}}$	-3.7863×10^{-8}	mol/m^2	Maximum NKA-ATPase Pump Rate	
$\mathbf{K_{NaiNeu}}$	10×10^{-3}	M	Na^+ threshold for NKA-ATPase	[3]
$\mathbf{K_{KENeu}}$	1.5×10^{-3}	M	K^+ threshold for NKA-ATPase	[3]
$\mathbf{[Na^+]_{Syn}}$	0.015	M	Na^+ concentration in the synapse	[3]
$\mathbf{[K^+]_{Syn}}$	0.1	M	K^+ concentration in the synapse	[3]

Table 9 Neuron Parameters (Both Experiments)

Parameter	**Value**	**Units**	**Description**	**Ref**
$\mathbf{g_{KNeu}}$	360	S/m^2	Maximum K^+ channel conductance	[3]
$\mathbf{g_{NaNeu}}$	1200	S/m^2	Maximum Na^+ channel conductance	[3]
$\mathbf{g_{LNeu}}$	3	S/m^2	Maximum leak channel conductance	[3]
$\mathbf{g_{KBNeu}}$	1.0522	S/m^2	K^+ Background channel conductance	[3]
$\mathbf{g_{NaBNeu}}$	2.3217	S/m^2	Na^+ Background channel conductance	[3]
$\mathbf{E_{KNeu}}$	-0.12	V	K^+ channel reversal potential	[3]
$\mathbf{E_{NaNeu}}$	0.115	V	Na^+ channel reversal potential	[3]
$\mathbf{E_{LNeu}}$	0.010613	V	Leak channel reversal potential	[3]
$\mathbf{C_m}$	0.01	F/m^2	Membrane capacitance	[3]

Acronyms

$[Ca^{2+}]_{GECS}$	Perisynaptic global ECS Ca^{2+} concentration
$[Ca^{2+}]_{PsC}$	Ca^{2+} concentration in the perisynaptic cradle
$[Ca^{2+}]_{PsECS}$	Perisynaptic extracellular Ca^{2+} concentration
$[Glu]_{ECS}$	Perisynaptic extracellular Glutamate concentration
$[Glu]_{PsECS}$	Glu concentration in the perisynaptic cradle
$[H^{+}]_{PsC}$	H^{+} Concentration in the perisynaptic cradle
$[H^{+}]_{PsECS}$	Perisynaptic extracellular H^{+} concentration
$[K^{+}]_{AS}$	K^{+} Concentration in the astrocyte soma
$[K^{+}]_{GECS}$	Perisynaptic global ECS K^{+} concentration
$[K^{+}]_{PsC}$	K^{+} concentration in the perisynaptic cradle
$[K^{+}]_{PsECS}$	Perisynaptic extracellular K^{+} concentration
$[K^{+}]_{Syn}$	K^{+} concentration in the synapse
$[Na^{+}]_{AS}$	Na^{+} Concentration in the astrocyte soma
$[Na^{+}]_{GECS}$	Perisynaptic global ECS Na^{+} concentration
$[Na^{+}]_{PsC}$	Na^{+} concentration in the perisynaptic cradle
$[Na^{+}]_{PsECs}$	Perisynaptic extracellular Na^{+} concentration
$[Na^{+}]_{Syn}$	Na^{+} concentration in the synapse
2-AG	2-arachidonyl glycerol (2-AG)
ADP	Adenosine diphosphate
ANNs	Artificial Neural Network
AP	Action Potential
AQP4	Aquaporin-4
ATP	Adenosine triphosphate
BCM	Bienenstock-Munro-Copper
BK	Big Potassium
C_m	Membrane capacitance
CNS	Central Nervous System
CSA_P	Process cross sectional area
CSA_{PS}	Perisynaptic cross sectional area
CSA_{Syn}	Synapse cross sectional area
CSF	cerebral spinal fluid (CSF)

$\mathbf{d_{EPS}}$	Perisynaptic external diameter
$\mathbf{d_{IPS}}$	Perisynaptic internal diameter
$\mathbf{d_{P}}$	Process diameter
$\mathbf{d_{Syn}}$	Synapse diameter
EAAT1/2	Excitatory amino acid transporter 1 and 2
ECME	EC coupling/mitochondrial energetics
ECS	Extracellular Space
$\mathbf{E_{KNeu}}$	K^+ channel reversal potential
$\mathbf{E_{KNeu}}$	K^+ channel reversal potential
$\mathbf{E_{LNeu}}$	Leak channel reversal potential
$\mathbf{E_{LNeu}}$	Leak channel reversal potential
$\mathbf{E_{NaNeu}}$	Na^+ channel reversal potential
EPSP	excitatory postsynaptic
ES	evolutionary strategy
F	Faraday constant
GABA	*gamma*-Aminobutyric acid
$\mathbf{g_{ECS}}$	Perisynaptic ECS leak conductance
GGC	glutamate-glutamine cycle
$\mathbf{g_{K}}$	K^+ background transport conductance
$\mathbf{g_{KBNeu}}$	K^+ Background channel conductance
$\mathbf{g_{Kir}}$	K_{ir} channel conductance
$\mathbf{g_{KNeu}}$	Maximum K^+ channel conductance
$\mathbf{g_{LNeu}}$	Maximum leak channel conductance
$\mathbf{g_{Na}}$	Na^+ background transport conductance
$\mathbf{g_{NaBNeu}}$	Na^+ Background channel conductance (Neurons)
$\mathbf{g_{NaNeu}}$	Maximum Na^+ channel conductance
HH	Hodgkin-Huxley
IICR	IP_3 Induced Calcium Release
$\mathbf{IP_3}$	inositol 1, 4, 5-trisphosphate
$\mathbf{IP_3Rs}$	inositol 1, 4, 5-trisphosphate Receptors
IPSP	inhibitory postsynaptic potential
$\mathbf{k_B}$	Boltzmann constant
KCC1	K-Cl co-transporter-1

K_{ir}	Inward rectifier K^+ channels
	($K_{ir4.1}$ Kir channel with protein number 4.1)
K_K	K^+ Poole-Frenkel channel constant
K_{KE}	K^+ threshold for NKA-ATPase
K_{KENeu}	K^+ threshold for NaK-ATPase
K_{Na}	Na^+ Poole-Frenkel channel constant
K_{Nai}	Na^+ threshold for NKA-ATPase
K_{NaiNeu}	Na^+ threshold for NK-ATPase (for Neurons)
l_P	Process length
LPLA2	lysosomal phospholipase A2
l_{PS}	Perisynaptic length
l_{syn}	Synapse length
LTD	Long Term Depression
LTP	Long Term Plasticity
MLFFNs	Multilayer Feed-forward Networks
MLP	Multi-Layer Perceptrons
NBC	sodium bicarbonate cotransporter
NCX	Sodium Calcium Exchanger
NKA	Sodium-Potassium Adenosine Triphosphatase
(Na^+/ K^+-ATPase)	
NKCC	Na-K-Cl co-transporters
NKCC1	Na^+/ K^+/Cl^- transporter
NKX	Sodium Potassium Exchanger (same as NKA)
PAP	perisynaptic astrocyte processes
pH	Potency of Hydrogen (from German: *Potenz-H^+*)
	pH=-log [H^+] at standard temperature and pressure
PMCA	Plasma membrane Ca^{2+} -ATPase
$P_{NaKmaxNeu}$	Maximum NaK-ATPase Pump Rate
PS	phosphatidylserine
PsC	Perisynaptic Cradle
PSD	postsynaptic density
PSP	postsynaptic potential
Q	Charge [in Coulombs]

QSCM	Quantitative Surface Conductivity Microscopy
R	Gas constant
$\mathbf{r_{EPS}}$	Perisynaptic external radius
r_g	Slope of glutamate uptake
$\mathbf{r_{IPS}}$	Perisynaptic internal radius
$\mathbf{r_P}$	Process radius
$\mathbf{r_{Syn}}$	Synapse radius
$\mathbf{SA_P}$	Process surface area
$\mathbf{SA_{PS}}$	Perisynaptic surface area
$\mathbf{SA_{PsECS\text{-}GECS}}$	Surface area between PsECS and GECS
$\mathbf{SA_{Syn}}$	Synapse surface area
s_g	Threshold for glutamate uptake
SHL	Supervised Hebbian Learning
SLFFNs	Single Layer Feed-forward Networks
STDP	Spike Timing Dependent Plasticity
STP	Short Term Plasticity
T	Temperature
TCA	Tricarboxylic Acid
$\mathbf{V_A}$	Astrocyte Membrane potential
$\mathbf{V_m}$	Astrocyte resting membrane potential
$\mathbf{Vol_P}$	Process volume
$\mathbf{Vol_{PS}}$	Perisynaptic volume
$\mathbf{Vol_{PsECS}}$	Perisynaptic ECS volume
$\mathbf{Vol_{Syn}}$	Synapse volume
XOR	Exclusive OR
$\mathbf{z_{Ca}}$	Calcium Valency
$\mathbf{z_{Glu}}$	Glu Valency
$\mathbf{z_K}$	K^+ Valency
$\mathbf{z_{Na}}$	Na^+ Valency
α_{EAAT}	Glutamate transport fitting parameter
β_{EAAT}	Glutamate transport fitting parameter
$\boldsymbol{\varepsilon_0}$	Vacuum permittivity
$\boldsymbol{\varepsilon_r}$	Relative permittivity of brain tissue

φ_w	Well activation energy

Acknowledgements

I am grateful for the support and assistance from my primary supervisor Professor Liam McDaid who provided feedback and direction on all my work, for his general assistance in tackling difficulties and setbacks during the PhD, and through his hard work and commitment I have become a lot more aware of the process of academic publishing and computational modelling, and conceptualisation of complex biological processes in particular.

I would like to thank Dr. KongFatt Wong-Lin and Dr John Wade for their assistance in both computational neuroscience and for his mathematical input particularly with regards to complicated numerical analysis and non-linear dynamics. I would like to thank Jim Harkin who introduced me to astrocytes and how they inspire new computational paradigms, and also for his feedback and direction in weekly meetings.

I would also like to thank Bronac Flanagan, Harm Van Zalinge, Steve Hall, Matthew Walker and Alexei Verkhratsky for their assistance with papers related with to the work in this thesis.

I of course would like to thank the School of Computing and Intelligent Systems for providing me with a desk and computing facilities and thanks all in the ISRC and the University who have helped me to get through my PhD.

I would like to express my gratitude to Kevin Baxter and John Laverty for their support on campus, their advocacy and their assistance with managing my PhD, and sometimes research-life balance. I would like to acknowledge the Department of Employment and Learning (which was merged into the Department for the Economy during my studies) for their financial support, which has enabled me to study at the University of Ulster, and the Doctoral College for providing administrative information and teaching key research skills.

Finally, I am hugely thankful for the inspiration of my late mother Mary who inspired my scientific interest, and who I deeply miss, the support of my father Patrick, my brothers John and Peter and to the rest of my family and friends who have supported me throughout my life.

Abstract

It is now known that astrocytes, the major class of glial cells, act as a third synaptic terminal and respond to neurotransmitters by releasing gliotransmitters. Structurally, astrocytes function primarily through their processes which are frequently extremely fine (<50 nm) with a large surface-to-volume ratio. They are rarely studied in live tissue, as they are not directly accessible to electrophysiology and are smaller than microscopic resolution. For this reason this thesis proposes that in order to advance our understanding of interactions between an astrocyte and nearby synapses, a computational modelling approach is essential.

The underlying hypothesis put forward in this thesis is that in thin astrocyte process, fixed negative charges existing in inner process membrane will be the dominant ionic conduction in the process cytoplasm. Specifically, it is proposed that these negative charges give rise to potential wells and therefore ions must hop from well to well as they move along the thin astrocyte process. Consequently this low conductance pathway serves to semi-isolate the astrocytic perisynaptic cradle (PsC) from the astrocytic main body.

A computational model of the PsC is developed which includes ionic hopping in the process cytoplasm. It made 4 key predictions:

1. The model gave results which agreed with experimental observation in that both Na^+ and K^+ microdomains form at the PsC, and that the mechanism underpinning this behaviour was the low conductance pathway between the PsC and the astrocyte soma: the low conductance pathway is a direct result of ion retention in the potential wells.
2. Additionally, a slow decay of Na^+ was also observed in our simulation after a period of glutamate stimulation which is in strong agreement with experimental observations. The pathological implications of microdomain formation during neuronal excitation are also discussed.
3. The model also predicted that the K^+ microdomain provides the driving force for the return of K^+ to the extracellular space for uptake by the neuron, thereby preventing K^+ undershoot. This observation is in direct contrast to the prevailing view of K^+ clearance, and may point towards a new mechanism for K^+ homeostasis at the PsC.
4. Furthermore, the model predicted that a Ca^{2+} microdomain can form due to reversal of the NCX extruder and the implications of this is significant in that a local source of Ca^{2+} is produced in the absence of the endoplasmic reticulum.

Note on Access to Content:

I hereby declare that with effect from the date on which the thesis is deposited in Research Student Administration of Ulster University, I permit:

1. The Librarian of the University to allow the thesis to be copied in whole or in part without reference to me on the understanding that such authority applies to the provision of single copies made for study purposes or for inclusion within the stock of another library.

2. The thesis to be made available through the Ulster Institutional Repository and/or EThOS under the terms of the Ulster eThesis Deposit Agreement which I have signed.*

IT IS A CONDITION OF USE OF THIS THESIS THAT ANYONE WHO CONSULTS IT MUST RECOGNISE THAT THE COPYRIGHT RESTS WITH THE AUTHOR AND THAT NO QUOTATION FROM THE THESIS AND NO INFORMATION DERIVED FROM IT MAY BE PUBLISHED UNLESS THE SOURCE IS PROPERLY ACKNOWLEDGED

_____

Kevin Breslin

January 2019

1.

Introduction

Background

I. The Human Brain

The adult human brain consists of three main parts, the cerebrum, the cerebellum and the brainstem. The cerebrum is the part of the brain which performs higher functions like interpreting sensory information, language, reasoning and fine motor control. The cerebrum is divided into two major parts, a right cerebral hemisphere and a left cerebral hemisphere [7]. The hemispheres are connected at the bottom by a corpus callosum which allows signals to be delivered between the hemispheres. Each hemispheres contains four main lobes (the temporal, frontal, parietal and occipital lobes) which connect to one another through complex connections. There are also several smaller but important parts of the brain, such as the thalamus, which serves as a connection point for nerve signals that enter and leave the cortex, the pituitary gland responsible for growth and developmental hormones, controlling the functions of organs and other glands and the pineal gland responsible for responses to light and dark environments [7]. The surface of the cerebrum forms the cerebral cortex, contains billions of neurons and neuroglia. This surface forms the grey matter of the brain, and beneath the cortex are fibres connecting neurons which form the white matter. The cerebellum is located at the back of the brain beneath the occipital lobes, it functions to coordinate muscle movement, posture and balance which gives rise to rapid and repetitive actions. It is separated from the cerebrum by the tentorium [8]. The brainstem is the posterior part of the brain that connects the nerves of the cerebrum and cerebellum to the spinal cord. It performs automatic functions such as digestion, respiration, temperature homeostasis and sleep. It contains three main parts, which are: the midbrain, pons and medulla. The midbrain is a centre for ocular motion, the pons co-ordinates eye and facial movements, facial sensation, hearing and balance, and the medulla controls breathing, heart rhythms, blood pressure and swallowing. The brain is

connected to the organs and muscles of the body through the nervous system to co-ordinate the adjustments and reactions of an organism to internal and environmental conditions (in combination with the endocrine system). The brain along with the spinal cord forms the central nervous system, with the rest of the nervous system being the peripheral nervous system and that is divided into the voluntary and autonomic nervous systems. At the tissue level, the nervous system is composed of neurons, glial cells, and extracellular matrix.

II. Origins of Modern Neuroscience and the Discovery of Glia cells.

Our knowledge of nerves dates back to Herophilos [9], and our understanding of the structure of nerve fibres ran in parallel with the development of anatomy and is attributed to work carried out by Luigi Galvani on animal electricity, which also aided the scientific understanding of the principles of electromagnetism [10]. The first anatomical description of neurons at a cellular level came through the advancement of microscopy. J.E. Purkinje in 1837 [11] helped develop the field of cell biology, and advanced the understanding of neurons beyond crude anatomical descriptions. Later Camillo Golgi and Ramón y Cajal stained branches of nerve cells and found that these cells could only touch, or synapse and from this Cajal postulated his neuron doctrine which states that the nervous system is a collection of individual cells called "neurons", which are interconnected to form a network and the shape of a cell determines its function [12]. Cajal systematically described the cellular organization of almost every part of the nervous system in all five classes of vertebrate as well as their embryogenesis [13]. Both Golgi and Cajal were jointly given the Nobel Prize in Physiology or Medicine 1906 in recognition of their work on the structure of the nervous system [12]. The concept of glia was coined by Swiss physiologist, Rudolf Virchow in 1858, to describe "a sort of nervenkitt (German for neural putty) in which the nervous system is embedded" [11]. In 1851 Heinrich Müller discovered the first type of glial cells, the Müller cells found in the retina. Otto Deiters (1860) and Jakob Henle (1869) helped discover stellate cells which were later named by Michael von Lenhoosek as Astrocytes (from the Greek for Star, astro and for cell, cyte) [11] [14]. Other glial cell types were discovered by Pio Del Rio-Horega: oligodendrocytes (from Greek for few "oligo", branches "dendro" and cell "cyte") and microglial to which he understood behave similar to white blood cells (phagocytes) [11] [14]. The final type, the Schwann cell, was discovered by Antione Ranvier in 1871, and named after Theodor Schwann who in 1839 determined there must be specialised cells to carry out the

function of creating a myelin sheath [11]. The above discoveries led to the belief that astroglia determine the architecture of neural tissue and maintain central nervous system (CNS) homeostasis [15] [16] [17] .

III. Astrocytes and their role in Homeostasis.

In this work we will focus on the ability of astrocytes to balance K^+, Na^+ and Ca^{2+} ions within a neuron-astrocyte system. Homeostasis is the tendency a system to move towards a relatively stable equilibrium between interdependent elements, especially as maintained by physiological processes [18]. It refers to a wide range of self-regulating processes in the body that maintain a complex number of elements including body temperature, fluid balance, blood pH, oxygen tension that are altered by the manner which the body consumes food, water and oxygen. It also refers to defence mechanisms in the body, such as excretion of toxins and waste products, acquired immune responses against illness and infection, repair against damage, pain and sensitivity response to damaging contact. [19] Some definitions of homeostasis include behavioural responses to maintain a psychotherapeutic balance [20]**.**

Astrocytes are organised into functional syncytia that show anatomical specialisation [21] [22], which allow intercellular diffusion of ions, secondary messengers and metabolites. Astroglial membranes closely enwrap the majority of excitatory synapses in the CNS and form astroglial cradle, [23] [24] [25] which is fundamental for synaptogenesis, synaptic maturation, synaptic transmission and synaptic extinction. Astroglial membranes are densely packed with transporters and ion pumps that maintain molecular homeostasis in the synaptic cleft and in the brain interstitium [26]. In particular astrocytes are central elements of potassium (K^+) homeostasis, which is critical for determining neuronal excitability [27] [28] [29]. Furthermore, astrocytes maintain homeostasis of many neurotransmitters and neuromodulators and supply neurons with glutamine. They are also an obligatory precursor for the synthesis of glutamate and GABA which are the main excitatory and inhibitory neurotransmitters respectively [30] [31] [32] [33].

K^+ homeostasis is a canonical function of astroglia proposed in the mid-1960s; both energy dependent Na^+/ K^+ATPase (NKA) and diffusional (inward rectifier K^+ channels) pathways were considered as molecular mechanisms [27] [34] [35]. Subsequently the Na^+/ K^+/Cl^- transporter NKCC1 was suggested to participate in K^+ buffering, especially at high (pathological) K^+ concentrations [36] [37] [28].

The local K^+ uptake by these channels and transporters is supposedly supported only by spatial K^+ buffering (K^+ diffusion through gap junctions from regions of elevated [K^+] to regions of lower [K^+]). Under physiological conditions, however, the main pathway for K^+ uptake is associated with NKA, whereas $K_{ir}4.1$ inward rectifying channels mediate K^+ export needed to restore K^+ gradients in neuronal compartments [36] [37] [28]. However, it is important to note these observations are at odds with the rapid diffusion of potassium in glia away from areas of synaptic activity, and are more consistent with compartmentalisation of potassium within astroglial processes.

Astroglial homeostatic function is, to a large extent, controlled by transmembrane sodium (Na^+) gradients and is regulated by cytoplasmic Na^+ signals [38] [39]. Dynamic fluctuations of $[Na^+]_i$ affect Na^+-dependent transporters and associated molecular cascades that link Na^+ dynamics to homeostasis of K^+ and neurotransmitters [38] [39]. Astroglial Na^+ signals are spatially heterogeneous with the existence of Na^+ microdomains; these Na^+ signals may also propagate through astroglial syncytia via gap junctions [40].

The main pathway for astroglial Na^+ entry occurs through the excitatory amino acid transporter1 and 2 (EAAT 1/2) [33]. Glutamate transport is powered by transmembrane ion gradients where 3 Na^+ and 1 H^+ ions are exchanged for one K^+ ion, hence the Na^+/glutamate transporter generates a net inward Na^+ current [41] [42]. In addition, glutamate opens astroglial ionotropic receptors (AMPA and NMDA receptors) and activates (indirectly through store-operated Ca^+ influx pathway) TRPC channels which further contribute to stimulus-dependent Na^+ entry [43] [44] [45] [25]. Glutamate transporters co-localise with sodium-calcium exchanger (NCX) that couple Na^+ and Ca^{2+} signalling [46] [47].

IV. The theoretical case for microdomains

The existence of astroglial ionic microdomains [48] [40] [39] indicates that there must be mechanisms that slow ionic diffusion along the processes. A candidate for this mechanism is associated with fixed negative charges existing in cell membranes. Previous experiments [49] have found localised fixed negative charges in the membranes of neurons and glia. Biological membranes consist of a continuous bilayer of lipid molecules in which membrane proteins are embedded. These bilayers are filled with polar and non-polar portions in their structure (amphipathic) [50]. All eukaryotic membranes are also asymmetric such that biophysical properties differ between the intracellular and extracellular surfaces; this asymmetry is necessary for many key cellular processes including cell fusion and cell clearance [51]. As both sides of the bilayer phospholipid membrane surface are negatively charged, and

the ions in contact with the membrane surface are in deep potential wells near the dipole heads of that membrane. As a result mobile ions cannot diffuse along the membrane easily but must "hop" from well to well slowing their diffusion as they transverse the process. [6] [52].

As astrocyte processes are, in some regions of the brain, very thin [16]. This thesis puts forward the hypothesis that fixed negative charges will have a dominant role in restricting ion conduction along the process. Specifically, it is proposed in this work that ion retention in the potential wells requires that ions must hop from well to well as they move along the thin astrocyte process and therefore this hopping effect serves to semi-isolate the astrocytic perisynaptic cradle (PsC) from the astrocytic main body. The aim of this thesis is to understand through modelling the mechanisms that control ionic homeostasis at the PsC and the associated intracellular/extracellular ionic processes. The roles that astrocytes have in homeostasis within the nervous system and regulating neural behaviour are of interest to the understanding of brain disorders and brain functions and possibly the development of new computational paradigms based around astrocyte interactions with neurons. To be able to model astrocytes and astrocyte-neuron interactions it is necessary to understand the mechanism involved in the influx/efflux of ions across cell membranes and between different cell types.

Objectives of the Thesis.

The objectives of the thesis are as follows:

- To develop a model that captures ionic conduction in thin astrocyte processes and to use the model to test a new hypothesis proposing that ionic conduction in these processes is surface dominated. Therefore, ionic flow in the process cytoplasm is constrained by ions hopping between potential wells due to the fixed negative charges that exist within a continuous bilayer of lipid molecules of the astrocyte membrane [50].

- To extend the ionic conduction model to include the influx/efflux of ions at the PsC and verify/use the model to explain the occurrence of ionic microdomains within the PsC during neuronal excitation. Experimental evidence has reported that a Na^+ microdomain forms within the PsC and the decay time is in the order of minutes after neuronal activity ceases [41] [39]. Furthermore, experimental evidence also shows that, in thin processes, no K^+ undershoot occurs post neuronal excitation.

- To use the model to investigate ionic homeostasis at the PsC where the focus will be on the interplay between Na^+, K^+ and Ca^{2+} ions. Effectively ionic microdomains represents a temporary "storage" mechanism for ions at the PsC and therefore a natural conclusion would be that K^+ ions are maintained there during neuronal excitation to be returned to the extracellular space post excitation. This points to a new theory for K^+ clearance and may also explain the absence of K^+ undershoot. Additionally, the occurrence of a Na^+ microdomain is very likely to reverse the NCX extruder providing a local source of Ca^{2+}.

- This local source of Ca^{2+} will also be investigated by further developing this model with the inclusion of Ca^{2+} ions to test whether the reversal of the sodium/calcium exchanger (NCX) due to the Na^+ microdomain, leads to the formation of a Ca^{2+} microdomain in the perisynaptic compartment. Moreover, the Ca^{2+} microdomain is remote from any Endoplasmic Reticulum (ER) mediated Ca^{2+} release and we propose that this local source of Ca^{2+} may provide a previously under explored form of astrocyte Ca^{2+} signalling.

Thesis Contribution

This thesis presents for the first time a detailed model that captures ionic homeostasis at the PsC where the focus of the model is on the interplay between Na^+, K^+ and Ca^{2+} ions. Specifically, this work will show that a slow leakage of ions away from the PsC could explain the formation of K^+ and Na^+ microdomains at the PsC, which points to a new theory for K^+ clearance. For example, it is widely reported [53] [27] that excitatory presynaptic neurons release K^+ into the extracellular space (ECS) which is subsequently cleared at the PsC and buffered away through diffusion to the main astrocyte body. However, it is proposed in this thesis that the flow of K^+ away from the PsC is not volume diffusion limited but rather is restricted due to the hopping effect along the process, and therefore a K^+ microdomain forms at the PsC during sustained presynaptic neuronal excitation. Furthermore, it will be shown through mathematical modelling, that the formation of a K^+ microdomain at the PsC may very well be advantageous as it facilitates a low energy return pathway for K^+ to the ECS, after neuronal excitation has ceased.

Additionally, ion retention along thin processes may also affect homeostasis for Na^+ ions as they also carry a positive charge. It has been shown in other work [41] that the decay rate of Na^+ following a sustained level of glutamate uptake through EAAT1/2 is in the order of seconds. Our model proposes that this slow decay rate is due to the restricted flow rate of Na^+ ions along thin processes which results in the formation of a Na^+ microdomain at the PsC: consequently Na^+ ions can only be removed by the NKA, reversal of NCX and other transporters.

Our model also proposes that the K^+ microdomain provides the driving force for the return of K^+ to the extracellular space via background K^+ channels, for uptake by the neuron via its NKA. Essentially, K^+ is transiently "stored" at the PsC during neuronal excitation where it decreases the electrochemical gradient of K^+, so reducing inward flow of K^+ through K_{ir}; this "stored K^+" is then available to replenish neuronal K^+ levels when the excitation ceases, thereby preventing K^+ undershoot in the extracellular space. These observations are consistent with *in vivo* experimental data [54], and partly explain why inward rectifying K^+ channels may play a prominent role for K^+ uptake at large volume glial processes (e.g. terminal endfeet of retinal Muller cells [55]) but not at low volume perisynaptic cradles. These results will also necessitate a reappraisal of the mechanisms and role of astrocytes in potassium accumulation during seizure activity [56], especially given the observation that the loss of function mutations

in the gene encoding $K_{ir}4.1$ are associated with a human epilepsy syndrome [57] and astrocyte $K_{ir}4.1$ expression is decreased in acquired epilepsy models [58]. Moreover, other conditions that have been proposed to be due to abnormalities of potassium homeostasis such as familial hemiplegic migraine are associated with mutations of the gene encoding the alpha2 subunit of NKA, which is predominantly expressed in astrocytes [59] .

It is now widely accepted that the perisynaptic astroglial compartment is devoid of the endoplasmic reticulum [60], hence excluding the metabotropic pathway for generation of local Ca^{2+} microdomains. It is also accepted that astroglial perisynaptic membranes express high densities of glutamate transporters of EAAT1/2 types, which couple glutamate transport with substantial Na^+ influx [41] [61]. These transporters are co-localised with NCX [46], and couple Na^+ and Ca^{2+} fluxes in opposite directions.

This thesis also tests another hypothesis that glutamate transporters and NCX working together are sufficient to create local Ca^{2+} microdomains in astroglial perisynaptic compartments. Our model demonstrates that stimulation of astrocytes with glutamate generates substantial Na^+ influx, which forms local microdomains due to the previously suggested mechanism of ion retention [3]. Moreover, the generation of Ca^{2+} microdomains have previously been reported but the underlying ionic fluxes (and channels/transporters contributing to) have not been examined. This computational modelling study has identified the molecular targets and their relative contributions to the formation of a Ca^{2+} microdomain in the absence of an ER region. Specifically, the Na^+ microdomain switches the NCX into reversed mode, thus generating Ca^{2+} influx which is sufficient to produce relevant focal Ca^{2+} signals. This mechanism, which does not depend on intracellular sources for Ca^{2+} directly links neuronal activity and glutamate release to the formation of Na^+ and Ca^{2+} microdomains in the perisynaptic astroglial processes, which are instrumental for generation of astroglial homeostatic response critical for maintenance of synaptic transmission.

Outline of the Thesis.

Chapter 2 of this thesis consists of a biophysical review covering the structure and basic physiology of neurons and neural glial cells. It also covers areas of applied biophysical principles in the development of artificial neural networks, and goes into detail about areas of physiological research used to develop the proposed model. Since both the neuron and astrocyte cells are the focus of this thesis, this review will provide information on the structure of these cells and the biological interplay. To understand these cells in detail, it is important to know the underlying physical principles of the cells environment. This includes the electrical factors such as membrane potential, electrodiffusion, ionic exchange between cells and the extracellular space and biological functions that are peripheral to this work: i.e., active transport by ATP transporters, volumetric changes due to osmotic pressure and finally chemical concentration gradients as a driving force for ions. What is central to the research presented in this thesis is fixed membrane charges and an in-depth review of their source and distribution will be included in this chapter.

Chapter 3 discusses existing biophysical models of astrocyte neuron interactions and highlight research into the underlining physiological issues. The computational modelling of astrocytes is essential to the understanding of the interactions between transport processes within and between cells. The review will also look at models of the signaling pathways between neurons and astrocytes and volumetric changes to cell structure. Additionally the review will cover existing models of astrocyte mitochondrial metabolism capturing the dynamics of underlying effects of the tricarboxylic acid (TCA) cycle that form and reform ATP in the EC coupling/mitochondrial energetics (ECME) model.

Chapter 4 proposes a new hypothesis where fixed positive membrane charges dominates ionic flow in thin astrocytic processes. Specifically in thin processes where the surface to volume ratio is high ionic flow is no longer electrodiffusion limited but rather is dominated by hopping between potential wells: these wells are due to potential fluctuations at the membrane inner surface as a results of the fixed negative charges. This chapter develops a computational model that will be taken forward in subsequent chapters to test the hypothesis. The model captures the interplay between different ionic types at the PsC and will be used to test whether or not the hopping effect within thin astrocytes can explain the formation of microdomains within the PsC, and other related phenomena such as K^+ undershoot in the extracellular space and Ca^{2+} influx due to the reversal of the NCX.

Chapter 5 will use the model developed in chapter 4 to test the hypothesis that ionic

retention in the potential wells directly results in microdomain formation in the PsC. Effectively the proposed model will show that in thin processes ionic conductance is impeded, and therefore the PsC is semi-isolated from the astrocytic main body. The proposed model will show that this semi-isolation can explain the formation of K^+ and Na^+ microdomains at the PsC, an observation recently reported by experimentalists [53] [27]. These microdomains can only be removed through active transport by the NKA, or electrostatically by reversal of NCX and other transporters.

Chapter 6 shows simulation results that predict that the combination of glutamate transporters and NCX working together is sufficient to create local Ca^{2+} microdomains in the PsC in the absence of an ER region. Specifically, the Na^+ microdomain switches the NCX into reversed mode, thus generating Ca^{2+} influx which is sufficient to produce relevant focal Ca^{2+} signals. This mechanism, which does not depend on intracellular sources for Ca^{2+}, directly links neuronal activity and glutamate release to the formation of Na^+ and Ca^{2+} microdomains in the perisynaptic astroglial processes, which are instrumental for the generation of astroglial homeostatic responses critical for maintenance of synaptic transmission.

Chapter 7 concludes the thesis followed by a discussion of further work.

2.

Biophysical Review

2.1 Introduction

This section will review existing biophysical studies on the structure and physiology of neurons and glia cells. This section will provide a review of the structure and basic physiology of neurons, neuroglial cells and neural architectures. There are two major cell types in the nervous system, neurons and neuroglial cells. Neurons are specialised for rapid communication in the body, while neuroglial are non-neuronal cells that carry out a broad range of ancillary functions [62] [63] [64]. In the nervous system neurons make up around 10-20% of the whole population of nervous system cells, and neuroglial cells make up the rest. Despite different shapes and sizes, neurons and glial cells have a similar microbiology. This is because most glia and neurons arise from common precursors [65]. This chapter presents a review of both neural and glial cells from the biophysical perspective where for the latter there is a particular focus on astrocytes. Neurons are specialised for rapid communication in the body, while the smaller but more common neuroglial cells carry out a broad range of ancillary functions [62] [63] [64]. Among the neuroglial cells are astrocytes, which along with neurons form the presynaptic cradle which is of particular interest in this thesis: the cradle region is studied in the context of ionic homeostasis. Astrocytes are abundant in the nervous system with the same receptors, channels, transporters and co-transporters as neurons possess and perform crucial functions like glutamate and K^+ clearance during neuronal excitation, the nature of these transporters will be explored in this section as will their role in K^+ buffering and K^+ clearance. Of particular interest is ionic homeostasis at the perisynaptic cradle in the presence of thin astrocyte processes. To underpin the core concept tabled in this work the review will focus on fixed negative charges in astrocyte membranes, relates the presence of these fixed charges to ionic homeostasis mechanisms such as microdomain formation at the perisynaptic cradle. The Chapter will look at neurons and neuroglial cells and then the transporters common in both cells. It will then explore the two key physiological mechanisms involved in this K^+ buffering and K^+ clearance, and the origins of fixed charges in thin astrocyte processes.

2.2. Neurons

2.2.1 Neuron structure

Neurons act as standalone functional units of the nervous system and are much bigger than glial cells and occupy most of its structure. An outline of the components of a neuron is given in Fig. 2.1 [62].

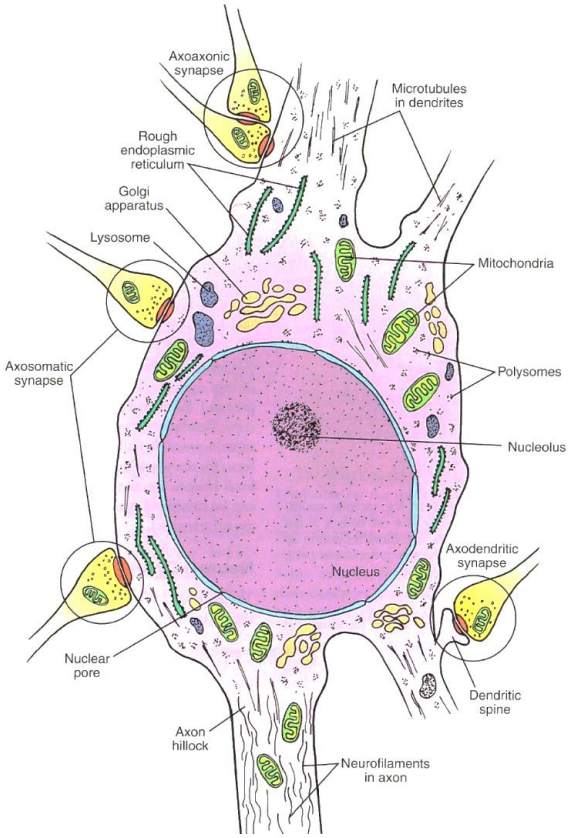

Figure 2.1: Components of a neuron from electron micrograph trace. Mitochondria are green, presynaptic terminals are yellow Figure 2.5 from [62] originally from [66]

Both neurons and glial cells contain a plasma membrane, or plasmalemma, which is a double layer of phospholipid molecules whose hydrophobic hydrocarbon chains are all directed toward the middle of the membrane. Embedded in this structure are protein molecules that include transporters, aquaporins and exchangers. The cytoplasm of the cell body is dominated by microstructures called organelles, which are used for protein synthesis (rough endoplasmic reticulum and polyribosomes) and for cellular respiration and energy production (mitochondria). Also present in both cells is a well-developed Golgi apparatus, which is a complex of vesicles and folded membranes involved in secretion and intracellular transport. The nucleus of a neuron (Figure 2.1) is usually in the centre of the cell body which contains its genetic material and a nucleolus which functions to create ribosomes and respond to cellular

stresses. Around the cell is an extracellular fluid which contains many sodium and chloride ions and inside the cell is a cytoplasm which contains mainly potassium and organic anions derived from amino acids. Both the extracellular fluid and the cytoplasm are electrically neutral with the same osmotic pressure which means the differences in charge concentrations produce a membrane potential. The inside potential is negative (≈−70 mV) with respect to the outside when the neuron is not conducting a signal, this is called the resting membrane potential. This potential opposes inward cation currents (e.g. K^+) and outward anion currents (e.g. Cl-) crossing the membrane. The membrane potential also controls voltage gated channels which can close preventing ions from being released or entering these channels.

Neuron diameters vary from 5 microns in complex circuits to 135 microns in large motor neurons. These cells have a main body called the soma which contains a nucleus and a cytoplasm: the cytoplasm containing organelles such as the mitochondria, endoplasmic reticulum and peroxisomes [62]. The soma consists of two main types of processes, the axon and the dendrites. The dendrites are processes that attenuate away from the cell body and function to carry signals to the soma. Dendrites, of which there are many in a neuronal cell, provide a large surface area for a synapse, so that multiple signal inputs can be collected and transmitted to the cell body. The axon of a neuronal cell is the most excitable part of the cell and serves to transmit information from the soma to nearby and distal synapses, and nerve terminals. Axons can vary from 100 microns to 1 meter long and from less than 1 micron in dimeter, without a myelin sheath, to 10 microns thick, with a myelin sheath. Indeed in the human cortex there are six kilometres of axons that assist the huge parallelism within the brain. Axons can branch into several processes which send information to synaptic target and the axon's excitability is due to the presence of a high density of voltage gated channels at the axon hillock where this region acts as the initiation site of action potentials. The myelin sheath formed by Schwann cells protect the signal from attenuation and alter the conducting properties of axons. Each Schwann cell is separated with gaps called the "nodes of Ranvier" which allow the signal to be amplified in the axon to prevent signal loss [63].

2.2.2 The Neuronal Communication Pathway

The membrane potential of a neuron at rest is approximately -70mV but this can depolarise rapidly due the influx/efflux of ions like K^+ and Na^+. If, at the soma, this potential is sufficiently depolarised beyond a threshold level then there is a rapid exchange of ions across the membrane which causes a rapid increase followed by an equally rapid decrease in the membranes

potential: this is termed a spike or an action potential and is the unit of excitation for neurons. The soma is therefore considered as the central processing unit that performs an important nonlinear processing step: aggregation of dendritic inputs followed by the generation of a spike of ions and neurotransmitters to the dendritic outputs to stimulate or inhibit their function (such as other neurons and glial cells, muscles tissue, blood vessels, organs, glands etc.) to normal levels.

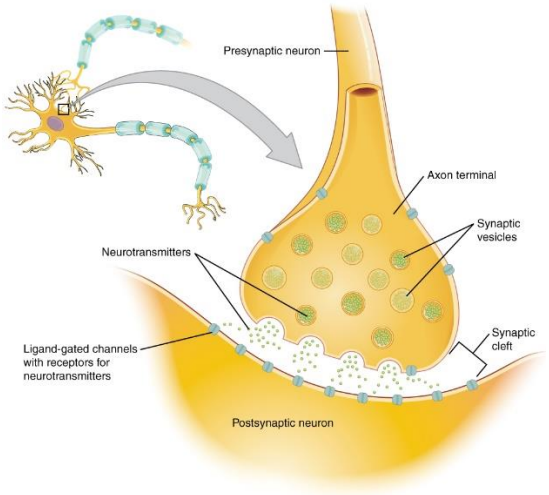

Figure 2.2: A diagram of proper synaptic connectivity [67]

Now consider the case where we have a presynaptic neuron whose axon makes close contact with the dendrite of a postsynaptic neuron. This junction is known as a synapse, as shown in Figure 2.2 where the terminal ending of the presynaptic axon fibre swells to form what is known as a synaptic bouton with neurotransmitters enclosed in vesicles contained within.

The synaptic bouton is not in intimate contact with the dendrite bouton and there exists a small spacing of about 20nm known as the synaptic cleft. When the presynaptic neuron is excited and emitting spikes, these spikes travel along the axon fibre and arrive the synaptic junction [63]. Most synapses are chemical; these synapses communicate using chemical messengers. Other synapses are electrical; in these synapses, ions flow directly between cells. At a chemical synapse, an action potential triggers the presynaptic neuron to release neurotransmitters. That bind to receptors on the postsynaptic cell and make it more or less likely to fire an action potential. In ionotropic based synapses this positive increase of potential at the synapse bouton causes an influx of Ca^{2+} which promotes the fusing of vesicles with the membrane and the subsequent release of neurotransmitter into the cleft. The neurotransmitter in the cleft diffuses and binds with receptors on the dendrite of the postsynaptic neuron. This chemical binding action leads to an influx of electrically charged ions into the postsynaptic terminal leading to a depolarisation of the postsynaptic neuron. This depolarisation is commonly referred to as the

postsynaptic potential or PSP. If the net flow of ions into the cell leads to an increase in the positive charge within the postsynaptic terminal then this is known as an excitatory postsynaptic potential or EPSP. Alternatively if the net flow of change into the terminal leads to a net negative charge increase within the postsynaptic terminal then this hyperpolarises the terminal and is known as an inhibitory postsynaptic potential or IPSP. The flow of ions out of the presynaptic neurons and into postsynaptic neurons (see Fig 2.2) alters the balance of charge in the intracellular space of both cells relative to their surrounding extracellular space at that junction and, as such, changes their membrane potential. Additionally, the flow rate of ions across the membrane of cells can be triggered by changes in the concentration gradient (due to the influx/efflux of ions) and/or the membrane potential. Details of these ion transporters are given in Section 2.2.2.

The above synapse is known as a chemical synapse but there also exists electrical synapses. Most synapses in vertebrates are chemical synapses and require chemical neurotransmitters but electrical synapses transport ions based only on a concentration gradient. Electrical synapses exist in a small number of sites in the central nervous system that are involved in synchronizing cortical functions due to the fast propagation of ions through the synapse. These synapses differ from chemical synapses in that they do not allow for synaptic integration, do not contain a synaptic clef and ionic transmission is bi-directional [63].

2.2.3 Synaptic Plasticity

Plasticity is the ability of the brain to change and adapt to new information where these changes occur at synaptic junctions. Plasticity is believed to be related to the level of activity at pre and postsynaptic neurons and this concept was first introduced by Donald Hebb in 1949 [68]. Synaptic plasticity is one of the most important areas in neuroscience since it underpins memory and it is now known that there are Short Term Plasticity (STP) and Long Term Plasticity (LTP). STP results from the depletion of neurotransmitters at the synaptic bouton whereas Short Term Facilitation (STF) results in an increase in the Probability of Release (PR) of neurotransmitter due to the influx of calcium after spike generation [69] [70] [71] [72] [73]. In contrast LTP is associated with activity dependent modification of neural circuits and has a much longer time scale than STP. Typically STP is in the millisecond to seconds range whereas LTP is hours to days or even longer.

LTP results in a persistent enhancement of synaptic transmission whereas in Long Term Depression (LTD) synaptic transmission is reduced. It is now known that LTP and LTD occur

at synaptic sites and underpin memory. From the computational perspective plasticity within a neural network containing spiking neurons is modelled by a change of weights associated with synapses where potentiation of weights models LTP while depression of weights represents LTD. Several learning rule have been proposed to relate weight change to neural activity and they are now discussed.

2.2.5 Unsupervised Learning Rules

There are a number of rules that implement plasticity at cellular level but one of the more commonly used is the Bienenstock-Munro-Copper (BCM) model [74] which compares correlated pre and post synaptic firing rates to a threshold in order to decide whether to induce LTP or LTD. The threshold slides as a function of the post synaptic activity to allow the weight to reach a stable state. However, BCM lacks biophysical underpinning unlike the Spike Timing Dependent Plasticity (STDP) rule which closely aligns with the Hebbian principle. STDP strengthens the weights if a presynaptic spike takes part in the firing of a postsynaptic spike otherwise the weights are weakened. More specifically, maximum efficacy occurs when a pre synaptic spike just precedes a postsynaptic whereas maximum weakening occurs when the presynaptic spike occurs just after the postsynaptic spike: The temporal ordering of spikes therefore dictates whether potentiation or depression occurs and so spike timing is important [75]. This is shown in the STDP associated plasticity window in Fig. 2.3, where it can be seen that the time difference between pre and post synaptic spikes sets the level of potentiation/depression [76].

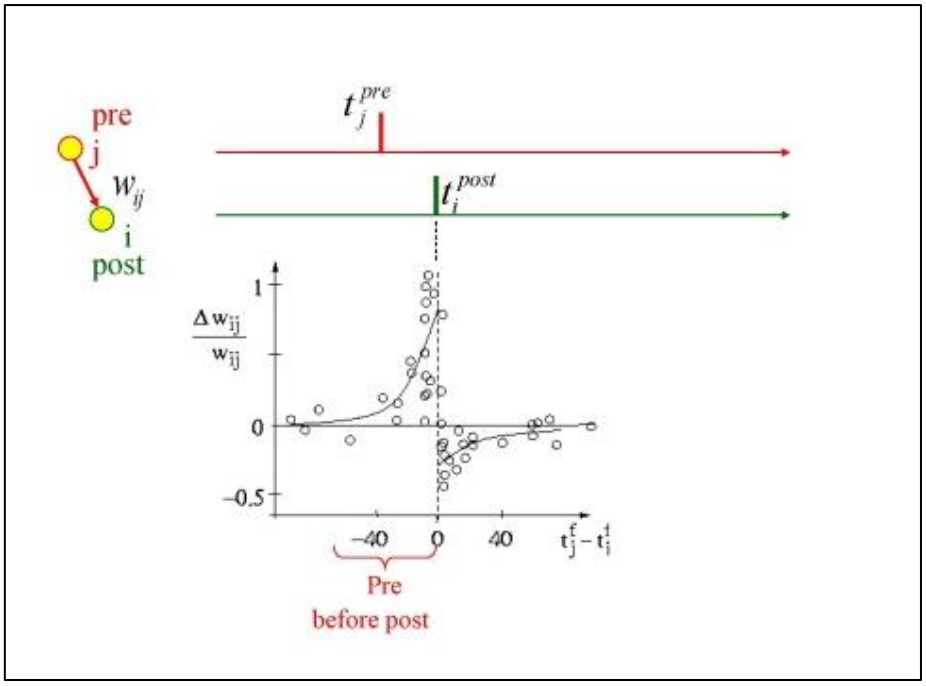

Figure 2.3: STDP learning Rate: The Plasticity Window relates to the time differential between pre-synaptic and post-synaptic spikes to weight updates [76]

2.1.6 Supervised Learning Rules

There exists several supervised learning methodologies and one of the most popular is SpikeProp. SpikeProp [77] [78] is a gradient decent training algorithm for SNNs that is based on backpropagation. The discontinuous nature of spiking neurons causes problems with gradient decent algorithms, but SpikeProp overcomes this issue by only allowing each neuron to fire once and by training the neurons to fire at a desired time. The topology utilises multiple delay lines for each synapse in order for the algorithm to determine the amount of delay so as to minimise the error as training progresses. However, the biological basis for such a training rule is questionable and since each neuron is only allowed to fire once, the algorithm can only be used in time-to-first-spike coding schemes, and therefore this algorithm cannot be used to learn patterns consisting of multiple spikes.

Another training algorithm uses an evolutionary strategy (ES) approach and this has been applied to SNNs [79] [80]. ES differs from genetic algorithms in that they rely solely on the mutation operator. The accuracy of the resulting SNN provides the basis for determining the fitness function and the ES population was shown to produce convergence to an optimal solution. [81]. A limitation of this approach appears to be that only the time-to-first-spike is considered [79]. Supervised Hebbian Learning (SHL) [82] [83] is arguably the most

biologically plausible supervised learning algorithm [84]. SHL simply seeks to ensure that an output neuron fires at the desired time, with the inclusion of a "teaching" signal. Since the teaching signal comprises of intracellular synaptic currents, supervision may be viewed as supervision by other neurons. Unlike other supervised learning algorithms SHL can learn firing patterns involving multiple spikes. However, SHL does suffer from the limitation that even after the goal firing pattern has been reached it will continue to change the weight values and therefore constraints must be added to the learning rule to ensure stability [83]

An algorithm that is closely related to SHL is the remote supervision method (ReSuMe) and this approach appears to avoid the drawbacks of SHL [84]. With this algorithm the teaching signal is not delivered as a current, as in the SHL case but rather is it an STDP-like Hebbian correlation that co-determines the changes in synaptic efficacy. In this algorithm the learning window is similar to STDP and ReSuMe has been shown to effectively learn patterns involving multiple spikes to a high degree of accuracy [84], and the learning process converges quickly and in a stable manner. Both SHL and ReSuMe are able to learn uncorrelated patterns of Poisson spike trains but implementing supervised learning with ReSuMe offers some advantages over SHL. For example SHL takes longer to train and ReSuMe is capable of continually adjusting weights because weight increase are dependent on input and output spikes timing and not on neuron activity.

2.1.7 Spiking Neural Networks (SNNs)

In order to capture how the brain processes information scientists have been implementing networks of neuron which loosely resemble the networks in our brain and these networks have been termed Artificial Neural Networks (ANNs). This section presents a brief review of the three generations of neural networks from their conception by McCulloch and Pitts in 1943.

ANNs are comprised of large arrays of interconnected computational elements (neurons) that attempt to capture the hugely dense and parallel processing ability of the brain [85]. The brain consists of approximately 10^{11} neurons forming approximately 10^{15} synaptic interconnections [86]. Early research into the functionality of brain networks is accredited to McCulloch and Pitts who were the first to propose an ANN that was loosely inspired by the networks in our brain. In this ANN each input is multiplied by a weigh and if the sum of the input weight vector exceeds a threshold then the neuron fires. An excited neuron is represented by a step function and therefore the resulting output is a binary 1, otherwise the output is binary 0 [87]. Following

on from this work, Donald Hebb (1949) suggested that it would be possible to train an ANN to give a certain output when presented with an input by means of learning. This gives rise to the Single Layer Perceptron (SLP) which had modifiable weights and an output threshold function [88] which allowed it to solve pattern recognition problems. More importantly the idea of adjustable weights triggered a new area in ANNs and a multitude of learning algorithms (e.g. Widrow & Hoff, 1960) [89]. However, a book released in 1969 [90] showed that SLP could only solve linearly separable problems and was incapable of solving the simple Exclusive OR (XOR) problem without a hidden layer of neurons. It took until 1986 for this to happen when Rumelhart and McClelland introduced the Multi-Layer Perceptron (MLPs) [91] which used what was called a back propagation learning algorithm. However, this algorithm exhibited a slow learning rate and required that the starting weights be optimised [92]. The algorithm however led to the second generation of neural networks, which used a sigmoidal activation function [93].

The best known unsupervised learning rule was Self Organising Maps (SOMs) proposed by Kohonen [94]. The algorithm updated weights using a form of competitive learning with a winner-take-all regime where all the weights in the winning neurons neighbourhood, for any given input, are updated.

The third generation of neural are known as Spiking Neural Networks (SNNs) where the neuron models are more closely associated with biological neurons in that when they are excited they fire a train of spikes: hence the name SNN. In the realisation of SNNs, much research has focused on developing models of biological neurons. These models have helped utilise the information contained in the temporal aspect of neuronal firing as well as that contained in the spatial distribution which was effectively utilised by the previous generation of neural networks. Numerous SNN models have been developed that can potentially implement a biological plausible artificial neuron and in the subsection below a brief review of spiking neural models is given.

2.1.8 SNN Neuron Models

Model 1: The Hodgkin-Huxley model

In 1952 Alan Hodgkin and Andrew Huxley carried out experiments on a nerve cell from a squid [95] which led to the development of a mathematical model of the AP found in these nerve cells. This model, known as the Hodgkin-Huxley model, was created to be an empirically based model to explain the AP of the squid giant axon as measured on an oscilloscope. They

were able to generate four differential equations that represented the variable conductances of sodium and potassium channels in that axon as well as a leak current I_L and an external current I_m.

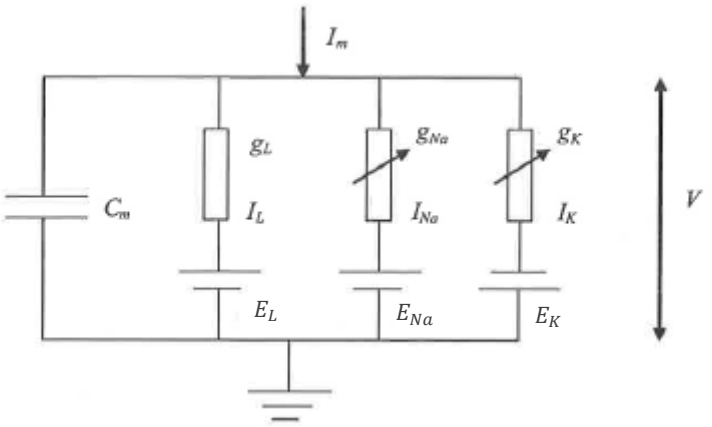

Figure 2.4 Equivalent Electrical Circuit of the Hodgkin and Huxley Model

The four coupled differential equations that define the Hodgkin-Huxley Model are:

$$C\frac{dV}{dt} = -g_K n^4(V - E_K) - g_{Na} m^3 h(V - E_{Na}) - g_L(V - E_L) + I(t) \quad (2.1)$$

$$\tau_n(V)\frac{dn}{dt} = -[n - n_0(V)] \quad (2.2)$$

$$\tau_m(V)\frac{dm}{dt} = -[m - m_0(V)] \quad (2.3)$$

$$\tau_h(V)\frac{dh}{dt} = -[h - h_0(V)] \quad (2.4)$$

The variable n describes the activation of K^+ channels, m the activation of Na^+ channels and h is the inactivation of Na^+ channels. For a fixed voltage V, the variables n, m, h approaches the respective target values (n_0,m_0, h_0) and respective time constants: (τ_n, τ_m,τ_m). The first equation is simply Kirchhoff's law for the conservation of charge for the system, the conductance parameters g_K, and g_{Na} are the conductances of the K^+ and Na^+ ion channels.

Model 2: The Integrate and Fire Model

The integrate-and-fire model is a simple spiking neuron model where the neuron and the cell membrane are represented by a single capacitor and a threshold device. When current is injected the capacitor will charge until a threshold is reached then an AP is produced [96]. This model does not represent a biological action potential but rather a simplified form of the

temporal coding behind one which is consistent with discoveries from neuroscience research [97] [96]. This is represented in the circuit of Figure 2.5.

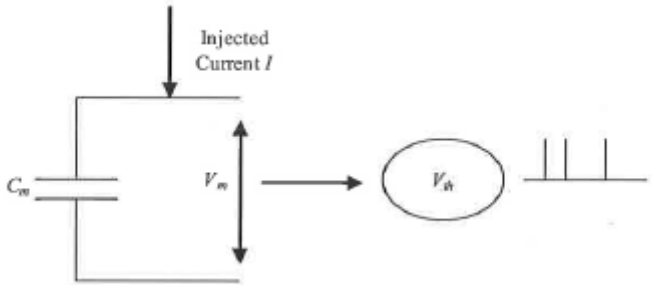

Figure 2.5: Integrate and Fire Neuron Model

The basic version of an integrate-and-fire neuron is called the perfect Integrate and Fire model, where the firing frequency of the neuron is proportional to the injection current. The charging of the cell membrane is determined by the current behaviour according to:

$$I_m(t) = C_m \frac{dV_m}{dt} \tag{2.5}$$

where C_m is the membrane capacitance, V_m is the membrane potential, and $I(t)$ is the stimulus current. By introducing a refractory period (t_{ref}) subsequent to a firing event, the neuron cannot fire again and the membrane potential is clamped to the resting potential for a fixed duration after firing has taken place. This changes the relationship between the current I_m and frequency f from

$$f = \frac{I_m(t)}{C_m V_{th}} \tag{2.6}$$

to

$$f = \frac{I_m(t)}{(C_m V_{th} + t_{ref} I(t))} \tag{2.7}$$

Model 3: The Leaky Integrate and Fire (LIF) Model

The LIF model captures the way that a neuron forgets about an input by allowing charge on capacitor plates to leak away. This is represented by a capacitor resistor circuit that provides a pathway for current to flow allowing the capacitor to return to an uncharged state [98]. This models neuron dynamics such as a time constant, voltage threshold (Eq. 2.11) and refractory period (Eq. 2.12) and is shown in Figure 2.6 [93]

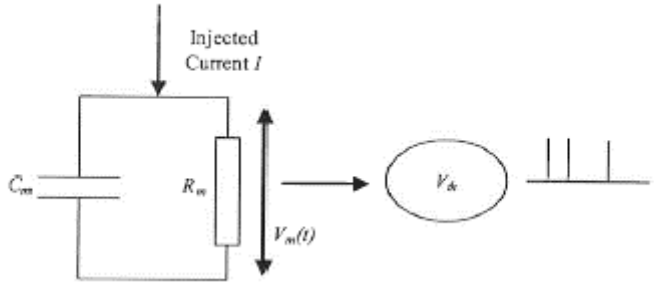

Figure 2.6 Leaky Integrate and Fire Model [93]

The LIF input current $I_m(t)$ stimulus to the cell is given by:

$$I_m(t) = C_m \frac{dV_m}{dt} + \frac{V_m}{R_m} \tag{2.8}$$

where C_m is the membrane capacitance, V_m is the membrane potential and R_m is the membrane resistance. Introducing a time constant ($\tau = R_m C_m$) modifies the equation to:

$$\tau \frac{dV_m}{dt} = -V_m(t) + RI_m(t) \tag{2.9}$$

Under stimulation by a constant current I_o with zero resting potential, the membrane potential of a spike at a time t, relative to a previous spike at the time $\mathrm{t}_{(0)}$ is given by:

$$V_m(t) + R_m I_o \left[1 - \exp\left(-\frac{(t - t_{(0)})}{\tau}\right)\right] \tag{2.10}$$

If $V_m(t)$ exceed a threshold voltage $V_{th}(t)$, then a spike is produced, otherwise no spike is produced (i.e. the neuron does not fire). By assuming that $V_m(t)$ reaches the threshold level at $t_{(1)} - t_{(0)}$, then we can write that:

$$V_{th}(t) + RI_o \left[1 - \exp\left(-\frac{(t_{(1)} - t_{(0)})}{\tau}\right)\right] \tag{2.11}$$

Solving this equation for a time interval $\mathrm{T} = \mathrm{t}_{(1)} - \mathrm{t}_{(0)}$ gives:

$$T = \tau \ln\left(\frac{RI_0}{RI_0 - V_{th}(t)}\right) \tag{2.12}$$

Model 4: Spike Response Model (SRM)

The Spike Response Model (SRM) is a variation of the LIF Model which depends on the time but $V_m(t)$ depends on the time of the last spike, where $V_m(t)$ term is calculated using time integration of all previous spikes [98], [77], [99]. In the case of an input generated by synaptic current pulses caused by presynaptic spikes, the SRM can be written as

$$V_m(t) = \sum_{t_i^{(f)} \in F_i}^{n} \eta_i \left(t - t_i^{(f)}\right) + \sum_{j \in \Gamma_j} \sum_{t_i^{(f)} \in F_i} \omega_{ij} \epsilon_{ij} \left(t - t_j^{(f)}\right) \quad (2.13)$$

where η_i models the AP generation, $t_i^{(f)}$ the final neuron firing time of neuron i, $t_i^{(f)}$ is the presynaptic input spike from neuron j, ω_{ij} is the synaptic strength between neurons i and j, ϵ_{ij} is the PSP of neuron i caused by a spike from neuron j, f is the set of all neuron firing times for i or j depending on subscript and Γ_j represents the set of all presynaptic j neurons to neuron i.

Model 5: The Izhikevich Model

The Izhikevich Model is a two dimensional model that can exhibit the firing pattens of all known cortical neurons and is defined by two differential equations [100]. The model is not based upon biophysical parameters but is a simple model that faithfully reproduces known firing patterns associated with neurons. The model is a two-dimensional systems having a fast voltage variable v and a slower "recovery" variable $u(t)$, which describe activation of the K^+ current or inactivation of the Na^+ current or their combination [101].

$$\frac{dv}{dt} = 0.04v^2(t) + 5v(t) + 140 - u(t) + I(t) \quad (2.14)$$

$$\frac{du}{dt} = a(bv(t) - u(t)) \quad (2.15)$$

Resetting of the membrane potential after a spike occurs is carried out with the following function.

$$If\ v \geq V_{th}, then \begin{cases} v \leftarrow c \\ u \leftarrow u + d \end{cases} \quad (2.16)$$

In this model, v is the membrane voltage, V_{th} is the firing threshold, u is a recovery variable, and a, b, c and d are parameters that can be adjusted to simulate different spiking activities.

While the model does faithfully reproduces all the known firing patterns, one difficult in using this model is determining the numerical values of the parameters to be used in simulations of the time evolution of the membrane potential for different stimuli [101].

Model 6: The FitzHugh-Nagumo Model

The FitzHugh-Nagumo model is based on the hypothesis that sodium activation channels and the membrane potential evolve on the same time scale. This allows channels on similar time scales to be grouped together [102], [103], [104]. It acts as a two-dimensional simplification of the Hodgkin-Huxley model. The model is described by:

$$\frac{dV}{dt} = V - \frac{V^3}{3} - W + I \tag{2.17}$$

$$\frac{dW}{dt} = \phi(V + a - bW) \tag{2.18}$$

where V is the fast activation channels, W is the slower activation channels and a, b and ϕ are positive variables [104]. The model allows a geometrical explanation of important biological phenomena related to neuronal excitability and spike-generating mechanism. These non-linear dynamical equations can be depicted in a phase portrait (Figure 2.7) with a V (polynomial line) and W nullcline (straight line); these lines intercept is an equilibrium point [105].

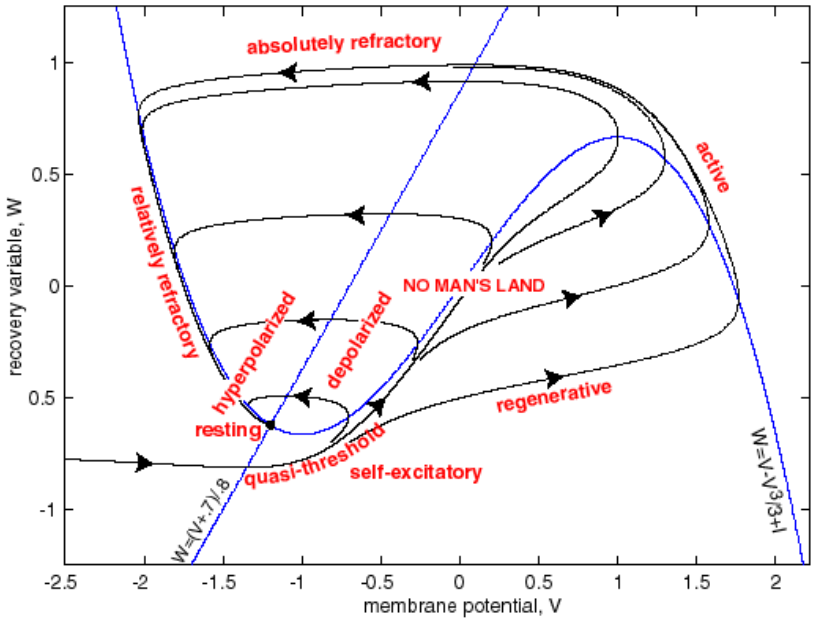

Figure 2.7: Phase portrait and physiological state diagram of FitzHugh-Nagumo model (modified from FitzHugh 1961) [105]

2.3 Neuroglial cells.

2.2.1 Neuroglial cell structure

There are five types of neuroglial cells, Astrocytes, Microglial cells, Oligodendrocytes Ependymal cells and Schwann cells. The main focus of this project will be on astrocytes and neurons but other glial cells have functions that contribute to the nervous system [62] [63] [64]. The main neuroglial cells of the nervous system are shown in Figure 2.8.

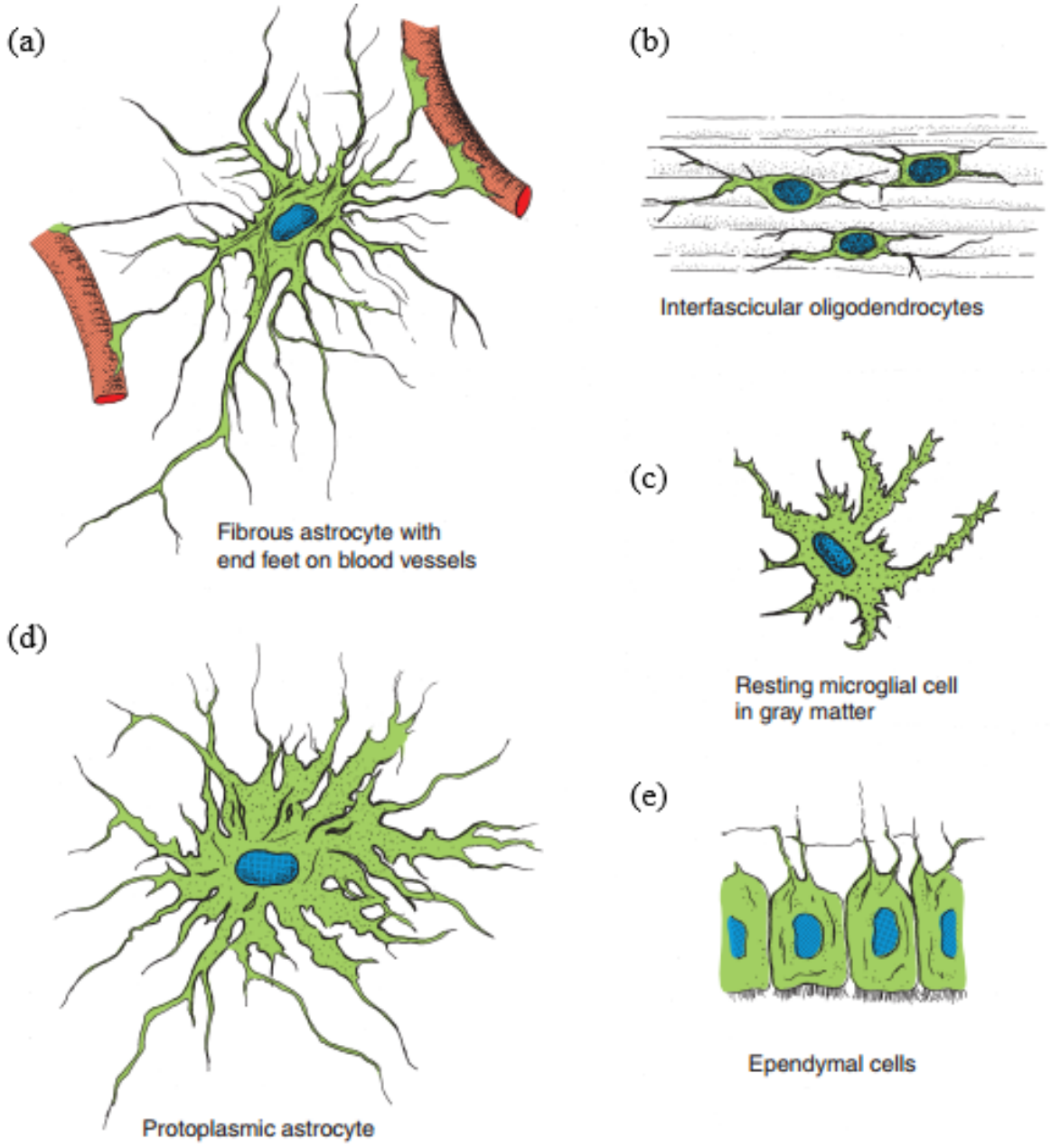

Figure 2.8: Neuroglial cells of the central nervous system {from [62]} a) Fibrous astrocyte with end feet on blood vessels b) Interfascicular oligodendrocytes, c) resting microglial cell in grey matter d) Protoplasmic astrocyte e) Ependymal cells

Microglial cells are cells that populate both grey and white matter in the nervous system. Their main properties are defensive and immunological. They do this by behaving like phagocytes when the central nervous system is diseased while also attacking viruses, micro-organisms and cancer cells [62].

Ependymal cells are cells of epithelium which cover the ventricles of the brain and the central canal of the spinal cord. These cells are divided into three main types. Ependymocytes which line the ventricular system in contact with the cerebral spinal fluid (CSF) which transmit molecules between this fluid and nervous tissue [62]. Tanycytes cells are ependymal cells with long basal processes that respond to endocrine changes in the CSF. Choroidal epithelial cells which cover the surface of the choroid plexus by opposing passive movements of substances from the blood to the CSF secreted by the cerebral ventricles [62].

Oligodendrocytes are cells with small nucleuses and long processes that have multiple microtubules and are involved in the connectivity between neurons mostly by myelination of the neurons in the CNS, especially in the white matter of the brain. They also have molecules associated with them that inhibit axonal growth [63]. Oligodendrocytes have two main types: Interfascicular oligodendrocytes are connected to myelinated axons in rows between the nerve fibres of the white matter of the CNS. Perineuronal (or Satellite) oligodendrocytes occur in close proximity to the somata of neurons around the cell bodies of some large neurons [62] [106]. There is also a third type of oligodendrocyte that doesn't myelinate but have cytoplasmic processes associated with long neurons [11].

Schwann cells are found only in the peripheral nervous system and their function is to insulate axons with myelin by wrapping around it in a spiral form. They form the myelin sheath of myelinated nerve fibres and provide support for non-myelinated nerve fibers [63]. Schwann cells also aid in cleaning up debris and guide the regrowth of axon by arranging themselves in a series of cylinders that serves as a guide for sprouts of regenerating axons [107].

Satellite cells are also glial cells that are found in sensory and autonomic ganglia called ganglionic gliocytes in the enteric nervous system similar to the ganglionic gliocytes and astrocytes. They provide structure and metabolic support for sensory, sympathetic, and parasympathetic nerves. It is also theorised that Satellite glial cells have a significant role in

controlling the microenvironment of the sympathetic ganglia due to the fact that they almost completely envelop neurons which can help regulate molecular diffusion across cell membranes [108] as well as having electrical properties which are very similar to those of astrocytes [109].

Astrocytes - are the most abundant type of glial cell in the brain, are important contributors in metabolic maintenance and are also very much involved in neuronal activity and information processing in the nervous systems [110] [111]. However, there is a severe lack of understanding regarding the biophysical mechanisms that underpin how they bi-directionally interact with neurons. Since the focus of this thesis is on the coupling between astrocytes and neurons, the remainder of this review will focus on astrocytes.

2.3.2 Astrocytes in the functional and dysfunctional brain

Current research has shown that astrocytes have a large number of receptors that are used to relay information about synaptic activity. For example, astrocytes have been found to possess binding sites for endocannabinoids or 2-arachidonyl glycerol (2-AG) which is a type of retrograde messenger released post-synaptically during neuronal depolarization [112]. Similar to neurotransmitter uptake, this leads to the Ca^{2+} oscillation within the astrocyte and the release of glutamate. This signalling pathway acts to modulate the transmission probability of the synapse and is a potential candidate for self-repair of damaged or low probability synapses [113]. This implies that astrocytes form connections with neurons thereby influencing their behaviour. In fact recent research now shows that approximately 50% of synapses are in intimate contact with astrocytes and consequently synapses exchange signals at three terminals, hence the name tripartite synapse [114] [115].

Although astrocytes cannot elicit propagating action potentials (PAPs) like neurons do, their "unit of excitation" is a transient increase in intracellular Ca^{2+} that is elicited by various neurotransmitters (e.g. glutamate, ATP, GABA, etc.) following binding to their respective receptors on the astrocytic membrane [115]. These astrocytic Ca^{2+} transients in turn lead to astrocytic release of transmitters (often referred to as "gliotransmitters") and to propagating Ca^{2+} waves [116]. Although the propagation of intracellular Ca^{2+} is not fully understood, the process is believed to be facilitated by propagating signaling proteins between micro-domain clusters of inositol 1, 4, 5-trisphosphate Receptors (IP_3Rs) [117] [118] [119] [120]. Astrocytes also communicate in a feedback mode with neurons at synaptic sites [121]. This bidirectional

communication between astrocytes and neurons results in various forms of synaptic modulation.

Astrocyte Pathology

Astrocytes provide a number of complex brain functions, where it is understood that changes to their physiology is involved in the development of many if not all neurological conditions. Impairments to any of these conditions such as neurotransmitter and ion regulation can trigger or exacerbate these conditions. It is also the case that astrocytes are included in numerous neuroprotective mechanisms against conditions such as Alzheimer's disease, Parkinson's disease or ischema. This is because they support neurons by providing a biological environment for repair and regeneration.

Nervous System Injury.

When the nervous system is damaged specific reactions of glia cells occur in what is known as reactive gliosis. This includes astroglial reactions (reactive astrogliosis), microglia activation, Wallerian degeneration and demyelination in oligodendrocytes and Schwann Cells [11]. Astrogliosis and microglia activation are common events to most CNS conditions. Astrogliosis response to CNS damage and disease is complex and multifaceted and can range from subtle and reversible alterations in gene expression and morphology to long-lasting changes associated with scar formation [122]. This process is controlled by specific signalling mechanisms that are dependent on the context of the trigger. Functions of astrogliosis and scar formation protect neural cells from degradation and dysfunction and restrict inflammation and infection, however it may also contribute or be the primary cause of CNS disorders through abnormal effects and loss of local functions. To treat astrogliosis disorders requires direct targeting of treatments to augment or attenuate specific aspects of astrogliosis.

Neurodegenerative Disorders

Alzheimer's disease - is a progressive, degenerative disorder that attacks the brain's nerve cells, or neurons and is the most common cause of dementia. The stages of the development of this condition is given in Figure 2.9 [11].

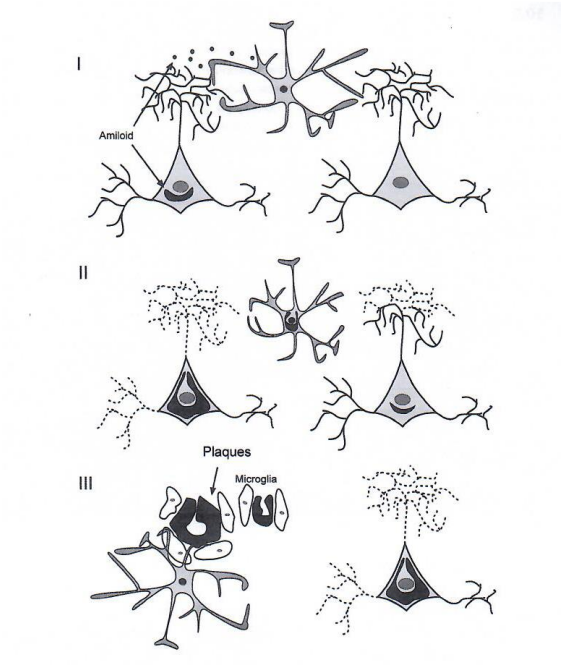

Figure 2.9: Diagram showing the stages Alzheimer's disease destroy astrocytes [11].

In the first stage of this condition astrocytes detect β–amyloid released by neurons, and respond by withdrawing processes from affected neurons whether they are affected or intact. In stage two neurites lacking astroglial support degenerate and astrocytes accumulate this amyloid. Thereafter in stage three, neurons and astrocytes die, triggering reactive astrogliosis in which microglial cells form a plaque from the amyloid debris.

Parkinson's disease - The reaction of glia cells are secondary in this condition, but the gliosis triggered by the neurodegeneration involved may contribute to progression of this disease. Parkinson's disease leads to activation of microglia and reactive astrogliosis where neurons in the substantia nigra are attacked by the microglia activity. It is also the case that dopaminergic neuron death increases in areas that are thinly populated by astrocyte cells [11].

Amyotrophic lateral sclerosis (ALS or Lou Gehrig's disease) - This condition is categorised by degeneration of neurons in the cortex, brainstem and spinal cord leading to progressive paralysis and muscle atrophy. One of the main causes of the neuron death found in ALS is deficient glutamate clearance. This deficient glutamate clearance is linked to the disappearance of astroglial transporter EAAT2 in affected brain regions. Astrocytes may participate in the

progression of neuron damage in biological environments which trigger astrocytes to become a glutamate source [11].

Stroke and Ischaemia

An ischemia is an insufficient supply of blood to an organ, usually due to a blocked artery, while a stroke is the sudden death of brain cells in a localized area due to inadequate blood flow. Astrocytes protect the brain from strokes and ischaemia in four ways: 1) they are a glutamate sink for the CNS, 2) they contain antioxidants that remove reactive oxide species, they support energy production in mild hypoxic conditions, 3) they buffer excess potassium stopping depolarized glutamate release and 4) scars produced by reactive astrogliosis fills a necrotic area. However, astrocytes may exacerbate damage where in severe conditions astrocytes may turn from the main glutamate sink, to a main glutamate source which can damage surrounding neurons. They can also increase the spread of infarction by causing loss of neuronal signal strength by glutamate signals triggered from astrocytes themselves or from calcium waves (See Figure 2.10.). Infarctions can also expand due to spreading depression which causes high extracellular K^+ concentrations inducing astrocytic collapse and a depolarising effect which causes astrocyte cells to swell and release more glutamate resulting in astrocyte death from functioning beyond its capabilities [11].

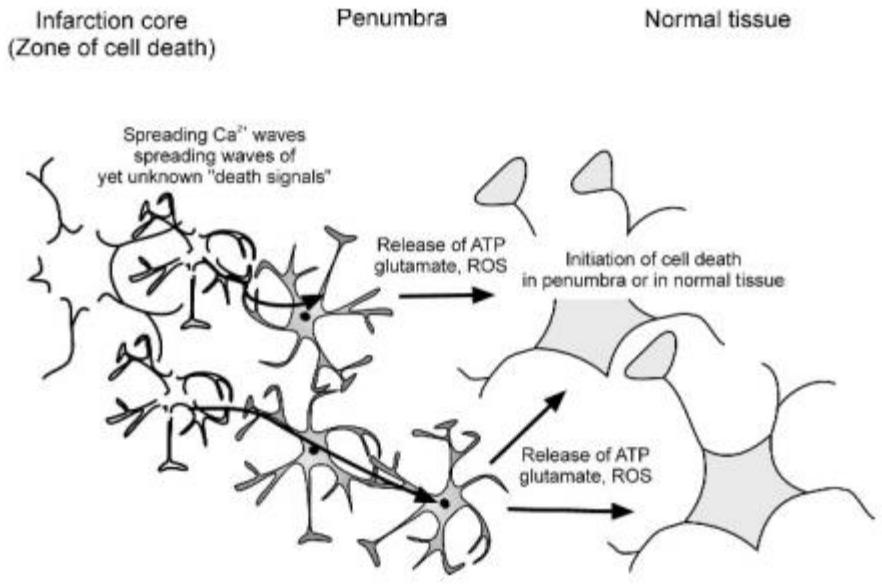

Figure 2.10 Astrocytes exacerbating infarction by propagating "death signals" or Ca^{2+} waves [11].

Viral and Bacterial infection

The only protection that the CNS has against infection within neurons and glia cells is the activation of microglia. Failures in microglia activation performance during an infection leads to irreparable CNS damage [122]. In cases of infections like meningitis the microglial responses can be mild, but types of pneumonia may trigger an over-activation of microglial cells which can increase brain damage [11]. Microglial cells like astrocytes can also be a target for different types of viruses leading to viral encephalitis for example in the case of herpes virus 6 or the human T lympotrophic virus. Dysfunction in these astrocytes will damage homeostasis mechanisms and cause endotoxicitiy [11]. Disruptions of perivascular astrocyte functionality may lead to the spread of inflammatory cells like lymphocytes to the CNS [122]. Even though the HIV-1 virus does not replicate much within astrocytes and the majority of viral replication occurs in microglial cells, reactive astrogliosis plays a role in potential neurological complications and the development of HIV associated dementia (HAD). Also astrocyte infections can contribute to increase neurotoxicity as well the loss of supportive and protective features such as the loss of glutamate homeostasis that contribute to this condition [122].

Neuropathic pain

Neuropathic pain occurs either as a result of either neurotropic infections or peripheral nerve injury. The roles of glial cells as primary mediators of pain. The precise role played by astrocytes in chronic pain is mostly undiscovered, however during chronic pain reactive astrogliosis occurs within the spinal cord and known pain receptors are expressed such as vanilloid receptor type 1 and cannabinoid receptor type 1 [11].

Psychiatric Processes

Glial malfunction has become a new area to investigate when it comes to the discoordination of synaptic transmission associated with the development of psychiatric disorders. However, knowledge of the underlying mechanisms involved remain speculative. Schizophrenia, bipolar disorder and major depressive disorders cause glial malfunction as well as neuronal malfunction. In all three conditions the number of astrocytes and their volume are reduced. GFAP (glial fibrillary acidic protein) expression is lost as well in these conditions. In bipolar disorder and major depressive disorder the reductions in astrocyte density occur in the prefrontal cortex. In schizophrenia there is increased demyelination in cortical areas as well as a loss of oligodendrocytes. Astrocytes also become involved in the early stages of the

pathogenesis of epilepsy, as reactive astrogliosis is observed to occur before neurological degenerative and fully developed seizures. It is believed that astroglial calcium waves, and the resultant glutamate release, triggers the paroxysmal depolarization shift associated with an epileptic seizure [11].

2.3.2 Astrocyte Processes

Astrocyte processes are often thin leaf-like structures capable of penetrating gaps between nerve branches and synapses [123] [46]. Some processes can be as thin as 20 to 50 nm (in the brain neuropil) which a separation distance of than 0.5μm [124]; [125]; [126]; [127]. This ensures they have a relatively high surface to volume ratio, which makes them ideal for sustained and localised sodium accumulation as this structure causes slow diffusion exchange but higher uptake of local Ca^{2+} entry via the sodium calcium-exchanger. The small breadth of individual astrocytic processes suggests a potential for having a role in chemical compartmentalization of local molecular activities concerning release and diffusion of signalling molecules such as Ca^{2+} ions [123].

Astrocytes also have the capacity to form functional perisynaptic processes on neurons in the hippocampus of adult mammals to strengthen synaptic transmission in these cells during neurogenesis [128] [126]. Perisynaptic processes have been identified as the third active element in chemical synapsis due to a unique molecular composition, structural plasticity and the capacity to form sheaths to interfere with neuronal information processing. However, understanding the mechanisms used by PAPs for responding to neurotransmission requires improved experimental measures, such as combinations of optical and electrophysiological methodologies in synergy [129]. PAPs contain a high density of transporters while devoid of calcium stores and have a high surface-to-volume ratio favourable for uptake of minerals. Other astrocyte processes further away from the synapse do have stores however, which can respond to Glu signalling. Therefore, communication is carried on outside the synapse rather than involving Ca^{2+} ions stores within the tripartite synapse [130]. PAPs also play a key role in the plasticity of perisynaptic astroglia during synaptogenesis as interactions between glial processes and pre- and postsynaptic partners suggest that glia can participate in some forms of structural synapse remodelling through reorganization of the postsynaptic density (PSD) around these synapses [127].

2.3 Transporters in astrocytes and neurons membranes

In the intracellular space astrocyte baseline sodium, chloride and calcium ion levels are low and baseline potassium ion levels are high, but in the extracellular space the baseline sodium and chloride levels are high with the baseline potassium levels low [131], [132]. During activity the concentration levels can increase and the resulting electrochemical gradient trigger transport mechanisms. The mechanism which allows transport of ions and small molecules across a membrane is called active transport. This occurs through a coupling effect in a transporter protein known as secondary active transport. This coupling effect stores energy in the form of an electrochemical or concentration gradient, where a driving ion/molecule moves down the gradient and a driven ion/molecule is moved against this electrochemical or concentration gradient. Two types of secondary active transport mechanism exists, co-transporters which is the driving ions and driven ions act in the same direction and ion-exchange mechanism when these ions are driven in opposite directions. The effectiveness that these transporters act against a gradient is determined by their stoichiometry. These transporters [41] and exchangers have many isoforms and features such as tissue location, coupling stoichiometry, substrate specificity that may vary in isoforms. Sodium is the main driver in the plasma membrane of cells in a multiple of processes and by simulating this mechanism we could understand how it drives other processes like potassium buffering. Figure 2.11 shows that there are a number of transporters that are involved in sodium driven mechanisms and some of them will form the focus of the project.

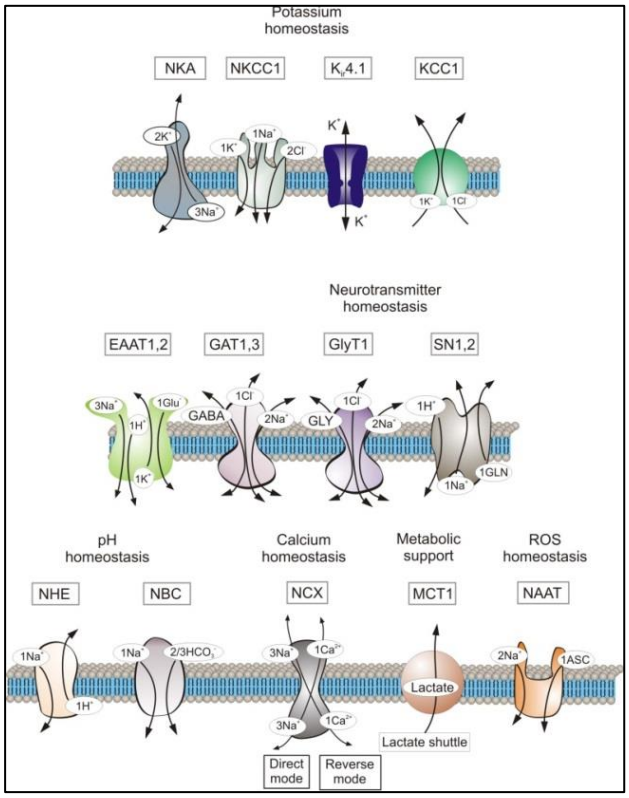

Figure 2.11 Astroglial homeostatic molecular cascades [25]

The function of the **Sodium Calcium Exchanger (NCX)** is to ensure that cytosolic Ca^{2+} can be extruded from a cell and Na^{+} entry into a cell against the direction of the electrochemical gradient can occur without additional energy (e.g. ATP) consumption [133]. The NCX is also reversible so that the electrochemical gradient and voltage can favour Na^{+} extrusion and Ca^{2+} entry during electrochemical changes that occur in cellular activity. NCX is considered to have a low affinity but a high capacity for Ca^{2+}. Na^{+} and Ca^{2+} are exchanged at a ratio of 3 Na^{+} ions for one Ca^{2+} ion.

The **Plasma membrane Ca^{2+}-ATPase (PMCA)** is an electrogenic pump on the membrane of animal cells that maintains a low concentration of Ca^{2+} ensuring proper cell signalling [133]. Unlike the NCX, the PMCA is not reversible and it does require the consumption of additional energy through ATP. PMCA finely regulates the concentration of cytosolic free Ca^{2+} around its basal value (100 nM) while NCX eliminates significant rises in intracellular Ca^{2+}. The NCX works in tandem with the PMCA to ensure the homeostasis of [Ca^{2+}] levels inside the cytosol of cells.

The **Sodium Potassium Exchanger (NKX) or Na^{+}/ K^{+}-ATPase (NKA)** enzyme keeps the internal [K^{+}] levels higher than external [Na^{+}] levels. It is activated by external [K^{+}] and

internal [Na^+] levels and the metabolic energy to transport Na^+ and K^+ inward comes from adenosine-triphosphatase (ATPase). A key role of this enzyme is to maintain the resting potential by changing the difference in concentrations of Na^+ and K^+ in response to an environmental change like an action potential [134].

Na-K-Cl co-transporters (NKCC1) [53] have been associated with electrically neutral ion transport, often operating u with a 1 Na: 1K: 2Cl stoichiometry. Their role in K^+ homeostasis has been revealed by optical methods where $[K^+]_0$ induces astrocytic swelling that is reversibly depressed by inhibiting $[K^+]_0$ with furosemide and bumetanide. NKCC1 was identified as the isoform expressed in astrocytes in optical nerves.

The K-Cl co-transporter (KCC1) mediates the coupled movement of K^+ and Cl^- ions across the plasma membrane of many animal cells. The transport process involves one for one movement of K^+ together with Cl^- and the net movement is outward [135].

There are four types of K^+ **voltage channels** present in neuroglia cells; inward rectifier K^+ channels (K_{ir}), delayed rectifier channels (K_D), rapidly inactivating A-type channels (K_A) and calcium activated K^+ channels (K_{Ca}). There are also voltage gated Na^+ channels (Nav), voltage gated Ca^{2+} channels and Cl^- and other anion channels. Inward Rectifying Potassium Channels (K_{ir}) [11] are the most prominent K^+ channel and are inwardly rectifying which mean that they pass current (positive charge) more easily in the inward direction (into the cell) than in the outward direction (out of the cell). K_{ir} channels underlie K^+ spatial buffering and there is interest in determining their macromolecular structure, mechanisms of targeting and modulation by both intracellular and extracellular factors.

There are 7 types of K_{ir} channel, 2 isomorphs are important and they are K_{ir} 4.1, which is largely at the end-feet and K_{ir} 2.1 which is expressed in the plasma membrane (Molecular machinery for astroglial K^+ and glutamate clearance) (see Figure 2.11). K_{ir} 2.2, K_{ir} 2.3, K_{ir} 3.1, K_{ir} 6.1 and K_{ir} 6.2 channels may also be expressed in glial cells. K_{ir} 4.1 channels have been demonstrated in both cultured and in situ astrocytes, and they are enriched in astrocyte processes enveloping synapses and blood vessels [136]. K_{ir} 2.1 channels show steep inwardly rectifying current voltage relationships, with minimal outward currents positive to E_K [137] while K_{ir} 4.1 are weakly rectifying with substantial outward currents [138], [53]**.**

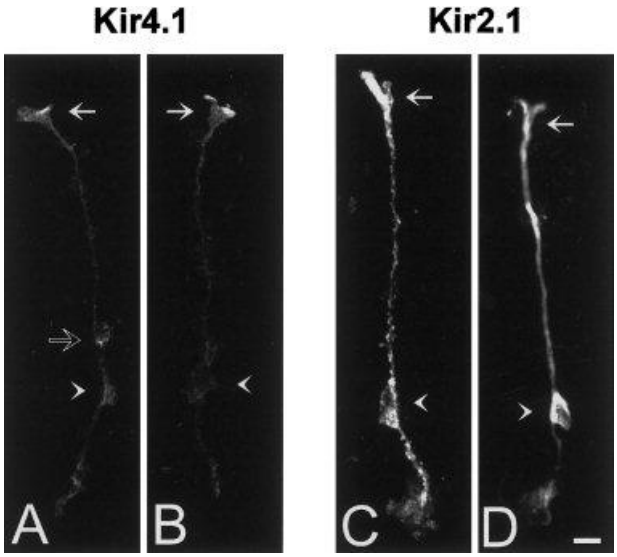

Figure 2.12 Acutely dissociated Müller cells display K_{ir}4.1 and K_{ir}2.1 immunoreactivity. Filled arrows indicate the endfeet; arrowheads indicate the somata of the cells. Unfilled arrow indicates strong K_{ir}4.1 immunoreactivity at a side branch, which perhaps contacted a blood vessel in situ. Scale bar = 10 µm [139].

Other K^+ channels *(*K_D, K_A, K_{Ca}*)* exist in neurons and glial cells to assist in the maintenance of the resting membrane potential, glial proliferation and reactivity. However, these channels are all closed at the resting membrane potential and are only active when the cell membrane is depolarised to values more positive than -40mV. The full functional roles of these channels are unclear.

The role of voltage gated Na^+ channels is not clear but it is believed they are involved in controlling glial proliferation, differentiation or migration [11]. Na^+ channels in astrocytes occur at a much lower density in comparison to neurons (10 μm^2 vs. 10,000 μm^2). Voltage gated calcium channels (Ca_v) are found in immature astrocytes and oligodendrocytes relevant for the growth and development of neuroglial precursors. However, the expression of voltage gated Ca^{2+} channels in mature glial cells is uncertain because of the inability to patch clamp.

Several types of Cl^- and other anion channels have been found in astrocytes; not only are they involved in Cl^- transport they also regulate the size of the cell and may be involved in astrocytic swelling. The activity of the Na^+/ K^+/Cl^- transporter can ensure that an astrocyte can accumulate high levels of Cl^- ions and these channels drive Cl^- ion efflux as the equilibrium potential for Cl^- ions is around -40mV. Finally there are Aquaporins which are responsible for the transport of water and water homeostasis. In astrocytes they are co-localised with K_{ir}4.1 channels, concentrated in astrocytic perivascular endfeet. AQP4 and to a lesser extent AQP9 are the aquaporin types most common to astrocytes.

2.4. Potassium Buffering

Astrocytes are also responsible for extracellular homeostasis of K^+ ions and extracellular pH, they synthesize neurotransmitters and neurotransmitter precursors and are generally involved in homeostasis of many neurotransmitters and neuromodulators [140]. These cells cannot generate action potentials due to the low densities of voltage-gated ion channels and high expression of K^+ channels that prevent substantial depolarization of their membranes. Instead astrocytes use intracellular signaling routes where local gradients of ions interact with intracellular targets and trigger physiological reactions. In addition astrocytes are physically connected into syncytia by means of intracellular contacts usually referred to as gap junctions [141].

K^+ transport [53] is a central mechanism involved in neuronal and neuro-astrocytic communication. Astrocytes encircle synapses and effect the distal (synapse end) processes of neurons. Potassium is expressed in astrocyte-neuron connections through two K^+ pumps (Na-K & NKCC) and inward rectifying potassium channels. The two K^+ pumps act to uptake potassium while K_{ir} channels are active in uptake and release. There are also BK (Big Potassium) channels that are Ca^{2+} sensitive and act at the end-feet near blood vessels alongside K_{ir} channels. The connections between neurons, astrocytes and blood vessels is called a neurovascular unit. K^+ ions can flow in multiple directions within astrocytes and in their extracellular regions, however the effects of this mechanism could be seen by K^+ undershoot or by excessive astrocytic uptake, which is balanced by K^+ removal by K_{ir} channels. In cerebral astrocytes these transporters are involved in spatial potassium buffering, which involves the movement of K^+ from the extracellular space to regions of low concentration by active uptake and release. Several physiological phenomena have been linked to K^+ buffering such as functional hyperemia. It is believed that there are two-way processes assumed to play a role in K^+ buffering. In a neurovascular unit forward activity occurs when astrocytes are stimulated by synaptic activity and reverse activity stimulated by blood vessels.

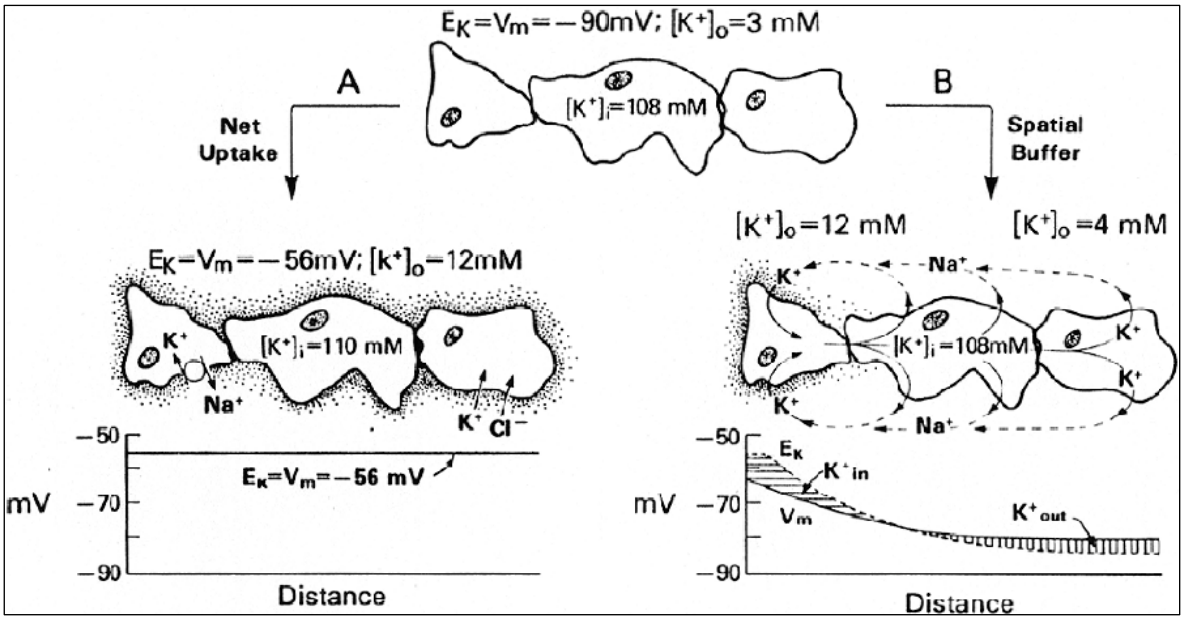

Figure 2.13: Diagram depicting role of glial cells in $[K^+]_0$ homeostasis. Top: Glial cells are electrically coupled via gap junctions forming a functional syncytium. (A) Net K^+ uptake mechanism. (B) K^+ spatial buffering mechanism [11].

There are two main processes involved in K^+ buffering, they are spatial buffering and net uptake (see Figure 2.13). In K^+ spatial buffering, the mechanism requires glial cells to transfer K^+ ions from regions of elevated $[K^+]_0$ to regions of lower $[K^+]_0$, through a membrane that is highly permeable to K^+. This K^+ current is driven by the difference between the membrane potential of the glial syncytium membrane and the local K^+ equilibrium potential. This causes K^+ to flow into the glial cells but K^+ entry causes at local depolarization that propagates through the glial cell and drives K^+ out of the glial cells. This results in very little net change in the K^+ levels inside the glial cell. Net K^+ uptaked is mediate mainly by the Na^+ K^+-ATPase pumps (Na^+ pump) and Na-K-Cl co-transporters. The Na^+ pump expels three Na^+ ions and moves two K^+ ions into the cell in order to maintain high intracellular K^+ and low intracellular Na^+. Local $[K^+]_0$ increases to ensure that K^+ ions are transported into the cell in exchange for the Na^+ ions, as long as the concentrations of extracellular K^+ is not saturated or Na^+ limiting [142]**.**

Spatial buffering requires two conditions in order to be efficient: 1) the glial cells should form a syncytium in which K^+ currents can travel relatively long distances and 2) these cells should be selectively and highly permeable to K^+. Evidence demonstrates that astrocytes form a functional syncytium allowing for intercellular diffusion of ions and signalling mechanisms [143], [144] and are highly permeable to K^+ ions. Inward rectifying potassium (K_{ir}) channels are the principle K^+ channels in glial cells in many CNS regions and steer K^+ ions inward only. Other types of K^+ channels including Ca^{2+} and voltage dependent channels don't express at

hyperpolarized glial resting conditions. Also required in the K^+ spatial buffering mechanism is the low permeability of glial cells to anions such as Cl^- in order to prevent the net uptake of KCl from occurring upon rises of $[K^+]_o$ which could lead to dangerous cell swelling [11]. There is no consensus concerning values for Cl^- permeability of glial cells in the native tissue [11].

2.4.1 Cell Swelling

Three models of interest [145] [146] and [131] have looked at cell swelling or volume changes that occur as a result of potassium buffering and other ion transportation. In a study of mechanisms of astrocytic K^+ clearance [145], high K^+ conductance was found to produce K^+ spatial buffering, while cells that lack K_{ir} channels or aquaporin channels have reduced K^+ clearance, and therefore swelling. In their model inwardly rectifying K^+ channels (K_{ir} 4.1) are distributed along the processes of the astrocyte and are co-localised with the aquaporin (AQP4) channels in microdomains. The lack of knowledge over which precise mechanisms are active in both K^+ clearance and buffering under high $[K^+]_{out}$ drove their research towards simulating these effects in a three compartmental model that is reviewed in the next chapter. In a previous paper [131], the researchers also highlight that there is a lack of consensus on an explanation of why the shrinkage in the extracellular space around astrocytes occurs 10-20 seconds after neuronal activity. The shrinkage has been linked to the clearance of potassium ions dispatched by the neuron during action potentials and postsynaptic potentials alongside water transport. They have created simulations trying to understand the complicated interactions of ion transporters, water transport by aquaporin channels and the operation of the Na^+- K^+-ATPase. The direction of water transport that is triggered by the setting up of an osmolarity gradient between the extracellular space and the astrocyte is of particular interest where water transport is through aquaporins and inorganic osmolyte transporters. These later transporters often allow solutes to move against an electrochemical gradient, and include the NKCCl, NBC (sodium bicarbonate cotransporter) and KCC1.

Experiments [146] have looked at the physical relationship between aquaporin dependent K^+ ions and water transport from the extracellular space to astrocytes following neuroexcitation. They explored physiological research that found that reduced aquaporin expression in mice showed a slower accumulation and clearance of K^+ from the ECS during neuroexcitation [147] [148] [149], and in epileptic humans [150] this has also been taken as evidence as aquaporins involvement in neuroexcitation. The possibility of a functional interaction between aquaporins and K_{ir} channels proposed by [151] was ruled out by patch clamp analysis of isolated human brain astrocytes [152], retinal Muller cells [153] and brain slices [149]: all of which suggest no

effect on K_{ir} channel function due to aquaporins. They explored the possibility that coupling of K^+ and water transport or diffusion limited transport could explain the link between aquaporin permittivity and K^+ uptake through simulation.

2.5 Fixed charges in astrocytes and neurons membranes

Biological membranes consist of a continuous bilayer of lipid molecules with some embedded membrane proteins as well. These bilayers are fluid with polar and non-polar portions in their structure (amphipathic) [50]. The lipid bilayers are asymmetric in all eukaryotic membranes ensuring opposite sides of the membrane have different biophysical properties to influence many key cellular processes including cell fusion and cell clearance [154]. Membrane lipid molecules come in three major classes: phospholipids, cholesterol, and glycolipids. There are four main types of phospholipids in mammalian cells - phosphatidylcholine, phosphatidylethanolamine, phosphatidylserine, and sphingomyelin. Of these four phospholipids only phosphatidylserine carries a net negative charge. Phospholipids also have a property that when placed in water they assemble spontaneously into bilayers, which form sealed compartments that reseal if torn. The assembly of these lipids is demonstrated in Figure 2.14 [50].

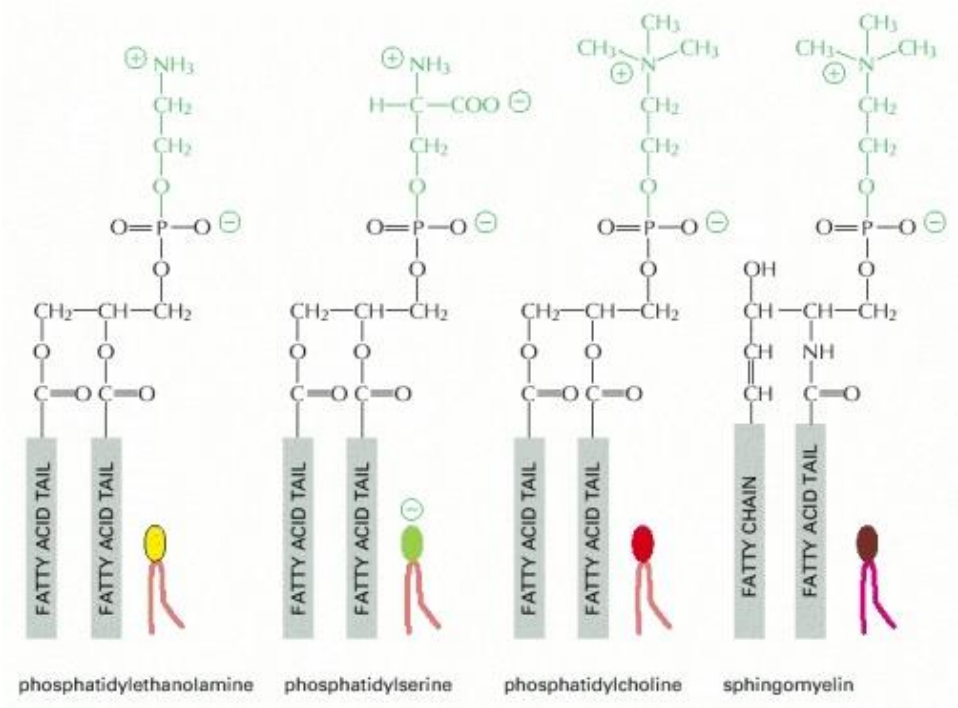

Figure 2.14: Four major phospholipids in mammalian plasma membranes. Note that different head groups are represented by different colours [50].

Investigations using Annexin V (a compound that binds to phosphatidylserine) have discovered that phosphatidylserine (PS) is found in the cytoplasmic face of the cellular plasmatic membrane and endoplasmic reticulum. Phosphatidylserine participates in cell signalling through the interaction with various signalling molecules [155]. A method for determining local surface charge density of a membrane can be found using quantitative surface conductivity microscopy (QSCM) involving a scanning nanopipette setup (scanning ion-conductance microscope) combined with an algorithm that takes account of the ionic current at the nanopipette tip [52]. Research on the excitable axon membrane of neurons show that the ions located on the membrane are tightly bound. This is because both sides of its bilayer phospholipid membrane surface are negatively charged, and the ions in contract with the membrane surface are in deep potential wells near the dipole heads of the membrane, which stops ions slipping along the membrane easily [6]. These surface charges also play a role in membrane-protein interactions [52]. The use of cationic amphiphilic drugs such as amiodarone (AMD) can be used to test the role of negatively charged lipids such as in membranes. It has been found that negatively charged lipid mediates lysosomal phospholipase A2 (LPLA2)-lipid membrane binding through an electrostatic interaction results in the amplification of the apparent LPLA2 activity [156]. Experimental work by R. Elul [49] found evidence for the presence of fixed negative charges within biological membranes of cells including neurons and glial cells. They were also able to rule out alternative hypothesis of electro-osmosis that could explain the cell movement but not account for the phenomenon. Fixed charge within the cell would have an impact on both the ion activities and the diffusion rates of the membrane. The physiological explanation is found by examining the polarity of the biological membrane. In the membrane each different phospholipid have a different negative charge on it which will be felt by cations at different strengths. The model will attempt to relate the presence of these fixed charges to the underlying dynamics of ionic homeostasis at the perisynaptic cradle.

2.6 Conclusion

This chapter is a literature review of biophysical studies that provide information about the structure and physiology of neurons and glia cells. Neurons are specialised for rapid communication in the body, while the smaller but more common neuroglial cells are non-neuronal cells that carry out a broad range of ancillary functions [62] [63] [64]. Neurons act as standalone functional units of the nervous system and are much bigger than glial cells. These cells have a main body called the soma which contains a nucleus and a cytoplasm: the cytoplasm containing organelles such as the mitochondria, endoplasmic reticulum and peroxisomes. Neurons have two main types of process called axons and dendrites. The axon of a neuronal cell is the most excitable part of the cell and serves to transmit information from the soma to nearby and distal synapses, and nerve terminals. Dendrites, of which there are many in a neuronal cell, provide a large surface area for a synapse, so that multiple signal inputs can be collected and transmitted to the cell body.

Of particular interest to the core research presented in this thesis is unsupervised and supervised learning rules. A well know unsupervised learning rule is the Spike Timing Dependent Plasticity (STDP) rule. STDP strengthens the weights if a presynaptic spike takes part in the firing of a postsynaptic spike otherwise the weights are weakened. More specifically, maximum efficacy occurs when a pre synaptic spike just precedes a postsynaptic whereas maximum weakening occurs when the presynaptic spike occurs just after the postsynaptic spike: The temporal ordering of spikes therefore dictates whether potentiation or depression occurs and so spike timing is important. Another well-known learning function is the Bienenstock-Munro-Copper (BCM) rule which correlated pre and post synaptic firing rates to a threshold in order to decide whether to induce LTP or LTD. The threshold slides as a function of the post synaptic activity to allow the weight to reach a stable state. However, BCM lacks biophysical underpinning. Supervised learning rules include SpikeProp, evolutionary strategy (ES), Supervised Hebbian Learning (SHL) and (ReSuMe). These supervised learning rules have been used successfully to train SNNs for a wide range of applications. A number of models that have been developed to replicate spiking neuron activity. An early but very biological realistic model is the Hodgkin-Huxley model, which was created to be an empirically based model to explain the action potential of the giant axon of a squid as measured from an oscilloscope. Other models include: the integrate-and-fire model, leaky integrate and fire model and spike response models where the latter does not use a capacitor-resistance

circuit. There are also two other models which are derived from two dimensional dynamical system models: the Izhikevich Model and the FitzHugh-Nagumo model.

The review in this chapter also focused on neuroglial cells where the most abundant glial cell in the brain is an Astrocyte. This cell is of particular interest in this thesis as it forms a cradle, often referred to as the presynaptic cradle, with a synapse. Astrocytes are abundant with the same receptors, channels, transporters and co-transporters as neurons possess and perform crucial functions like glutamate and K^+ clearance during neuronal excitation. Of particular interest is ionic homeostasis at the perisynaptic cradle in the presence of thin astrocyte processes. To underpin the core concept tabled in this work the review focused on fixed negative charges in astrocyte membranes. All biological membranes consist of a continuous bilayer of lipid molecules with some embedded membrane proteins as well. These bilayers are fluid with polar and non-polar portions in their structure and are described as amphipathic. Fixed charge within the cell due to phosphatidylserine (which carries a net negative charge) would have an impact on both the ion activities and the diffusion rates of free cytosolic ions. Subsequent contribution chapters relates the presence of these fixed charges to ionic homeostasis at the perisynaptic cradle.

3.

Review of Computational Models

3.1 Computer Modelling of Astrocytes

Computational modelling of astrocytes are essential to the understanding of the interactions between transport processes within the brain and between cells. A recent paper [157] investigated a broad ranges of processes involved in Na^+ homeostasis, transients in response to neuronal activity, astrocyte function and neuron-glial interaction, the loss of sodium balance under metabolic stress and its role in transmitter uptake and volume regulation. A model of astrocytic ion concentration dynamics [5] focuses on changes of ionic fluxes crossing the astrocyte membrane controlled by a Na^+/K^+ exchanger and K^+, Na^+ and Cl^- channels [158]. However, this model does not take into account calcium signalling and its interactions with these charge carriers. An electrodiffusion model [159] which is adaptable to astrocyte cells allows channels to be distributed in different ways and gating parameters can be altered to match experimental data. However, this method ignores extracellular details such as surrounding astrocytes and microvilli. Another recent paper [160] deals with 3 scenarios of glial mediated regulation: ion concentration regulation, synaptic neurotransmitter release and synaptic plasticity. Notable research [158] on an astrocyte-neuron system presents a one dimensional electro-diffusive model to simulate the role of astrocytes in K^+-removal from high concentration regions. The membrane mechanisms were based on four channels, the passive Na^+ and Cl^- channels, the Na^+/K^+ pump and the inward rectifying K^+- K_{ir} channel (K_{ir}) with transmembrane fluxes. The K^+/Na^+ pump uses energy (ATPase) to exchange 2 K^+ ions with 3 Na^+ ions and contributes 2 K^+ ions to the influx and 3 Na^+ ions to the efflux of ions in each pumping. Intercellular Ca^{2+} waves and oscillations in astrocytes [161] have also been modelled to investigate control and plasticity and identifying mechanisms that may be involved in neuron to astrocyte intracellular signalling. More advanced modelling has focused on local details in the morphology and function of cells. For example [162] provided detailed information on NCX allo-allosteric, bind-competition, electrical effects of the membrane on the NCX from

modelling myocytes in rabbits. This is also important at looking at the mitochondrial source of ATP used in the NCX. A recent paper [163] investigated the contribution of morphology (surface to volume ratio) in Ca^{2+} dynamics of dendrites. We will look at effects of volumetric changes within the astrocyte, in particular the role of osmosis. Osmosis can change the number of anions and cations at the PsC and the extracellular space, as well as the volumetric and membrane potential changes of both these regions via the transport of water by aquaporin channels and ion kinetics occurring due to ionic exchangers between cells and the extracellular space. Osmosis is an important phenomenon to consider because it could alter the morphology of narrow processes, their surrounding space and the PsC volume. Greater details on these approaches are highlighted in this chapter.

3.2 Models of Astrocyte and Neuron interaction

An investigation into bidirectional communication between neurons and astrocytes underpins dynamical coordination between neuron clusters helped design a composite astrocyte-neuron model [164]. This is applied to simplified neural structures and limited to coordination between localized neurons, the principle (which embodies structural, functional and dynamic complexity), and the modelling strategy may be extended to coordination among remote neuron clusters. A similar model [165] demonstrates that astrocytes are capable of bidirectional communication with neurons which leads to modulation of synaptic activity, and that indirect signalling through retrograde messenger's leads to modulation of synaptic transmission probability of release. This work also modelled astroglial syncytia in self-repairing SNNs that draws from the ability of astrocytes to coordinate repair. They do this by first identifying when faults occur and subsequently reinstating the activity of neurons by adjusting connections. A fault tolerant mechanism was modelled in a coupled astrocyte-neuron system. Endocannabinoid mediated self-repair that is reported to occur in astrocytes, and involves the dynamics of natural intermediate molecules such as IP_3 and glutamate, control the feedback signal that indicates the success of establishing a repaired connection. It is governed by a spike dependent plasticity mechanism (STDP) combined with a BCM learning rule [166] at tripartite synapses (see Figure 3.1). This mechanism was used to create an astrocyte neural mechanism which was then tested to provide simulation results demonstrating both cellular and network level repair.

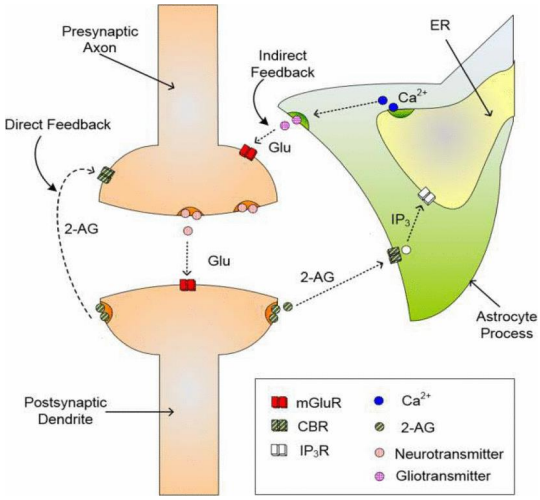

Figure 3.1: A Tripartite Synapse showing an axon, dendrite and astrocyte process [165].

A core pathway is the IP_3 dependent release of Ca^{2+} storage which leads to astrocyte-to-neuronal feedback. In particular, the key equation which describes the IP_3 and Ca^{2+} dynamics is given by [166]:

$$\frac{dIP_3}{dt} = \frac{IP_3^* - IP_3}{\tau_{ip3}} + r_{ip3}y \tag{3.1}$$

IP_3 is the concentration in the cytoplasm and IP_3^* is the baseline level within the cytoplasm when the cell is in a steady state and receiving no input, r_{ip3} is the rate at which IP_3 is produced, τ_{ip3} is the IP_3 decay rate and y is the amount of neurotransmitter released into the cleft. Ca^{2+} dynamics are described by the Li-Rinzel model using three channels, given by [166]:

$$\frac{dCa^{2+}}{dt} = J_{chan}(Ca^{2+}, h, IP_3) + J_{leak}(Ca^{2+}) - J_{pump}(Ca^{2+}) \tag{3.2}$$

J_{pump} which models how Ca^{2+} is stored within the ER by pumping Ca^{2+} out of the cytoplasm into the ER via Sarco-Endoplasmic-Reticulum Ca^{2+} -ATPase (SERCA) pumps. Here r_C is the maximal CICR rate, h is the fraction of activated IP_3Rs, C_0 is the total free Ca^{2+} cytosolic concentration, C_1 is the ER/cytoplasm volume ratio and m_∞ and n_∞ are the IP_3 Induced Calcium Release (IICR) and CICR channels respectively. J_{chan} models the opening of Ca^{2+} channels by the mutual gating of Ca^{2+} and IP_3 concentrations and is given by:

$$J_{chan} = r_C m_\infty^3 n_\infty^3 h^3 (C_0 - (1 + C_1)Ca^{2+}) \tag{3.3}$$

J_{leak} describes the amount of Ca^{2+} released by leakage through the ER membrane and J_{leak} is the Ca^{2+} which leaks out of the ER and r_L is the Ca^{2+} leakage rate. J_{leak} is given by:

$$J_{leak} = r_L(C_0 - (1 + C_1)Ca^{2+}) \tag{3.4}$$

J_{pump} is the amount of Ca^{2+} pumped from the cytoplasm into the ER via the SERCA pumps and is given by:

$$J_{pump} = v_{ER}\frac{(Ca^{2+})^2}{k_{ER}^2+(Ca^{2+})^2} \tag{3.5}$$

where r_L is the Ca^{2+} leakage rate, v_{ER} is the maximum SERCA pump uptake rate and k_{ER} is the SERCA pump activation constant.

There is still a need to explore new approaches to achieving highly adaptive autonomous computing paradigms that can match the astrocyte role in the CNS. Further research is required to demonstrate self-repair at the level of useful large-scale networks. Importantly, it is not clear how spatially extended astrocyte models with leaky membranes support these mechanisms.

3.3 Models of effects of volumetric changes within the astrocyte.

A recent model [131] [167] uses ordinary differential equations to calculate the changes in the number of Na^+, K^+ and HCO_3^- bicarbonate ions in the astrocyte and the extracellular space, as well as the volume changes of both these regions. By deriving the volume to area ratio based on the electro-neutrality principle and assuming space-charge neutrality, the following relationships are defined

$$[Na^+]_i + [K^+]_i - [Cl^-]_i - [HCO_3^-]_i - \frac{z_i X_i}{w_i} = 0 \tag{3.6}$$

$$[Na^+]_o + [K^+]_o - [Cl^-]_o - [HCO_3^-]_o = 0 \tag{3.7}$$

where the subscripts "o" and "i" define variables in the extracellular and intracellular space respectively, X_i is the number of impenetrable ions trapped within the astrocytic membrane area A with volume to area ratio given by w_i and z_i is the average valence of the ions.
The number (N) of each ion S in each region (i / s) is defined by the product

$$N_{i,S} = w[S]_i \tag{3.8}$$

and the model equations are defined as following:

$$\frac{dN_{i_{Na}}^+}{dt} = \frac{g_{Na}}{F}[V_m - E_{Na}] - 3J_{NaKATPase} + \theta_{NKCCl}J_{NKCC1} + \theta_{NBC}J_{NBC} \tag{3.9}$$

$$\frac{dN_{i_K}^+}{dt} = \frac{g_K}{F}[V_m - E_{Na}] + 2J_{NaKATPase} + \theta_{NKCCl}J_{NKCC1} \tag{3.10}$$

$$\frac{dN_{i_{HCO_3^-}}^+}{dt} = 2\theta_{NBC}J_{NBC} \tag{3.11}$$

$$\frac{dN_{o_{Na}}^+}{dt} = -k_C f(t) - \frac{dN_{i_{Na}}^+}{dt} \tag{3.12}$$

$$\frac{dN_{o_K}^+}{dt} = -k_C f(t) - \frac{dN_{i_K}^+}{dt} \tag{3.13}$$

$$\frac{dN_{i_{HCO_3^-}}^+}{dt} = -\frac{dN_{i_{HCO_3^-}}^+}{dt} \tag{3.14}$$

$J_{NaKATPase}, J_{NKCC1}, J_{NBC}$ are the fluxes of the Na-K-ATPase pump and the NKCC1 and NBC co-transporters, while $k_C f(t)$ is a function defining the flux rate membrane area of Na^+ and K^+ between the extracellular space and the neuron area. The theta terms (θ_t) are a binary number indicates if the transporter mentioned in the subscript of the term is active or not. When active the theta term is 1, and when inactive it is 0. The assumed electroneutrality condition demands

that the algebraic sum of all electric currents into the astrocyte has to be zero at every instant. The membrane potential V_m is derived by:

$$V_m = \frac{g_{Na}E_{Na}+g_K E_K+g_{Cl}E_{Cl}+\theta_{NBC}g_{NBC}E_{NBC}-J_{NaKATPase}}{g_{Na}+g_K+g_{Cl}+\theta_{NBC}g_{NBC}} \quad (3.15)$$

where L_p is the water permeability per unit area of the astrocyte membrane, and $\frac{X_i}{w_i}$ is the number of impermeable molecules per volume to area ratio.

$$\frac{dw_i}{dt} = L_p([Na^+]_i + [K^+]_i + [Cl^-]_i + [HCO_3^-]_i + \frac{X_i}{w_i} - [Na^+]_o + [K^+]_o + [Cl^-]_o + [HCO_3^-]_o) \quad (3.16)$$

It is assumed also that the total volume of the space occupied by the astrocyte and the extracellular space remains constant and can be expressed as:

$$w_o + w_i = w_{tot} \quad (3.17)$$

where w_o and w_i are the width (or volume to surface ratio) of the extracellular and intracellular space respectively and w_{tot} is the total of both.

Another model [146] invested a number of mechanisms that could relate aquaporin activity to potassium ion uptake. These included AQP4-dependent: (a) K^+ permeability, (b) resting ECS volume, (c) ECS contraction during K^+ reuptake and (d) diffusion-limited water/ K^+ transport coupling. A model was developed to compute transport and diffusion for an astrocyte–ECS interface that could expand and contract [146]. A diagram showing these transporters in neurons and astrocytes surrounded by the ECS is shown in Figure 3.2

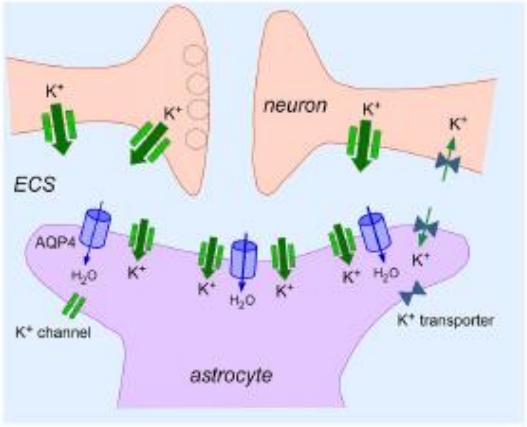

Figure 3.2: A diagram showing these transporters working in neurons and astrocytes surrounded by the ECS [146]

The astrocyte membrane potential ψ for this model is computed from the Nernst-Planck equation in which parameters α and β describe effects of non- K^+ ions

$$\psi = \left(\frac{RT}{F}\right) \ln\left[\frac{\alpha + [K^+]_e}{\beta + [K^+]_a}\right] \tag{3.18}$$

The K^+ flux is described by the Goldman-Hodgkin-Katz equation, in which a pump term ($J^a_{K\,pump}$) is included (corresponding to Na^+/K^+ ATPase) to balance resting K^+ leak to give $J^a_K(0)$=0 [168] [169] [170].

$$J^a_K = P_K \left(\frac{\psi F}{RT}\right) \left(\frac{\left([K^+]_a - [K^+]_e exp\left(\frac{-\psi F}{RT}\right)\right)}{\left(1 - exp\left(\frac{-\psi F}{RT}\right)\right)} \right) - J^a_{K\,pump} \tag{3.19}$$

K^+ pump flux was calculated as a function of $[K^+]$ and an astrocyte-ECS K^+ gradient $\Delta[K^+]$ from experimental findings. The $J^a_{K\,pump}$ term is given by:

$$J^a_{K\,pump} = 2J^a_{K\,pump}\,(0) \left[1 + \frac{[K^+]_e(0)}{(\Delta[K^+] - \Delta[K^+](0) - 2[K^+]_e(0))}\right] \tag{3.20}$$

The water flux J^a_V (i.e. volume (V) flux) between the extracellular space (with osmolarity Φ_e) to astrocyte (with osmolarity Φ_a) compartments is given by:

$$J^a_V = P_f v_w (\Phi_e - \Phi_a) \tag{3.21}$$

Where P_f is the water permeability of the astrocyte and v_w is the partial molar volume of water (18 cm³/mol).

When the water is transported into and out of the astrocyte cell the width of the space alters (See Figure 3.3).

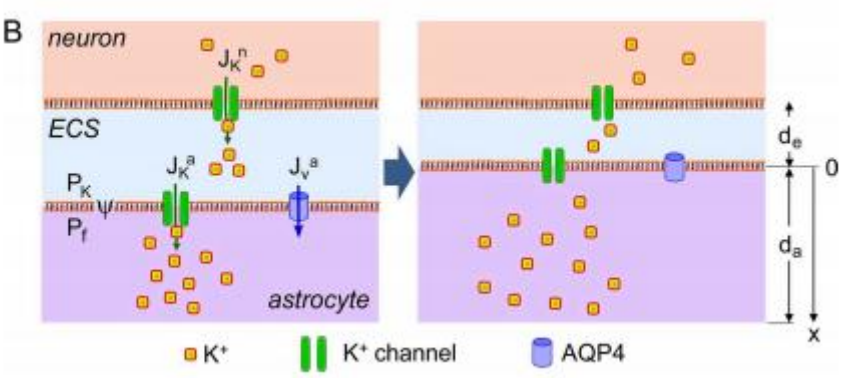

Figure 3.3: Schematic of Neuronal, Astrocyte and ECS compartments before and after ECS shrinkage [146].

Extracellular space width (d_e) produced by the water flux (J_v^a) from the ECS to the astrocyte volume is given by

$$\frac{d(d_e)}{dt} = J_v^a \tag{3.22}$$

Astrocyte width (d_a) produced by this water flux J_v^a is given by

$$\frac{d(d_a)}{dt} = -J_v^a \tag{3.23}$$

The new extracellular space [K⁺] concentration resulting from this volume change is given by

$$\frac{d[K^+]}{dt} + \left(\frac{J_v^a}{d_e}\right)[K^+] = \frac{J_K^a}{d_e} \tag{3.24}$$

The time dependent astrocytic [K⁺] concentration resulting from this volume change is given by

$$\frac{d[K^+]}{dt} - \left(\frac{J_v^a}{d_a}\right)[K^+] = -\frac{J_K^a}{d_a} \tag{3.25}$$

where the extracellular osmolality Φ_e is calculated by the integral below where the factor of 2 is included for electroneutrality

$$\Phi_e = \frac{\Phi_e(0)}{d_e} + \frac{2}{d_e}\left(\int J_K^a \, dt\right) \tag{3.26}$$

The astrocytic osmolality is given an initial astrocytic osmolarity $\Phi_a(0)$ calculated as

$$\Phi_a = \frac{\Phi_a(0)}{d_e} + \frac{2}{d_a}(\int J_K^a \, dt \,) \tag{3.27}$$

and the osmolarity of Non-[K^+] ions is calculated as

$$[\text{non } K^+]_a = \Phi_a(t + \Delta t) - 2[K^+]_a \tag{3.28}$$

In the diffusion limited model the equation for the potassium ion diffusion is given by Fick's second law with a diffusion constant D_a

$$\frac{\delta[K^+]}{\delta t} = D_a \frac{\delta^2[K^+]}{\delta x^2} \tag{3.29}$$

and the non-potassium diffusion by a similar version with the same diffusion constant.

$$\frac{\delta[non\ K^+]}{\delta t} = D_a \frac{\delta^2[non\ K^+]}{\delta x^2} \tag{3.30}$$

The flux boundary condition is given by

$$\frac{\delta[K^+]_a}{\delta t} = -J_K^a/\delta \tag{3.31}$$

where δ is the buffer region length.

A three compartmental model [145] simulated the kinetics, membrane potential, ion transport and cell volume changes of a system, where an astrocyte uptakes potassium ions from a synaptic cleft and a main body and releases it in a perivascular space as shown in Figure 3.4 .

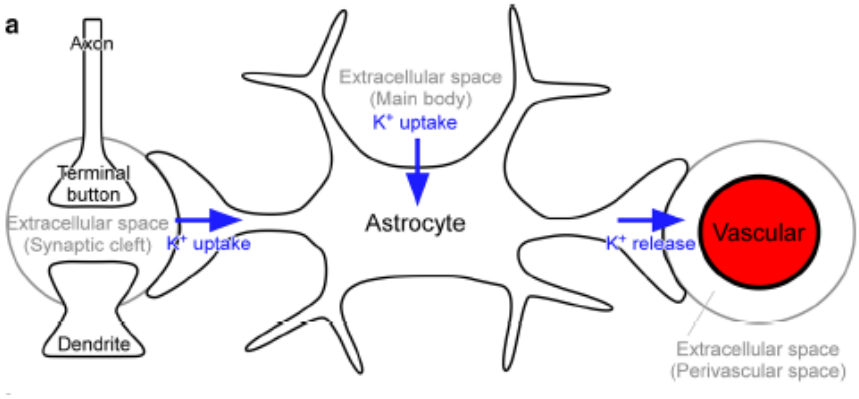

Figure 3.4 Potassium ion dynamics in a synapse-astroyte-vascular system [145].

The three compartmental model is demonstrated in Figure 3.5 where K_{ir} and aquaporin channels are localised at the synaptic cleft and vascular end-feet of the body and a K_{ir} channel and ion transporters are located in the main body. The investigations looked at how high $[K^+]_{out}$ (representing high neuronal activity) would change the flow of ions and water though changing ion concentrations, electrochemical gradients, membrane potential and volume through osmosis gradients.

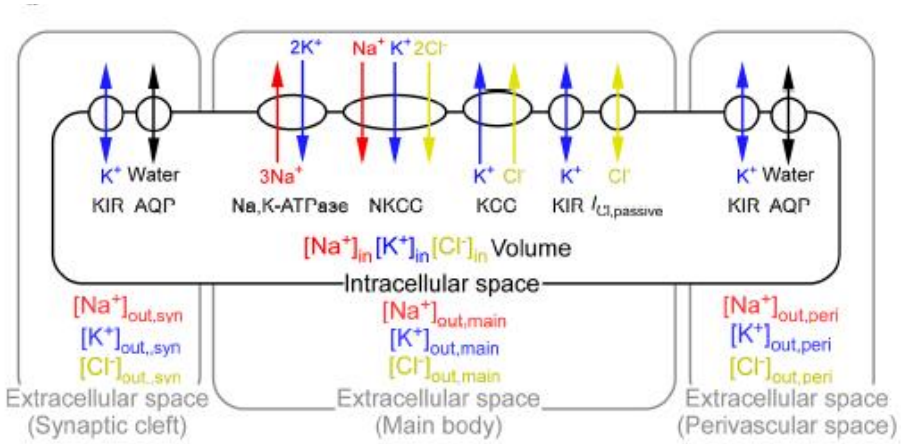

Figure 3.5: Compartmental model schematic showing the synaptic part, main body part and perivascular part. [145]

All parts of the model share the same membrane potential, and the same intercellular concentration. The concentrations in the extracellular space around the three parts of the

astrocyte however can be different. In this model the membrane potential (V_m), volume (Vol) and ion concentrations ($[Na^+]_{in}$, $[K^+]_{in}$, $[Cl^-]_{in}$) are described in the following dynamic equations, where C_m is the total membrane capacitance, and (I_{Na}, I_K, I_{Cl}) are the currents through the membrane and J_{water} is the water flux through the aquaporin channels. The F in these equations is Faraday's Constant.

$$\frac{dV_m}{dt} = \frac{\sum -I_{Na} - I_K - I_{Cl}}{C_m} \tag{3.32}$$

$$\frac{d[Na^+]_{in}}{dt} = \frac{\sum -I_{Na}}{F \cdot Vol} \tag{3.33}$$

$$\frac{d[K^+]_{in}}{dt} = \frac{\sum -I_K}{F \cdot Vol} \tag{3.34}$$

$$\frac{d[Cl^-]_{in}}{dt} = \frac{\sum I_{Cl}}{F \cdot Vol} \tag{3.35}$$

$$\frac{dVol}{dt} = J_{water} \tag{3.36}$$

The ionic currents are calculated by summing the ionic currents through the transporters and ion channels:

$$I_{Na} = I_{Na,NaK} + I_{Na,NKCC} \tag{3.37}$$

$$I_{K,KIR} = I_{K,KIR,syn} + I_{K,KIR,main} + I_{K.KIR,peri} \tag{3.38}$$

$$I_K = I_{K,NaK} + I_{K,NKCC} + I_{K,KIR} \tag{3.39}$$

$$I_{Cl} = I_{Cl,NKCC} + I_{Cl,passive} \tag{3.40}$$

where $I_{i,j}$ represents the current of ion (i) through transporter or ion transporter (j) and $I_{K,KIR,k}$ represents the current of through the channel at part k (syn for synapse, main for main body or peri for perivascular. These are calculated by a regional K_{ir} channel equation given by [145]:

$$I_{K,KIR,i} = \overline{g_{KIR,i}} \cdot A_i \cdot \sqrt{[K]_{out,i}} \cdot (V_m - E_{K,i}) \cdot \left(\frac{1}{1 + \exp\left(\frac{V_m - E_{K,i} - 91.7}{25.6} \right)} \right) \tag{3.41}$$

3.4 Models of Mitochondrial effects.

A model of astrocyte mitochondrial metabolism [171] uses a modified Magnus-Keizer model to capture the dynamics of a large number of variables including the mitochondrial membrane potential ($\Delta\Psi_M$)), ADP, Ca^{2+} ions, NADH, protons in the mitochondria and the ADP in the cytosol. Ca^{2+} in the cytosol is divided into two categories, Ca^{2+} unconnected to buffers, the free calcium's IP_3 receptor pore and the mitochondria's Ca^{2+} uniporter. The model takes account of changes in cell volume and membrane potential as a result of ion flows due to voltage-gated channels and Na^+/K^+ pumps. The dynamics of the tricarboxylic acid (TCA) cycle, mitochondrial Ca^{2+} and oxidative phosphorylation, the metabolic process which reforms ATP are looked at in more detail in the EC coupling/mitochondrial energetics (ECME) model of [172]. In this model the dynamics of the K^+ ions into astrocyte by K_{ir} and Na^+-K^+ATPase out via K^+_{in} leak are given by

$$\frac{dK_{in}^+}{dt} = -\frac{D_K}{z_K Vol_{in} * F}(-I_{Kleak} + 2\overline{I_{NaK}} * \frac{A_{cap}}{V_{astro}} + I_{Kir}) \tag{3.42}$$

Where I_{Kleak} is the K^+_{in} leak current, $\overline{I_{NaK}}$ is the net Na^+-K^+-ATPase current from the astrocyte, D_K is the diffusion constant for K^+, A_{cap} is the Capacitative cell surface area, V_{astro} the astrocyte volume and z_K is K^+ valence.

The rate of $[Na^+]$ out of astrocyte by Na Leak and Na^+/K^+ Pump are given by

$$\frac{dNa_{in}^+}{dt} = -\frac{D_{Na}}{z_{Na} Vol_{in} * F}\left(-3 \cdot \overline{I_{NaK}} * \frac{A_{cap}}{V_{astro}} - I_{Naleak}\right) \tag{3.43}$$

Where $\overline{I_{NaK}}$ is the astrocytic Na^+_{in} leak current, D_{Na} reflects the diffusion constant for Na^+, z_{Na} is Na^+ valence.

The rate of $[K^+]$ into ECS by K^+ leak and neuron pulse is given by

$$\frac{dK_{out}}{dt} = -\frac{1}{z_K Vol_{out} * F}(I_{K,neuro} + I_{Kleak} - 2\overline{I_{NaK}} * \frac{A_{cap}}{V_{astro}} - I_{Kir}) \tag{3.44}$$

The astrocyte membrane potential V_m is then calculated by

$$\frac{dV_m}{dt} = \frac{1}{C_m}\left(\overline{I_{NaK}} * \frac{A_{cap}}{V_{astro}} - I_{Naleak} + I_{neuro} + I_{Kleak}\right) \tag{3.45}$$

ATP dynamics are calculated by a) (V_{ANT}) the concentration flux rate (V) of the adenine nucleotide translocator, b) V_{CK}^{mito} the concentration flux rate of the creatine kinase system (CK) in the mitochondria, c) V_{AM} the concentration flux rate across the myofibrillar ATPase (AM), d) J_{up} is the SERCA Pump rate, e) I_{pCa} The current due to the Sarcolemmal Ca^{2+} pump (pCa) f) I_{NaK} the $Na^{+}K^{+}$-ATPase (NaK) current. V_{astro} is the volume of the cell (with V_{myo} for myocyte used in the diagram) and A_{cap} is the Capacitative cell surface area. [173]

$$\frac{d[ATP]_i}{dt} = V_{ANT} \cdot \frac{V_{mito}}{V_{myo}} - V_{CK}^{mito} - V_{AM} - \frac{1}{2}J_{up} - \left(I_{pCa} + I_{NaK}\right)\left(\frac{A_{cap}}{\mathbf{V_{astro}}F}\right) \tag{3.46}$$

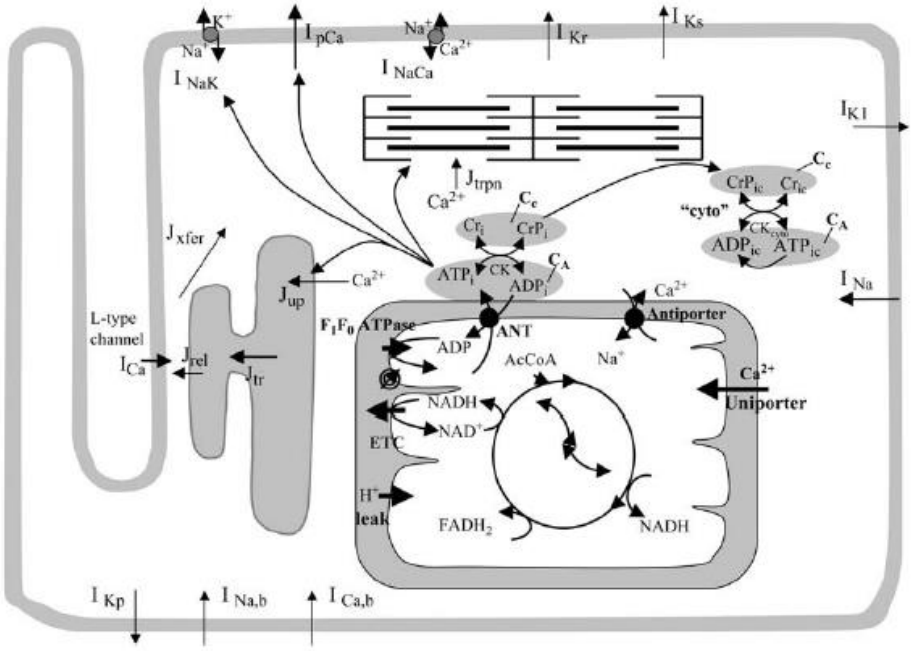

Figure 3.6: General scheme of the EC coupling/mitochondrial energetics (ECME) model. The TCA cycle occurring in the mitochondria (singular rectangular shape). Sarcolemma (disjointed H shape) as well as other cytoplasmatic compartments [173].

The TCA cycle helps to regulate the production of chemicals NADH and $FADH_2$ which drive a proton motive force and the F_1F_0-ATPase pump. The TCA cycle enzymes are regulated by a mitochondrial matrix calcium concentration, which are determined by Ca^{2+} uniporter and a Na^{+}/ Ca^{2+} exchanger. This is a model described by twelve ordinary differential equations for the time rate of the mitochondrial membrane potential and matrix concentrations of Ca^{2+}, NADH, ATP and TCA cycle intermediates.

3.5 Conclusion

This chapter looks at computational modelling of astrocytes, which is essential to the understanding of the interactions between transport processes within and between cells. A summary of a broad range of research areas that are developed in detail later was initially given.

The first model deal with astrocyte and neuron retrograde signalling where the focus is on self-repair in a bi-directionally coupled astrocyte-neuron (AN) system. This work also modelled the astroglial syncytia in self-repairing SNNs and highlights the ability of astrocytes to coordination repair in a network of neurons. They do this by first identifying when faults (failed synapses) occur and subsequently reinstating the activity of neurons by adjusting connections or re-learning new pathways (repair). A fault tolerant mechanism was modelled in a coupled astrocyte-neuron network where the endocannabinoid pathway was shown to mediate self-repair. Essentially the retrograde messenger endocannabinoid released by neurons activates receptors on the astrocyte membrane which in turn releases the IP_3 secondary messenger resulting in a Ca^{2+} oscillation. Gliotransmitters are then released which starts the re-learning process and a repair process is initiated. The re-learning is effected by opening the STDP plasticity window and when the neuron activity is reinstated the plasticity window is shut: the process of modulating the height of the plasticity window is governed by the BCM learning rule [166]. This mechanism was used to create an astrocyte neural self-repairing network which was shown to provide both cellular and network level repair.

The review also focuses on three models of volumetric changes within astrocytes due to osmosis. The model reported [136] [167] uses ordinary differential equations to calculate the changes in the number of Na^+, K^+ and HCO3- bicarbonate ions in the astrocyte and the extracellular space, as well as the volume changes of both these regions. The model framework appears sufficiently detailed and constrained to guide future key experiments and pave the way for more comprehensive astroglia–neuron interaction models for normal as well as pathophysiological situations. In one model [146] a number of mechanisms that could relate aquaporin activity to potassium ion uptake were investigated against experimental predictions. These included AQP4-dependent: (a) K^+ permeability, (b) resting ECS volume, (c) ECS contraction during K^+ reuptake and (d) diffusion-limited water/K^+ transport coupling. A model was developed to compute transport and diffusion for an astrocyte–ECS interface that could expand and contract. A third model was created [145] which is a three part compartmental model to simulate the kinetics, membrane potential, ion transport and cell volume changes of

a system where an astrocyte uptakes potassium ions from a synaptic cleft and a main body and releases it in a perivascular space.

This chapter also focused on modelling astrocyte mitochondrial metabolism using a modified Magnus-Keizer model which looks at the astrocyte's internal source of ATP. The model integrates the dynamics of cell membrane potential, ion homeostasis, cell volume, mitochondrial ATP production, mitochondrial and endoplasmic reticulum Ca^{2+} handling, IP_3 production and GTP-binding protein-coupled receptor signalling.

In conclusion, the models provided in this section provide insights into astrocyte and neuron retrograde signalling that underpin the work in this thesis. These papers modelling the complete synapse offer a mathematical insight into modelling the physical processes involved in ion and molecular transport procedures, but the list of transporters for ionic efflux and influx will be broader later. Also these models would have to be adapted to take account of the ionic transport within the process, the morphology of the synapse and astrocyte (which will be modelled as the combination of compartments) and the inclusion of the charge hopping transport phenomenon discussed in chapter 2. The charge hopping transport phenomenon is central to the hypothesis that fixed ions are responsible for microdomain formation in thin processes. Phenomena such as volumetric changes and mitochondrial metabolism were also looked at. Integrating these areas of consideration would assist in creating more physiologically realistic but complex astrocyte models in the future.

4.

Ionic Microdomains in the Perisynaptic Complex: A New Hypothesis

4.1 Introduction

The existence of astroglial ionic microdomains [39], [48], [40] at the PsC indicates that there must be mechanisms that slow ionic diffusion along the processes. A candidate for this mechanism is associated with fixed negative charges existing in cell membranes, which was reviewed in chapter two. Previous experiments [49] had found localised fixed negative charges in the membranes of neurons and glia. Biological membranes consist of a continuous bilayer of lipid molecules in which membrane proteins are embedded. These bilayers are filled with polar and non-polar portions in their structure (amphipathic) [50]. All eukaryotic membranes are also asymmetric such that biophysical properties differ between the intracellular and extracellular surfaces; this asymmetry is necessary for many key cellular processes including cell fusion and cell clearance [51]. In this chapter we develop modelling equations that captures how fixed negative ions in the membrane of thin astrocyte processes influence the formation of microdomains at the PsC. The work presented here formed part of a peer reviewed journal. [3]

4.2 Hypothesis

This thesis proposes that, in thin astrocyte processes with large surface to volume ratio, fixed negative charges existing in inner process membrane will be the dominant mechanism controlling free ion conduction in the cytoplasm. These negative fixed charges present on the membrane are due to phosphatidylserine (PS) which is composed of phosphatidic acid (PA), with the negatively charged phosphate group attached to the amino acid serine at the hydroxyl end [50]. Specifically, it is hypothesised that the fixed negative charges give rise to potential wells and therefore free cytosolic ions must hop from well to well as they move along the thin astrocyte process. Consequently this low conductance pathway serves to semi-isolate the astrocytic perisynaptic cradle (PsC) from the astrocytic main body. This thesis shows, for the first time, that this low conductance pathway could explain the formation of K^+, Na^+ and Ca^{2+} microdomains at the PsC and points to a new theory for K^+ clearance. For example, it is widely reported [27], [53] that excitatory presynaptic neurons release K^+ into the extracellular space (ECS) which is subsequently cleared at the PsC and buffered away through diffusion to the main astrocyte body. However, this thesis proposes that the flow of K^+ away from the PsC is not volume diffusion limited, but rather is restricted due to the hopping effect along the process, and therefore a K^+ microdomain forms at the PsC during sustained presynaptic neuronal excitation: effectively the PsC acts as a K^+ store during neuronal excitation.

Furthermore, this thesis will show through mathematical modelling, that the formation of a K^+ microdomain at the PsC may very well be advantageous as it facilitates a low energy return pathway for K^+ to the ECS, after neuronal excitation has ceased. Additionally, ion retention along thin processes may also affect homeostasis for Na^+ ions and indeed other ions such as Ca^{2+}. It has been shown in other work [174] that the decay rate of Na^+ following a sustained level of glutamate uptake (in the absence of extra-cellular K^+ change) through EAAT1/2 is in the order of seconds. This thesis will also show that this could potentially result from the restricted flow rate of Na^+ ions along thin processes which results in the formation of a Na^+ microdomain at the PsC that can only be removed by the NKA, reversal of NCX and other transporters. The overall aim of the thesis is to mathematically prove the proposed hypothesis thus providing experimentally testable biological based concepts that potentially explain the existence of ionic $[Na^+]$, $[K^+]$ and $[Ca^{2+}]$ microdomains at the PsC. The remainder of this chapter details the mathematical models used throughout this thesis.

4.3 Astrocyte Process Ionic Transport Model

As was eluded to in Chapter two, phospholipids have different negative charge levels [50] which will interact with the flow of free ions in the process cytoplasm. The variation in charge distributions will lead to differing spatial capture strengths E for ions by each lipid, as shown in Figure 4.1.

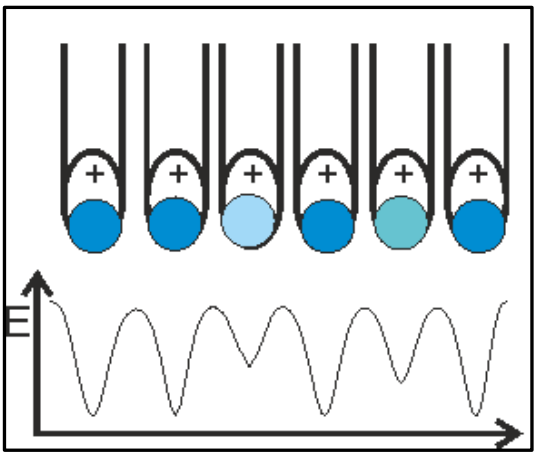

Figure 4.1 Dipole strengths of lipids in a membrane layer: higher blue represents a more negative electric dipole with varying capture strengths E. ***(Diagram created by Harm Van Zalinge)***

Similarly to how charges move through a purely crystalline material, a charged particle could move towards these potential wells from an energetically unfavourable region to a more preferable site at the energy minima of the well [175]. Ions could however move out of these wells through thermal excitation if the donated energy is greater than U, as shown in Figure 4.2 (a). These liberated ion would then hop to a neighbouring preferred position in what is termed diffusion by hopping: a type of Brownian motion. When an external electric field is applied, as shown in Figure 4.2 (b), the electric potential energy on a mobile ion will now have a downward slope.

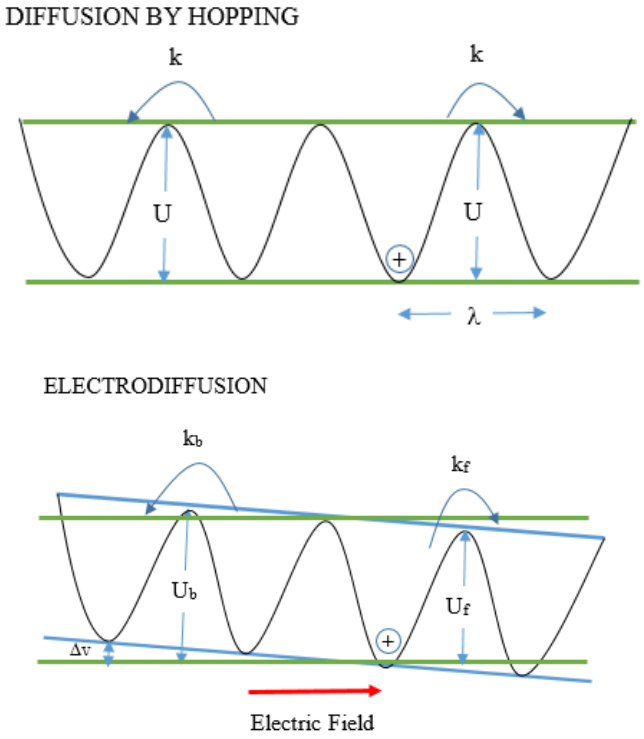

Figure 4.2: (a) Ionic diffusion by ion hopping and (b) electric field assisted ion hopping: electrodiffusion

This has the effect of lowering the activation energy barrier on one side from U to U_f and raising the barrier on the other side from U to U_b. This would mean that the number of hops per second in the direction of the field is much greater than in the reverse direction and the mobile ion is driven by electrodiffusion.

Both sides of the bilayer phospholipid membrane surface are negatively charged, however, it has been shown that the distribution of charge is non-uniform at the atomic scale [52]. This non-uniform distribution gives rise to a potential profile including deep potential wells that can trap ions close to the membrane. Basic quantum mechanics show that regardless of the depth of a well it will have at least one energy state that can trap the travelling ions. The main effect of the depth of the well is the energy needed for the ion move out of the well and continue its motion. This means that the ions cannot move easily along the membrane and must "hop" from well to well [52] [6].

4.3.1 Charge Hopping Model

Charge hopping transport has been extensively studied in dielectric and semiconductor materials. The present case is particularly complex because of the presence of mobile ions in the cytoplasm which causes the formation of an electrical double layer near the interface between the cytoplasm and the membrane. The associated negative charge will cause ions to move towards the membrane creating a dynamic space charge distribution in the cytoplasm as ions move from one well to an adjacent one; that is, there will be a net movement of ions due to the electric field along the length of the process. This leads to a complex and dynamic 3D potential distribution, which would require extensive atomic level modelling, and is beyond the scope of this thesis. However, in order to investigate the interplay between retention of ions along the process length and the formations of microdomain at the PsC we draw on a well-established charge hopping model for electrons in dielectrics containing Coulombic trapping centres [176]. In our case, the membrane fixed charge and associated potential wells are deemed analogous to Coulombic trapping centres. The current flow I_{iPF} through the thin process is then represented as:

$$I_{iPF} = K_i \frac{V_A - V_m - V_r}{l} exp\left[- \frac{Q_i\left(\varphi_w - \sqrt{\frac{Q_i(V_A - V_m - V_r)}{l\pi\epsilon}}\right)}{k_B T} \right] CSA_P \tag{4.1}$$

where K_i is a constant which represents mobility and concentration of mobile ions, V_m is the resting membrane potential of the astrocyte, φ_w is the well activation energy or potential barrier to ion flow, l is the length of the process, Q_i is the charge on a single ion taken as the charge on an electron, T is the absolute temperature, CSA_P is the cross-sectional area of the process, ϵ is the dynamic permittivity and is given by $\epsilon = \epsilon_0 \epsilon_r$, where ϵ_0 is the absolute permittivity and ϵ_r is the relative permittivity of the cytoplasm and k_B is the Boltzmann constant. It has been shown that φ_w lies typically in the range $(1 – 20) \times k_BT$ [6] and is initially taken as $10\ k_BT$ in this work. However, the effect of changing φ_w will be considered later. Also the membrane potential (Vm) across the length of the process is assumed linear in this formulation; that is the lateral electric field is constant. The square root term in the argument of the exponential term of Eqn. (4.1) represents the field-dependent lowering of the activation energy, φ_w. The 'trapping centres' are assumed to be spaced relatively widely such that their potential distributions do not overlap.

The concentrations of K^+ and Na^+ in the astrocyte soma are held constant but will be continuously changing at the PsC thus establishing a dynamic concentration gradient

associated with these cations. Consequently, we formulate a Nernst-like reversal potential for Na^+ and K^+ between the astrocyte soma (AS) and the PsC as:

$$V_r = \frac{RT}{F} ln\left(\frac{[i]_{AS}}{[i]_{PsC}}\right) \tag{4.2}$$

where *i* is the ion under consideration. A schematic of the hopping concept for K^+ ions is shown in Fig. 4.3.

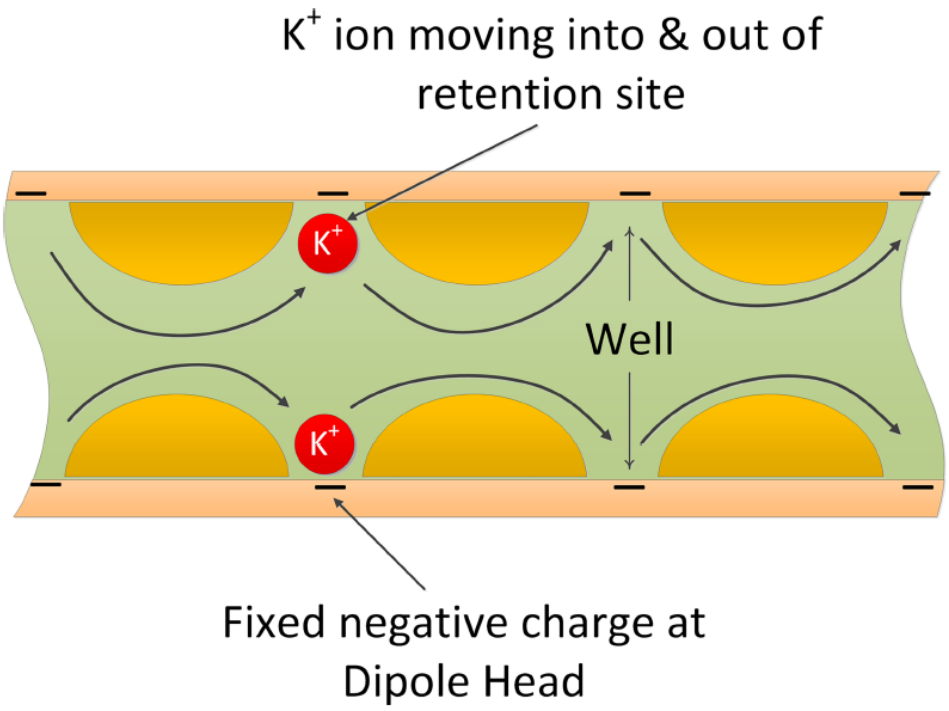

Fig. 4.3 Thin astrocyte process showing charge hopping transport mechanism [3]. The fixed negative charge on the inner membrane surface attracts positively charged cations into the wells causing hopping from well to well along the astrocyte process.

Figure 4.3 assumes a cylindrical process to simplify the model and also that ion hopping dominates over electrodiffusion over the entire cross section of the process. Therefore, the fixed negative charge on the inner membrane surface attracts positively charged ions everywhere into wells causing hopping from well to well along the length of the process.

4.4 PsC Multi-Compartmental Model

To explore the effects of ion retention in thin astrocytic process, a multi-compartmental model was developed consisting of a single synapse surrounded by an astrocytic perisynaptic complex (PsC). Previous imaging studies [177] [127] [126] [178] have highlighted the detailed neural/astroglial biological framework which is comprised of complex geometrical structures making modelling of these shapes extremely complex. To overcome the computational overhead associated with the morphology of a synapse, where the influx/efflux of ions is 3-dimensional, and at the same time capturing the cradle-like structure [127] formed by the PsC around a synapse, this thesis compartmentalises regions of interest using cylindrical arrangements, as shown in Fig. 4.4.

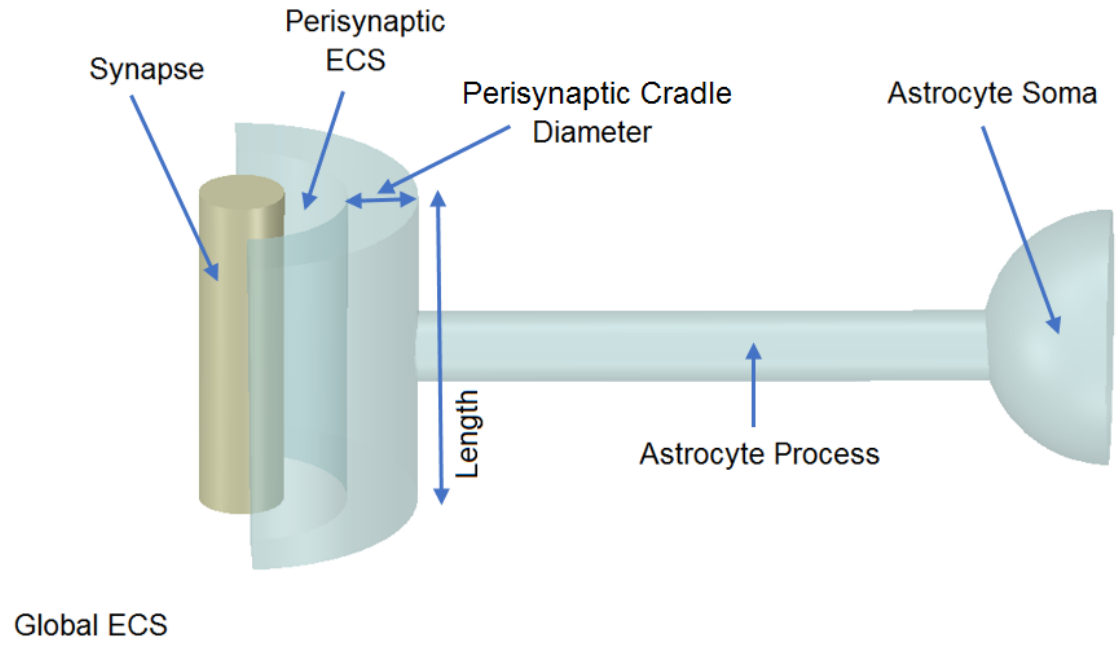

Fig 4.4 Model morphology. A 3-dimensional representation of a single synapse enwrapped by a single astrocyte. In total there are six compartments, 1) Global ECS (GECS), 2) Synapse, 3) Perisynaptic ECS, 4) Perisynaptic complex, 5) Process, and 6) Astrocyte Soma. Each compartment is modelled as a simple cylindrical structure except the GECS and soma which are not given dimensions because ionic concentrations remain constant within these compartments [3].

Fig. 4.4 approximates a biological synapse by modelling the complete synapse (pre and post) as a single cylinder with the same length as the PsC. The PsC was modelled as a hollow half cylinder where the perisynaptic volume was calculated based on the wall thickness of the cylinder. This structure models the cradle-like morphology [127] formed by the PsC surrounding a synapse. The perisynaptic extracellular space (PsECS) volume was modelled by subtracting half the volume of the synapse from the hollow portion of the PsC. Since the PsC does not completely enwrap the synapse, ions are free to diffuse from the PsECS into a much

greater extracellular volume which we denote as a global extracellular space (GESC). Note: within this model the ionic concentrations within the astrocyte soma and GECS are held constant and therefore these compartments are not assigned a volume.

4.5 Ionic Efflux/Influx Transport Models

The synapse and PsC contain various ionic channels, exchangers and pumps to provide homeostasis and dynamic exchange of ions between the two cells and extracellular space, and is described in Fig 4.5.

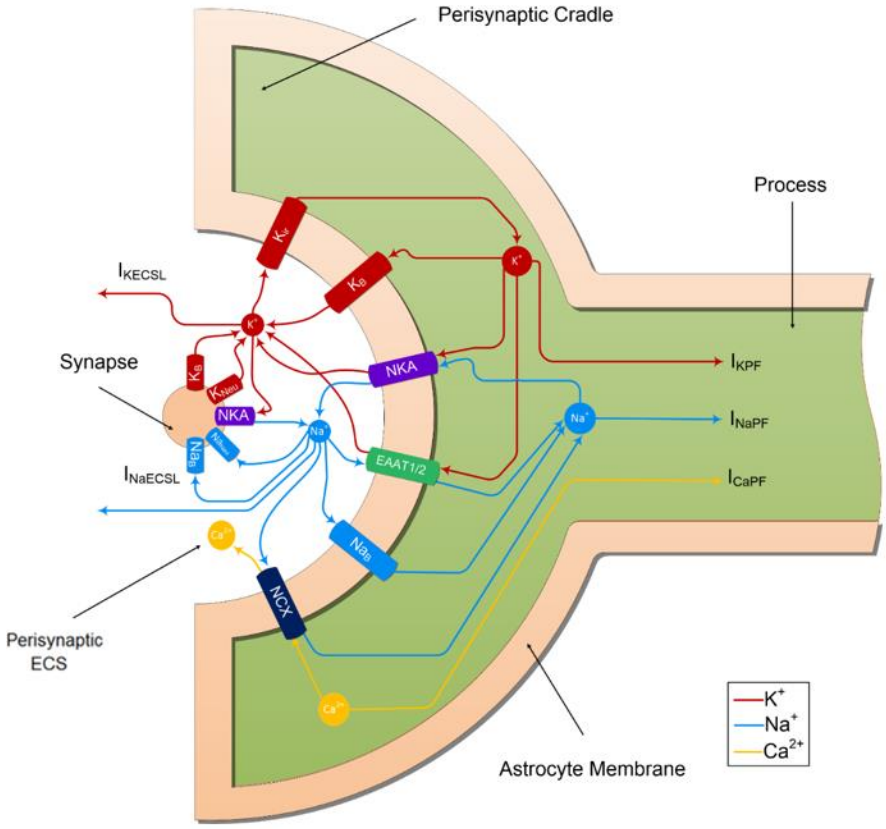

Fig 4.5 Ion transport machinery of the perisynaptic and synapse.

Fig. 4.5 captures eleven transport mechanisms which move ions across the membranes. The neuron model exchanges K^+ and Na^+ with the PsECS via a potassium channel (K_{Neu}) and a Na^+ potassium pump (NaK_{Neu}). The astrocyte exchanges K^+, Na^+ and Ca^{2+} with the PsECS via the Na^+ leak channel (Na_{Leak}), potassium inwardly rectifying channel (K_{ir}), Calcium leak channel (Ca_{Leak}), Na^+-Ca^{2+} exchanger (NCX), Na^+-K^+-ATPase (NaK), and a glutamate-sodium-potassium cotransporter (EAAT). It also allows K^+, Na^+ and Ca^{2+} ions to flow along the process

to the soma via the three currents I_{iKPF} where i is one of the 3 ions. The mathematical descriptions of these components are now described in detail.

The perisynaptic model comprises six compartments, the synapse, PsC, Perisynaptic Extracellular Space (PsECS), Global Extracellular Space (GECS) the astrocyte process and the astrocyte soma. Each of these compartments comprises four ionic concentrations, K^+, Na^+, Ca^{2+} and Chloride (Cl^-). All channels sensitive to these ions reside on the perisynaptic astrocyte membrane and we assume no channel, transporter, co-transporter or pumps at the astrocyte process membrane. The kinetic equations for the changes of ionic concentration of each of these ions is given below. Note: z_xFVol_y is used to convert the total ionic current of ion x into a concentration for the volume y. All initial conditions and parameters for this model are described in Tables 1, 3, 5, 7 and 9 of the introduction section**.**

4.5.1 Mathematical Transport Models

The diffusion of K^+ between the PsECS and the GECS is modelled as a simple gradient controlled channel and is given by:

$$I_{KECSL} = g_{ECS} E_{ECS} SA_{ECSL} \tag{4.3}$$

where g_{ECS} is the conductance of the channel, SA_{ECSL} is the surface area between the PsECS and the GECS, and E_{ECS} is the Nernst like potential of the channel given by:

$$E_{ECS} = \frac{RT}{F} ln\left(\frac{[K^+]_{PsECS}}{[K^+]_{GECS}}\right) \tag{4.4}$$

The change in K^+ in the PsC is given by:

$$\frac{d[K^+]_{PsC}}{dt} = -\left(\frac{I_{Kir}+I_{KNaK}+I_{KEAAT}+I_{KPF}}{z_K F Vol_{PsC}}\right) \tag{4.5}$$

where I_{Kir} is the K_{ir} channel current, I_{KNaK} is the K^+ current through the NaK, I_{KEAAT} is the K^+ current created by the glutamate transporter, and I_{KPF} is the K^+ current from the PsC to the astrocyte soma resulting from ion hopping flow along the process. K^+ changes in the PsECS are given by:

$$\frac{d[K^+]_{PsECS}}{dt} = -\left(\frac{I_{KECSL}+I_{KNeu}-I_{Km}}{z_K F Vol_{PsECS}}\right) \tag{4.6}$$

where I_{KECSL} is current due to K^+ leakage from the PsECS to the GECS, I_{KNeu} is the K^+ current from the neuron and I_{Km} is the total K^+ current flowing through the astrocyte membrane. K^+ is held constant in the GECS and astrocyte soma compartments. Changes in the perisynaptic Na^+ are given by:

$$\frac{d[Na^+]_{PsC}}{dt} = -\left(\frac{I_{NaL}+I_{NaNaK}+I_{NaEAAT}+I_{NaNCX}+I_{NaPF}}{z_{Na} F Vol_{PsC}}\right) \tag{4.7}$$

where I_{NaL} is a current due to Na^+ leakage across the membrane, I_{NaNaK} is the Na^+ dependent current component of the NaK, I_{NaEAAT} is the Na^+ current component of the glutamate transporter, I_{NaNKCC} is the Na^+ current through the NKCC, I_{NaNCX} is the Na^+ current flow due to

the NCX, and I_{NaPF} is the Na^+ current from the PsC to the astrocyte soma resulting from the ion hopping flow along the process. [Na^+] changes in all other compartments are not considered and remain constant. Perisynaptic Ca^{2+} concentration ($[Ca^+]_{PsC}$) varies according to:

$$\frac{d[Ca^{2+}]_{PsC}}{dt} = -\left(\frac{I_{CaNCx}+I_{CaPF}}{z_{Ca}FVol_{PsC}}\right) \tag{4.8}$$

where I_{CaNCX} is the Ca^{2+} dependent component of the current flow through the NCX and I_{CaPF} is the Ca^{2+} current from the PsC to the astrocyte soma resulting from ion hopping flow along the process. [Ca^{2+}] changes in all other compartments are not considered and remain constant at baseline..

The membrane voltage of the astrocyte is assumed to be at the same level across all compartments of the astrocyte and varies according to:

$$C_m \frac{dV_{Astro}}{dt} = I_{Km} + I_{Nam} + I_{Cam} \tag{4.9}$$

Where C_m is the membrane capacitance, I_{Km}, I_{Nam} and I_{Cam} is the total current flow across the perisynaptic membrane ion channels and are given by:

$$I_{Km} = I_{Kir} + I_{KNaK} + I_{KEAAT} \tag{4.10}$$

$$I_{Nam} = I_{NaL} + I_{NaNaK} + I_{NaEAAT} + I_{NaNCX} \tag{4.11}$$

$$I_{Cam} = I_{CaNCX} + I_{CaL} \tag{4.12}$$

The K_{ir} channel is a voltage dependent ion channel with a high affinity to K^+. The current flow through this channel is given by [53]:

$$I_{KIR} = g_k\sqrt{[K^+]_{PsECS}}(V_{Astro} - E_K)SA_{PsC} \tag{4.13}$$

where g_k is the channel conductance. Note: the value of g_k is chosen in such a way that at steady state $I_{Km} = 0$. V_{Astro} is the astrocyte membrane voltage, SA_{PsC} is the surface area of the perisynaptic membrane, and E_K is the Nernst potential of the channel and is given by:

$$E_K = \frac{RT}{F} log\left(\frac{[K^+]_{PsECS}}{[K^+]_{PsC}}\right) \quad (4.14)$$

where *R* is the Gas Constant, *T* is the temperature in Kelvin and *F* is Faradays constant.

The Na^+ leak channel is a plasma membrane pore which allows Na^+ to pass through based on the electrochemical gradient between the PsC and ECS. Since Na^+ concentration inside the cell is much less than outside, this channel usually results in influx of Na^+ into the PsC under normal physiological conditions. It was modelled as a simple passive electrochemical gradient dependent channel given by [179]:

$$I_{NaL} = g_{Na}(V_{Astro} - E_{Na})SA_{PsC} \quad (4.15)$$

where g_{Na} is the channel conductance. Note: the value of g_{Na} is chosen in such a way that at steady state $I_{Nam} = 0$. V_{Astro} is the astrocyte membrane voltage, SA_{PsC} is the surface area of the perisynaptic membrane and E_{Na} is the channel Nernst potential and is given by:

$$E_{Na} = \frac{RT}{F} log\left(\frac{[Na^+]_{PsECS}}{[Na^+]_{PsC}}\right) \quad (4.16)$$

The NaK exchanges intracellular Na^+ for extracellular K^+ against the gradient of both ions and has a stoichiometry of 2:3. The K^+ current component of the pump is given by [178]:

$$I_{KNaK} = 3\ F\ P_{NaKmax} \frac{[Na^+]_{PsC}^{1.5}}{[Na^+]_{PsC}^{1.5} + K_{Nai}^{1.5}} \frac{[K^+]_{PsECS}}{[K^+]_{PsECS} + K_{KE}}\ SA_{PsC} \quad (4.17)$$

and the Na^+ current component of the pump is given by:

$$I_{NaNaK} = -2\ F\ P_{NaKmax} \frac{[Na^+]_{PsC}^{1.5}}{[Na^+]_{PsC}^{1.5} + K_{Nai}^{1.5}} \frac{[K^+]_{PsECS}}{[K^+]_{PsECS} + K_{KE}}\ SA_{PsC} \quad (4.18)$$

where P_{NaKmax} is the NaK maximum pump rate, K_{Nai} is the Na^+ threshold of the pump, and K_{KE} is the K^+ threshold of the pump.

Glutamate released into the extracellular PsECS in the course of neurotransmission is assumed here to be entirely removed by astrocytic EAAT1/2. A transport cycle involves the co-transport of 3 Na^+ and 1 H^+ with 1 glutamate and counter-transport of 1 K^+ [180] [181]. EAAT1/2 proteins are trafficked to the plasma membrane to facilitate the rapid removal (~3ms) of glutamate from the cleft. Glutamate bound to these proteins is then transported to the astrocytic cytosol over a longer period: in this work a complete transport cycle is assumed to be 30 ms [182] [33]. Existing EAAT mathematical formulations do not capture adequately this rapid binding and slow release function and therefore in this work we adopt a different approach. To model the stoichiometry and cycle rate we assume that initially a release of glutamate instantaneously binds to membrane-bound proteins and thereafter the flux of Na^+ through the EAAT transporter pore follows an exponentially decaying rate given by:

$$\frac{dJ_{NaEAAT}}{dt} = -\frac{J_{NaEAAT}(t)}{\tau} + J_0\delta(t - tsp) \tag{4.19}$$

where J_{NaEAAT} is the flux rate of Na^+through the EAAT1/2, *Jo* is the max flux rate through the transporter, δ is the Dirac Delta function, *t* is time, and *tsp* is the previous neuronal spike time. In our model we view the membrane as a capacitor charged with bound glutamate and J_{NaEAAT} as a discharging flux.

The EAAT is responsible for the uptake of extracellular glutamate from the PsECS. Among other ions, it also transports K^+ and Na^+, for every glutamate ion taken up it releases 1 K^+ ion and takes up 3 Na^+ ions [180]. To model this stoichiometry, we adjust the model presented by [183] which describes glutamate uptake by the astrocyte. Therefore, the K^+ current component of the transporter is given by:

$$I_{KEAAT} = -\frac{V_{mg}}{\left(1-exp(r_g s_g - r_g Glu_{PsECS})\right)} \tag{4.20}$$

and the Na^+ current component is given by:

$$I_{NaEAAT} = 3\frac{V_{mg}}{\left(1-exp(r_g s_g - r_g Glu_{PsECS})\right)} \tag{4.21}$$

where V_{mg} is the maximum uptake of glutamate, r_g is the slope of the glutamate uptake, s_g is the threshold of the glutamate uptake, and Glu_{PsECS} is the PsECS concentration of glutamate. Note, as no account is taken intracellularly of glutamate no change in PsECS glutamate is calculated.

The diffusion of K^+ between the PsECS and the GECS is modelled as a simple gradient controlled channel and is given by:

$$I_{KECSL} = g_{ECS} E_{ECS} SA_{ECSL} \tag{4.22}$$

where g_{ECS} is the conductance of the channel, SA_{ECSL} is the surface are between the PsECS and the GECS, and E_{ECS} is the Nernst like potential of the channel given by:

$$E_{ECS} = \frac{RT}{F} log\left(\frac{[K^+]_{PsECS}}{[K^+]_{GECS}}\right) \tag{4.23}$$

The neural model utilised in the work consists of the biophysical Hodgkin and Huxley (HH) model [95] with added NaK pump which changes $[K^+]_{PsECS}$ [184]. All parameters values for this model can be found in Table 7-9.

The membrane potential of the neuron is described by the Hodgkin and Huxley (HH) model [95] for a neuron and is given by.

$$C_m \frac{dV_{Neu}}{dt} = -g_{NaNeu} m^3 h (V_{Neu} - E_{NaNeu}) - g_{KNeu} n^4 (V_{Neu} - E_{KNeu}) - g_{LNeu} (V_{Neu} - E_{LNeu}) \tag{4.24}$$

where C_m is the membrane capacitance, g_{NaNeu} is the Na^+ channel conductance, g_{KNeu} is the K^+ channel conductance, g_{LNeu} is the leak channel conductance and V_{Neu} is the neuron membrane voltage with an initial condition of -0.01 volts. E_{NaNeu} is the Na^+ channel reversal potential, E_{KNeu} is the K^+ channel reversal potential and E_{LNeu} is the Leak channel reversal potential, and *m*, *n* and *h* are channel gating variables.

The Na^+ activation variable is given by:

$$\frac{dm}{dt} = \alpha_m (1 - m) - \beta_m m \tag{4.25}$$

where

$$\alpha_m = 0.1\frac{V_{Neu}+40}{1-exp\left(-\left(\frac{V_{Neu}+40}{10}\right)\right)} \tag{4.26}$$

and

$$\beta_m = 4exp\left(-\left(\frac{V_{Neu}+65}{18}\right)\right) \tag{4.27}$$

The Na^+ inactivation variable is given by:

$$\frac{dh}{dt} = \alpha_{mh}(1-h) - \beta_h h \tag{4.28}$$

where

$$\alpha_h = 0.07exp\left(-\left(\frac{V_{Neu}+65}{20}\right)\right) \tag{4.29}$$

and

$$\beta_h = 0.1\frac{1}{exp\left(-\left(\frac{V_{Neu}+35}{10}\right)\right)+1} \tag{4.30}$$

The K^+ activation variable is given by

$$\frac{dn}{dt} = \alpha_n(1-n) - \beta_n n \tag{4.31}$$

where

$$\alpha_n = 0.01\frac{V_{Neu}+55}{1-exp\left(-\left(\frac{V_{Neu}+55}{10}\right)\right)} \tag{4.32}$$

and

$$\beta_n = 0.125exp\left(-\left(\frac{V_{Neu}+65}{80}\right)\right) \tag{4.33}$$

The HH model simulates current flow of K^+ through a voltage gated channel, therefore the current flow of K^+ from the neuron can be modelled as:

$$I_{KNeu} = -g_K n^4 (V_{Neu} - E_{KNeu}) SA_{Syn} \tag{4.34}$$

Similar to the astrocytic NaK, the neuronal NaK exchanges intracellular Na^+ for extracellular K^+ against the gradient of both ions and has a stoichiometry of 2:3. The K^+ current component of the pump is given by [5]:

$$I_{KNaKNeu} = 3\ F\ P_{NaKmaxNeu} \frac{[Na^+]_{Syn}^{1.5}}{[Na^+]_{Syn}^{1.5} + K_{NaiNeu}^{1.5}} \frac{[K^+]_{PsECS}}{[K^+]_{ECS} + K_{KENeu}} SA_{Syn} \quad (4.35)$$

where $P_{NaKmaxNeu}$ is the NaK maximum pump rate, K_{NaiNeu} is the Na^+ threshold of the pump, K_{KENeu} is the K^+ threshold of the pump, and SA_{syn} is the surface area of the synapse. $[Na^+]_{Syn}$ is the Na^+ concentration level within the synapse. Since the neural model does not contain all the necessary ion channels for homeostasis, Na^+ changes due to the neural NaK pump both inside and outside the synapse are ignored. The value of $P_{NaKMaxNeu}$ was chosen in such a way that $I_{KNaKNeu} = I_{KNeu}$ at steady state.

The Sodium Calcium Exchanger (NCX) is a bidirectional ion transporter which uses the electrochemical gradient of Na^+ to exchange 3 Na^+ ions for 1 Ca^{2+} ion across the membrane. During normal physiological operation, the transporter operates in forward mode and Na^+ is transported into the cell while Ca^{2+} is extruded. However, the direction transporter can be reversed during membrane depolarisation resulting in an influx of Ca^{2+} and efflux of Na^+ [185]. The Na^+ current component of the transporter is given by [186]

$$I_{NaNCX} = \bar{I}_{NCX} \left(\frac{[Na^+]_{PsC}}{[Na^+]_{PsECS}}\right)^3 e^{\frac{\gamma FV}{RT}} - \left(\frac{[Ca^{2+}]_{PsC}}{[Ca^{2+}]_{PsECS}}\right) e^{\frac{(\gamma-1)FV}{RT}} SA_{PsC} \quad (4.36)$$

where $\bar{I}_{NCX}$ is the NCX exchanger conductance and γ is a partition parameter.
The Ca^{2+} current component is given by:

$$I_{CaNCX} = -2\left(\frac{I_{NaNCX}}{3}\right) \quad (4.37)$$

Another variable in this model is leakage from perisynaptic ECS to global ECS. This diffusion of K^+ and Na^+ between the PsECS and the GECS is modelled as a simple gradient controlled channel and is given by:

$$I_{iECSL} = g_{iECS} E_{iECS} SA_{ECSL} \quad (4.38)$$

where i is the ion under consideration, g_{iECS} is the conductance of the channel, SA_{ECSL} is the surface area between the PsECS and the GECS, and Ei_{ECS} is the Nernst like potential of the channel given by:

$$E_{iECS} = \frac{RT}{F} ln\left(\frac{[i^+]_{PsECS}}{[i^+]_{GECS}}\right) \tag{4.39}$$

4.6 Conclusion

This chapter develops a new model that will be used to test the hypothesis that in thin astrocyte processes with large surface to volume ratio, fixed negative charges existing in inner process membrane will be the dominant mechanism controlling free ion conduction in the cytoplasm. Specifically, it is hypothesised that the fixed negative charges give rise to potential wells and therefore free cytosolic ions must hop from well to well as they move along the thin astrocyte process. It is proposed that the flow of K^+ away from the PsC is not volume diffusion limited, but rather is restricted due to the hopping effect along the process, and therefore a K^+ microdomain forms at the PsC during sustained presynaptic neuronal excitation: effectively the PsC acts as a K^+ store during neuronal excitation. Furthermore, this thesis will show through mathematical modelling, that the formation of a K^+ microdomain at the PsC may very well be advantageous as it facilitates a low energy return pathway for K^+ to the ECS, after neuronal excitation has ceased.

To explore the effects of ion retention in thin astrocytic process, a multi-compartmental model was developed consisting of a single synapse surrounded by an astrocytic perisynaptic complex (PsC). The new complete model contains 11 transport mechanisms which move ions across the cellular membranes. To overcome the computation overhead associated with the morphology of a synapse, where the influx/efflux of ions is 3-dimensional, and at the same time capturing the cradle-like structure [124] formed by the PsC around a synapse, we compartmentalise regions of interest using cylindrical arrangements. The perisynaptic extracellular space (PsECS) volume was modelled by subtracting half the volume of the synapse from the hollow portion of the PsC. The model captures eleven transport mechanisms which move ions across the membranes. The neuron model exchanges K^+ and Na^+ with the PsECS via a potassium channel (KNeu) and a Na^+ potassium pump (NaKNeu). The astrocyte exchanges K^+, Na^+ and Ca^{2+} with the PsECS via the Na^+ leak channel (NaLeak), potassium inwardly rectifying channel (K_{ir}), Ca^{2+} leak channel (CaLeak), Na^+-Ca^{2+} exchanger (NCX), Na^+-K^+-ATPase (NaK), and a glutamate-sodium-potassium cotransporter (EAAT). It also allows K^+, Na^+ and Ca^{2+} ions to flow along the process to the soma via the three currents I_{iKPF} where i is one of the 3 ions. The model created in this chapter will be used to simulate K^+ and Na^+ microdomains in chapter five.

5.

Simulations of K^+ and Na^+ Microdomains

5.1 Introduction

This chapter focuses on applying the model outlined in Chapter 4 to test the hypothesis that retention in thin astrocyte processes directly results in K^+ and Na^+ microdomain formation at the PsC. Note that in this chapter we are only focusing on K^+ and Na^+ microdomains but chapter 6 will extend the model to include Ca^{2+}. Specifically this chapter will provide compelling evidence that ion retention in PsC impedes the flow of free ions into the astrocyte process cytoplasm thus leading to the formation of K^+ and Na^+ microdomains at the PsC. Additional simulation results will also show that K^+ retention at the PsC points to a new theory for K^+ clearance from the synaptic cleft. This finding is in direct contrast with the accepted theory that only excitatory presynaptic neurons release K^+ into the extracellular space (ECS) which is subsequently cleared at the PsC and buffered away through diffusion to the main astrocyte body [36] [37].

The first simulation will test the contribution of conventional electrochemical diffusion to ionic microdomains the equation by modelling pure electrodiffusion with no hopping effect. The second simulation will explore how K^+ retention in the astrocyte process gives rise to a K^+ microdomain at the PsC and eliminates K^+ undershoot. In the third simulation, the role of glutamate transport via EAAT1/2 is investigated and results will examine the cell membrane voltage and concentrations and the perisynaptic K^+ currents and perisynaptic Na^+ currents. The final simulation we examine what happens when K^+ is released by the neuron as before and a 100 μM puff of glutamate is released into the PsECS, with each spike event. Having analysed

the formation of microdomains in the previous three simulations this thesis now explores the sensitivity of the model to its parameters. These parameters are PsC surface area, the maximum NKA pump rate, Pmax, and the potential barrier to ion flow along the process, φw. In these simulations a neuronal firing rate of 40Hz was chosen.

Our results will show that the flow of K^+ away from the PsC is not volume diffusion limited, but rather is restricted due to the hopping effect along the process, as outlined in chapter 4. Therefore, a K^+ microdomain formed at the PsC during sustained presynaptic neuronal excitation represents a temporary store for K^+ ions which can be returned to the ESC after neuronal excitation dies off: furthermore, the formation of a K^+ microdomain at the PsC may very well be advantageous as it facilitates a low energy return pathway for K^+ to the ECS, after neuronal excitation has ceased. This chapter will show that ion retention along thin processes also affects homeostasis for Na^+ ions as they carry a positive charge. Specifically it will be shown via simulations of both K^+ and glutamate clearance that because of Na^+ retention in thin astrocyte processes a microdomain of Na^+ ions forms at the PsC which is removed, after neuronal excitation dies off, by the NKA, reversal of NCX and other transporters. This removal mechanisms result in a slow decay rate for the Na^+ microdomains (in the order of minutes). This finding is in agreement with other work [174] where the decay rate of Na^+ following a sustained level of glutamate uptake (in the absence of extra-cellular K^+ change) through EAAT1/2 is in the order of minutes. However, it is necessary to establish prior to simulation of ion retention the extent to which conventional electrochemical diffusion contributes to microdomain formation in thin processes. The following section address this issue

5.2 Electrochemical Diffusion in Thin Processes

This thesis proposes a new theory whereby ion retention in thin astrocyte processes serves to semi-isolate the PsC from the astrocytic main body thus causing ionic microdomains to form at the PsC. This chapter focuses on Na^+ and K^+ related transporters only and the associated transport machinery is shown in Fig. 5.1. To test the contribution of conventional electrochemical diffusion to ionic microdomains the equation to model the currents I_{KPF} and I_{NaPF} where replaced with a pure diffusion equations.

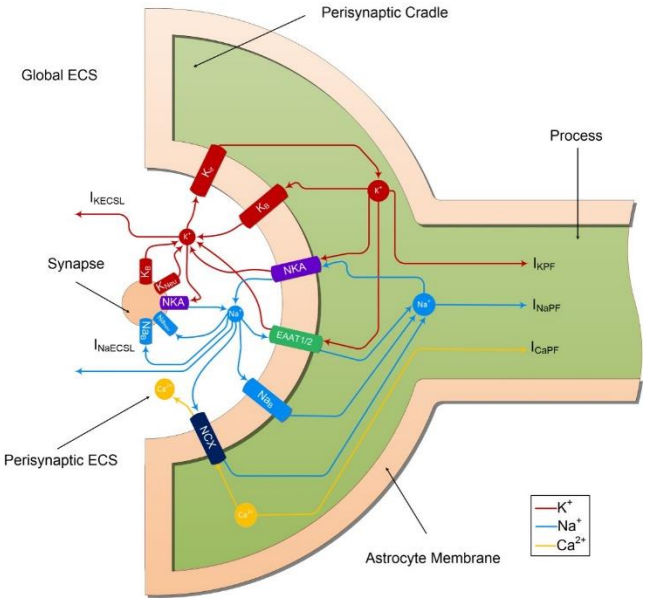

Fig 5.1. Ion transport machinery of the perisynaptic cradle and synapse. The simplified model contains 7 transport mechanisms which move ions across the membranes. The neuron model exchanges K^+ and Na^+ with the PsECS via a K^+ channel (K_{Neu}) and a sodium potassium pump (NKA_{Neu}), Note: neuronal NKA K^+ binding site is completely saturated, so the only ion that activated neuronal NKA is cytosolic Na^+ **[3]**.

In this work we used an expression for ionic diffusive fluxes [187]

$$J_{ion_{Diff}} = \frac{D_{ion}}{V_{process}} \cdot l_{process} \cdot CSA_{process} \cdot (Ion_B - Ion_{eff}) \tag{5.1}$$

where D_{ion} is the diffusive constant of the respective ion (e.g. Na^+, K^+), $V_{process}$, $l_{process}$, $CSA_{process}$ are the volume, length and cross-sectional area of the process, and $(Ion_B - Ion_{eff})$ is the difference between the respective ion concentrations at the body and at the cradle. Equation (5.1) was used to model the flow of Na^+ and K^+ ions along the astrocyte process and the simulation results in Figure 5.2 were obtained.

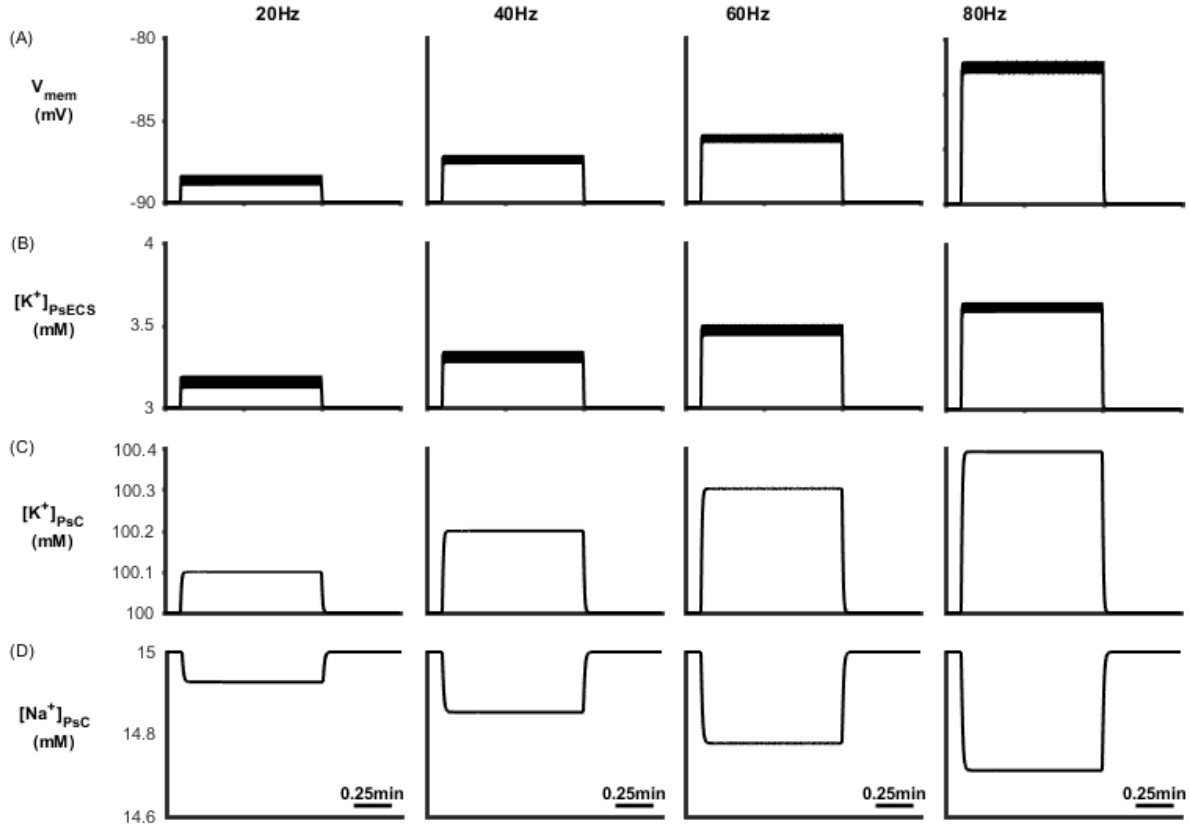

Fig 5.2. Neuron Membrane Voltage and End-foot Concentrations (A) Astrocyte Membrane Voltage (B) Potassium Concentration in the Ps ECS (C) Potassium Concentration in the Perisynaptic ICS (D) Sodium Concentration in the Perisynaptic ICS.

Fig. 5.2 (A-D) shows the membrane voltage and ionic concentrations at the PsC for different presynaptic neuron frequencies. In this simulation glutamate was held constant in the cleft and only K^+ was released with each presynaptic neuron spike. The spike leads to -2% and 0.4% relative increases at 80Hz in the levels of Na^+ and K^+ respectively. Clearly the levels of K^+ and Na^+ remain virtually at baseline ($[Na^+]$ = 15mM and $[K^+]$ =100mM) indicating that no microdomain is formed in the case of pure electrodiffusion. Note also that the concentration of these ions both within the PsC and in the ECS remain constant for the duration of the presynaptic neuron excitation. This is because of the rapid removal of Na^+ ions away from the PsC by electrodiffusion causing the NKA to function at a slower rate initially allowing K^+ to build up rapidly in the ECS until the rate of removal of K^+ by the NKA is equal to the rate of emission of K^+ from the presynaptic neuron. Thereafter, ionic concentration everywhere remains constant and this will be the case for all frequencies. Note that the thicker horizontal lines in Figure 5.2 A and B indicate oscillatory behaviour in $[K^+]_{PsECS}$ which is due to puffs of K^+ which are released at every spike event, and also as K^+ uptake is by K_{ir} channels there will

be an associated rise is the membrane potential (Vm) with frequency.

In conclusion, this section shows that ionic microdomains cannot be formed in the presence of conventional electrochemical diffusion and this finding sets the scene for subsequent simulations. The remainder of this chapter will focus on testing the proposed hypothesis: in thin processes where the surface to volume ratio is large, surface conduction dominates and therefore the flow of ions is restricted to a hopping mechanism which effectively semi-isolate the PsC from the astrocytic main body.

5.3 Microdomain formation and K^+ Undershoot

To explore how K^+ retention in the astrocyte process gives rise to a K^+ microdomain at the PsC and eliminates K^+ undershoot, several simulations were carried out with the presynaptic neuron stimulated using external currents to produce firing rates of 20Hz, 40Hz, 60Hz and 80Hz. These firing rates are all within physiological frequencies of most cortical pyramidal neurons and fast spiking neurons. The neural stimulus has a duration of ~1 minute where the first 0.1 minute allows the model to reach a steady state condition and the stimulus ceases after 1min. Although this is a significant period of time, it allowed an investigation into how extracellular and intracellular ionic concentrations would be affected during a sustained period of neural activity. For each simulation, PsECS [Glu] was held constant at the background level. The simulation results presented in this section were carried out using Matlab 2015b 64 bit (Windows version) by Mathworks and all morphological values required for our model are listed in the table of parameters at the beginning of the thesis. The forward Euler method of integration was used for simulation with a fixed time step of 10μs.

5.3.1 PsC membrane voltages and ionic concentrations against time.

Fig 5.3 describes $[K^+]$ and $[Na^+]$ dynamics for each of the 4 different stimuli where it can be seen that neuronal release of K^+ into the PsECS leads to an increase in the astrocyte membrane voltage (V_A in Fig 5.3A) because of the change in ionic currents through the PsC membrane.

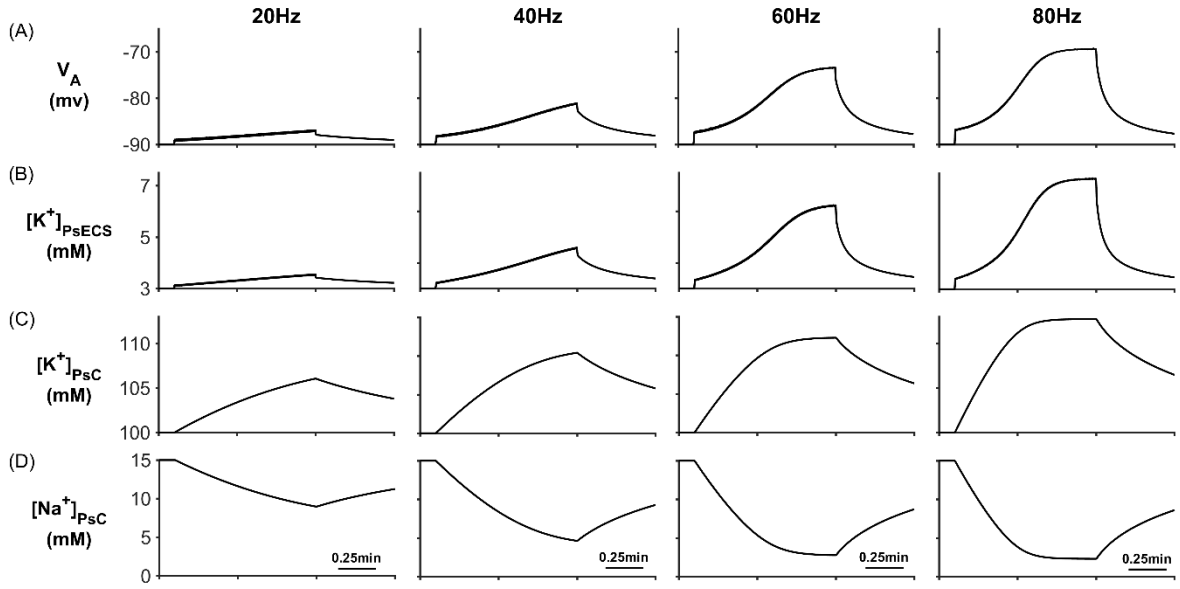

Fig 5.3. PsC membrane voltages and concentrations against time. (A) Astrocyte membrane voltage (V_A). (B) $[K^+]_{PsECS}$. (C) $[K^+]_{PsC.}$ transient. (D) $[Na^+]_{PsC}$ transient.

It can also be seen that K^+ steadily increases within the PsECS ($[K^+]_{PsECS}$ in Fig 5.3 B) and after a period of ~0.8 minutes it approaches steady state at higher frequencies where the release rate of K^+ by the presynaptic neuron equates to the clearance rate by NKA, K_B on both the PsC and the presynaptic terminal and also K^+ lost into the GECS. It is also worth noting that as the concentration of K^+ increase in the PsC ($[K^+]_{PsC}$ in Fig 5.3 C), the $[Na^+]$ within the PsC decrease due to efflux by NKA at the PsC ($[Na^+]_{PsC}$ in Fig 5.3 D). Note: the astrocyte membrane voltage V_A, $[K^+]_{PsECS}$ and $[K^+]_{PsC}$ all increase with the presynaptic neuron firing rate while $[Na^+]_{PsC}$ decreases.

5.3.2 Perisynaptic K^+ currents.

During neural activity, the NKA and K_{ir} channel currents are responsible for K^+ uptake while the background K^+ and KPF currents release K^+ from the PsC.

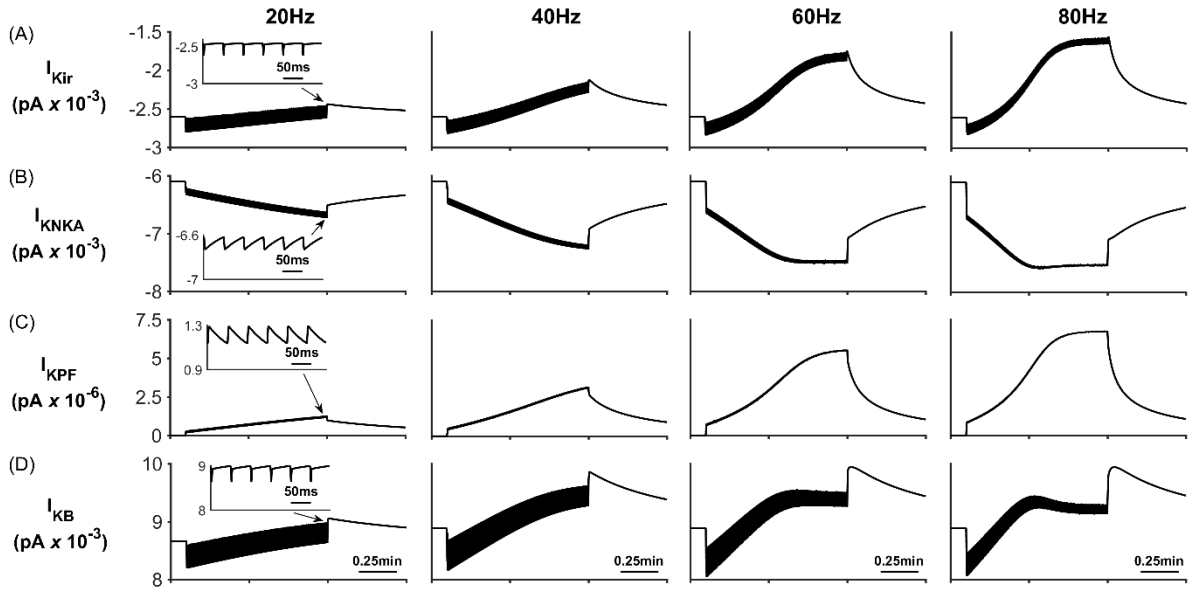

Fig 5.4 Perisynaptic K^+ currents. (A) K^+ K_{ir} current. (B) K^+ NKA current. (C) K^+ current along the process. (D) Background K^+ current.

These currents can be seen in Fig 5.4 where Fig 5.4 B shows that, contrary to the current thinking [184], the NKA is the dominant driving force for K^+ uptake while K_{ir} channel (Fig 5.4 A) is much less so for K^+ clearance. Furthermore, clearance by K_{ir} diminishes over time because the changes in the associated reversal potential due to the $[K^+]_{PsC}$ microdomain. Fig 5.4 C shows that I_{KPF} is several orders of magnitude lower than I_{Kir} and therefore this slow leakage of K^+ away from the PsC appears to be a plausible explanation for the emergence of a K^+ microdomain. Note the saturation and subsequent fall off of I_{KB} at higher frequencies is a direct result of the K^+ background reversal potential approaching V_A. This is caused by the rapid build-up of K^+ in the PsECS and cradle. The high frequency oscillatory behaviour which appears as a thickening of Fig 5.4 A-D is due to the astrocytic response to the pulsed nature of presynaptic neuronal K^+ release. As K^+ in the PsECS fluctuates so does the astrocyte NKA pump and to a lesser extent the astrocyte membrane voltage. These fluctuations in the NKA and membrane voltage are also reflected in Na^+ and K^+ currents. Inserts in Fig 5.4 A-D, column 1, are used to show detail of astrocyte K^+ current dynamics in response to neuron K^+ release. Note: for clarity only the first column shows this detail as the dynamics for each current is similar for each of the stimulus frequencies.

5.3.3 Total perisynaptic membrane K^+ current and K^+ process current.

When the neuron stops releasing K^+ (~ 1min) K^+ quickly flows from the PsECS into the ECS which reduces the K^+ gradient between the PsECS and PsC thereby reducing NKA pump rate, after which a net efflux of K^+ takes place from the stored K^+ in the associated microdomain. This points to a new theory whereby K^+ microdomain formation during neuronal excitation (due to ion retention in the astrocyte process) provides the driver for the return of K^+ to the PsECS, via background K^+ leak and $K_{ir}4.1$ channels, for uptake by the neuron. Fig 5.5 A shows the net transfer of K^+ across the perisynaptic membrane while Fig 5.5 B shows the net current flow along the process (out of the perisynaptic cradle). During stimulation (0.1 min to 1min) it can be seen that there is a net transfer of K^+ into the perisynaptic cradle across the membrane (Fig 5.5 A). Since the current flowing along the process to the soma (Fig 5.5 B) is 3 orders of magnitude smaller than the currents entering the cradle, there is a net build-up of K^+. Essentially a K^+ microdomain forms because of the low conductance pathway from the cradle to the astrocyte soma: this is strong evidence for the proposed hypothesis. Furthermore, this microdomain allows the efflux of K^+ from the PsC into the PsECS after neuron stimulation ceases. This can be seen as a spike like current in Fig 5.5A after 1min and is more pronounced in the 80Hz simulation.

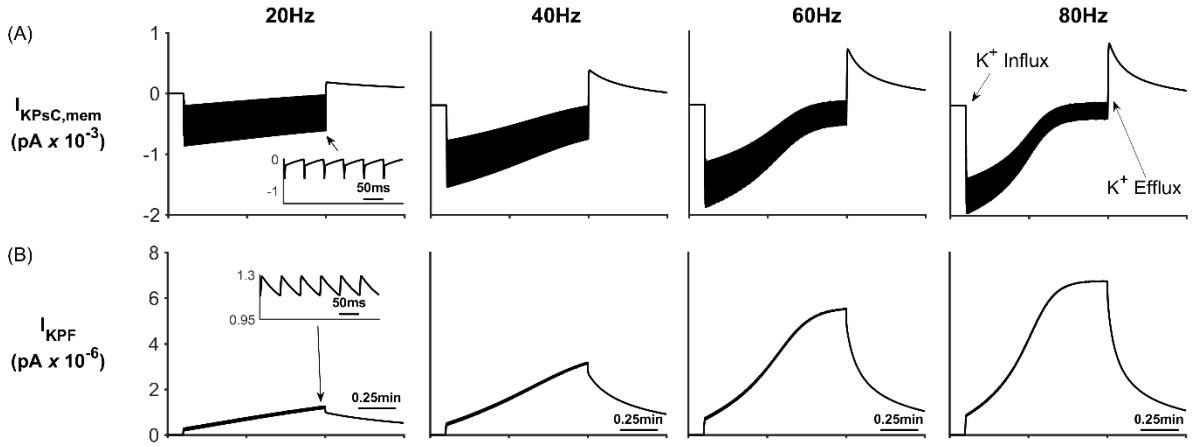

Fig 5.5. Total perisynaptic membrane K^+ current and K^+ process current. (A) The total K^+ current flowing across the perisynaptic membrane (IKPSC,mem). During neural activity (Start = 0.1 min) K^+ in the PsECS is removed by NKA and there is a net influx of K^+. When neural activity stops (1min), K^+ is released back into the PsECS mediated by the background K^+ channel. This influx/efflux can be seen in A column 4. (B) K^+ current flowing along the process (IKPF).

5.3.4 Perisynaptic Na^+ Currents

Fig 5.6 shows the Na^+ currents for the four different stimulus frequencies. All Na^+ channels, except the NKA (Fig 5.6B) Na^+ current, result in Na^+ influx to the PsC. When the neuron stops firing there is a net influx of Na^+ into the PsC. The decrease in I_{NaB} (Fig 5.6A) can be explained as follows. Since I_{NaB} is dependent on the astrocyte membrane potential as well as Na^+ gradient there is a sharp decrease in the current due to the astrocyte membrane potential depolarising.

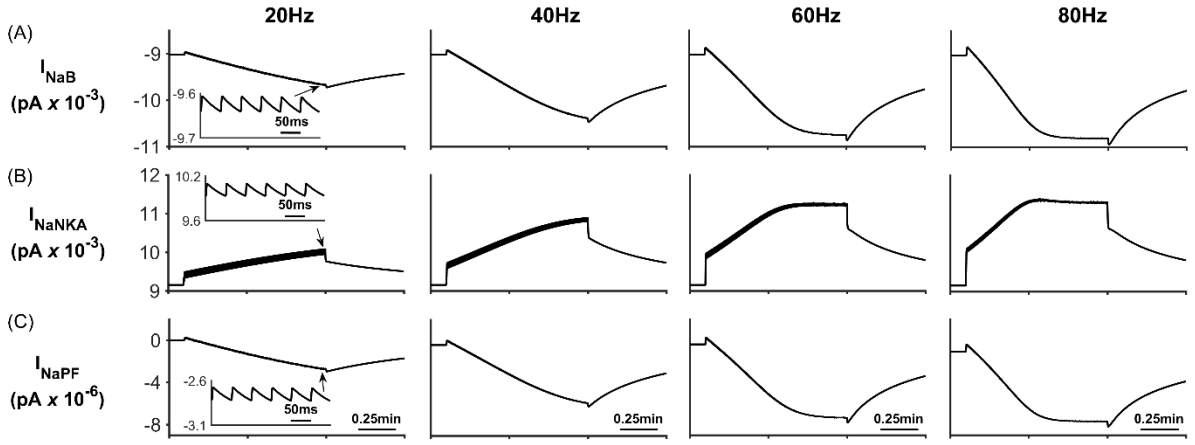

Fig 5.6. Perisynaptic Na^+ currents. (A) Background Na^+ current. (B) NKA current. (C) Na^+ current along the process. During neural activity, the NKA pumps Na^+ from the cell to allow for K^+ uptake, therefore there is a net decrease in $[Na^+]_{PsC}$. When the neuron stops firing, NKA slows down and there is a net uptake of Na^+ via the remaining channels.

5.3.5 Process and Background Channel Reversal Potentials for K^+ and Na^+

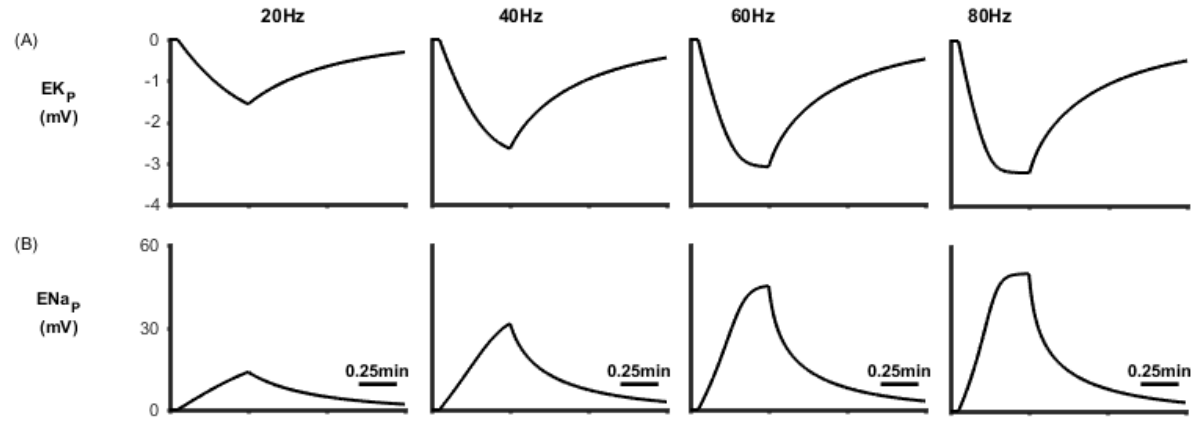

Fig 5.7: Process Reversal Potentials for K^+ and Na^+ at different frequencies.

Figure 5.7 shows the process reversal potentials for K^+, and Na^+. With reference to Fig. 5.7 (A) it is clear that the reversal potential for K^+, PRP_K, continually decreases with increasing presynaptic neuron activity and drops to approximately -2.7mV at 80Hz. When the presynaptic stimulus stops at 1 min PRP_K has reached this maximum and thereafter begins to return to a

baseline level of zero. This behaviour can be explained with reference to Fig. 5.3 (B-C). This figure shows that the ratio of K^+ concentration in the PsC to that in the PsECS continually decays with frequency. This is because NKA is saturated even at 20Hz and therefore pumps K^+ from the PsECS to the PsC at a constant rate across all frequency ranges: remember NKA is the dominant mechanism for removing K^+ from the PsECS. Consequently as PRP_k depends on this ratio then it will reduce at the ratio drops. A similar explanation hold for PRP_{Na} but in this case the Na^+ concentration in the PsECS is held constant at the baseline level. As the firing frequencies of the presynaptic neuron increase PRP_{Na} increases to approximately 32mV at 80Hz and thereafter decreases to its baseline level of zero [174]. During neural activity, the NKA pumps Na^+ from the cell causing Na^+ to drop from its baseline level in the PsC and therefore the ratio of Na^+ in the PsECS to that in the PsC is increasing with frequency. Consequently PRP_{Na} shows an increasing trend with frequency.

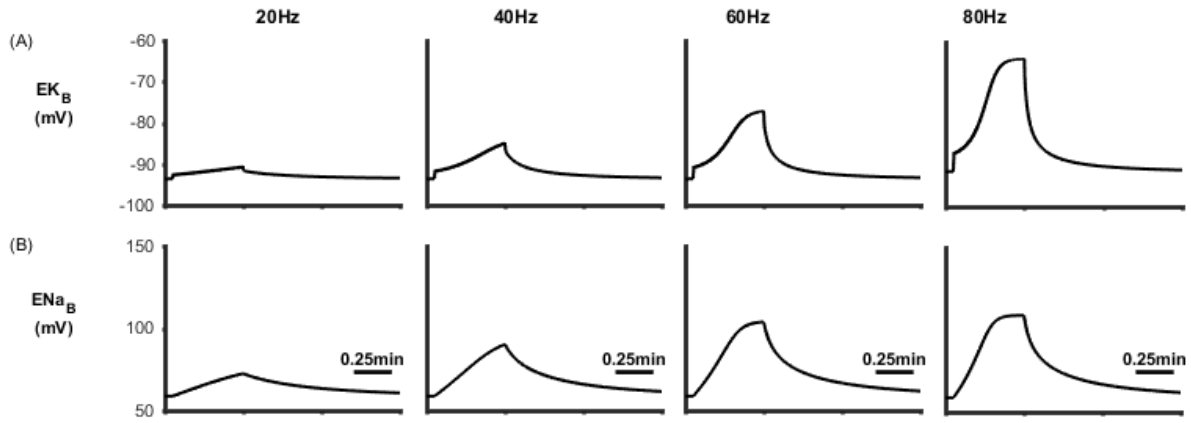

Fig 5.8: Background Channel Potentials for K^+ and Na^+

Figure 5.8 shows the background channel reversal potentials for K^+, and Na^+. The background K^+ reversal potential (Figure 5.8A) increases due to the K^+ gradient by the rapid build-up of K^+ in the PsECS and cradle, as stated before, as the reversal potential approaches the astrocyte membrane voltage V_A where it depolarises causing subsequent fall off of I_{KB} and a return of EK_B to background levels. The Na^+ reversal potential (Figure 5.8B) increases due changes in the Na^+ gradient but reaches a saturation point, as show in the higher frequencies. At this saturation point the depolarisation of the astrocyte membrane results in a decrease in the I_{NaB} current (Fig 5.6A) and there is a net influx of Na^+ into the PsC as the efflux of Na^+ by the NKA (Fig 5.6B) reduces when the neuron stops firing.

5.4 Glutamate driven PsC Na^+ microdomain formation

As well as K^+ buffering, astrocytes also provide a critical role in glutamate uptake and recycling via the glutamate-glutamine cycle (GGC) [188]. In this simulation, the role of glutamate transport via EAAT1/2 is investigated and results will show that the slow leakage of Na^+ ions in the astrocyte process causes Na^+ to increase in the PsC before being returned to the PsECS via the NKA. These results support previously published experimental work [174]: there is no neuronal excitation and therefore the concentration of K^+ in the PsECS is held constant.

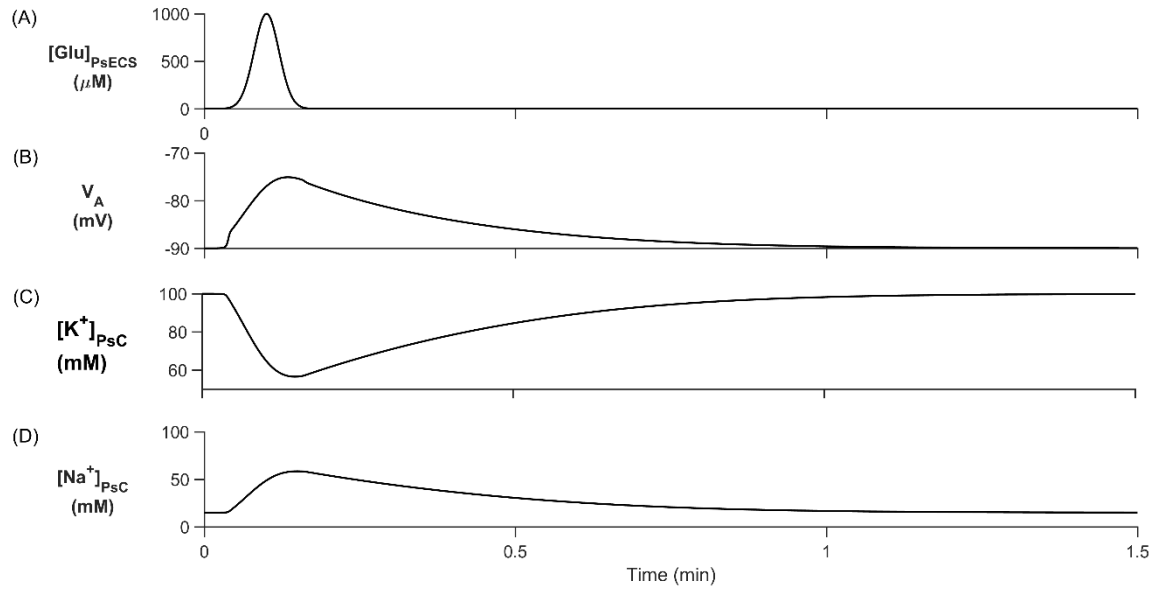

Fig 5.9. Cell membrane voltage and concentrations. (A) Glutamate is injected into the PsECS with a Gaussian distribution for ~10s with a maximum concentration of 1000μM. (B) PsC membrane voltage depolarises with ionic changes in the PsC. (C) $[Glu]_{PsECS}$ increase causes EAAT1/2 activation and a thereby removing K^+ and (D) the uptake of Na^+.

The concentration of glutamate in the PsECS was modulated using a Gaussian function as shown in Fig 5.9A. Figure 5.9 B shows that the PsC membrane voltage depolarises with ionic changes in the PsC. Fig 5.9 C-D presents the results of the PsC ionic $[K^+]_{PsC}$ and $[Na^+]_{PsC}$ concentrations. From Fig 5.9 C-D we clearly see that the $[K^+]_{PsC}$ decreases while $[Na^+]_{PsC}$ increases, this is the opposite dynamics to that observed in Fig 5.3 C-D. This is because K^+ in the PsECS is now held constant at 3 mM and therefore all K^+ channels except the NKA, represent a slow leakage through the astrocyte process removing K^+ from the PsC (Fig 5.10 A-B, Fig 5.10 D-E) resulting in a net K^+ efflux. The main driving force behind Na^+ uptake by the PsC is the EAAT1/2 transporter which is also responsible for the removal of glutamate from the PsECS (Fig 5.11A).

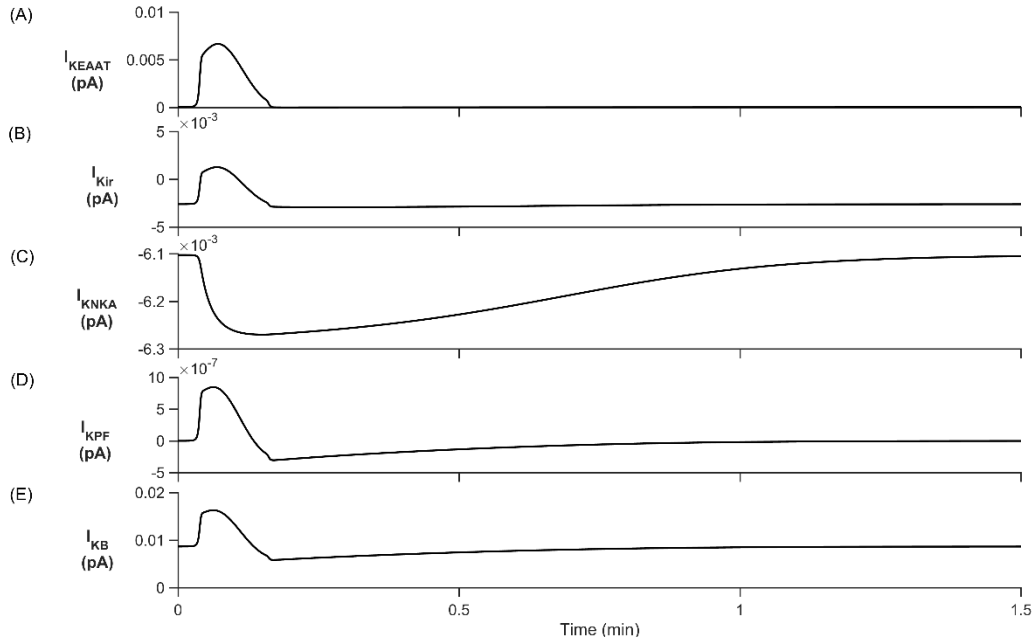

Fig 5.10 Perisynaptic K^+ currents. (A) K^+ EAAT1/2 current. (B) K^+ K_{ir} current. (C) K^+ NKA current. (D) K^+ current along the process. (E) K^+ background current.

During $[Glu]_{PsECS}$ injection, the EAAT1/2 and K_{ir} release K^+ at an accelerated rate. This is opposed by NKA and the transport of K^+ from the astrocyte soma to the PsC. When glutamate falls to baseline levels, the EAAT1/2 (Fig 5.10 A) and K_{ir} channels (Fig 5.10 B) quickly revert to their initial rates. NKA (Fig 5.10 C) and transport of K^+ from the astrocyte soma (Fig 5.10 E) is then able to establish baseline ionic concentrations at the PsC.

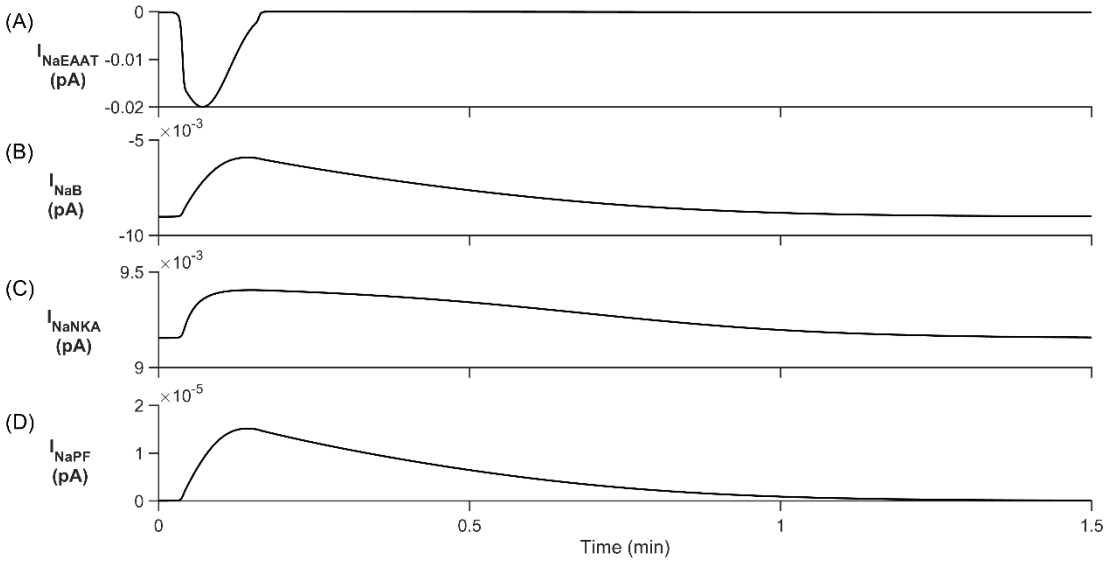

Fig 5.11. Perisynaptic Na^+ currents. (A) Na^+ EAAT1/2 current. (B) Background Na^+ current. (C) Na^+ NKA current. (D) Na^+ current in the astrocyte process.

As is the case for K^+, retention of Na^+ ions as they flow within the astrocyte process substantially limits the transport rate of these ions away from the PsC as shown by the INaB (Figure 5.11B). In this case, Na^+ is restricted and therefore a Na^+ microdomain forms at the PsC. Note: similar to the results presented in [174] there is a long decay (~80s) transient of Na^+ (Fig 5.9D)which far outlasts the glutamate signal decrease (Fig 5.9A) and this thesis proposes that this is due to the slow removal of Na^+ by the NKA.

With the increase of $[Glu]_{PsECS}$, EAAT1/2 transport rate is increased to remove glutamate from the PsECS, which also results in Na^+ being taken up. Furthermore, as $[Na^+]_{PsC}$ increases, the rate of Na^+ influx from the background channel decreases. All other channels remove Na^+ until $[Na^+]_{PsECS}$ reaches steady state conditions.

5.5 ECS K^+ and glutamate driven PsC microdomain formation

The previous two simulations have shown that K^+ or Na^+ microdomains form in the PsC when the system is stimulated with changes in K^+ or glutamate respectively. However, while these simulations show that our hypothesis could potentially explain experimental observations, we now wish to use our model to predict ionic dynamics at the PsC under physiological conditions where both K^+ and Glu are released at the presynaptic terminal. In these simulations K^+ is released by the neuron as before and a 100 µM puff of glutamate is released into the PsECS, with each spike event. Firing rates in the presynaptic neuron are 20Hz, 40Hz, 60Hz and 80Hz, for a period of 0.1min to 1min.

5.5.1 PsC membrane voltages and concentrations against time.

The results presented in Fig 5.3 show that the overall behaviour of the model, i.e. microdomain formation of K^+ in the PsC, occurs. The astrocyte membrane voltage V_A oscillates (~7mV amplitude) as shown in Fig 5.12 A).

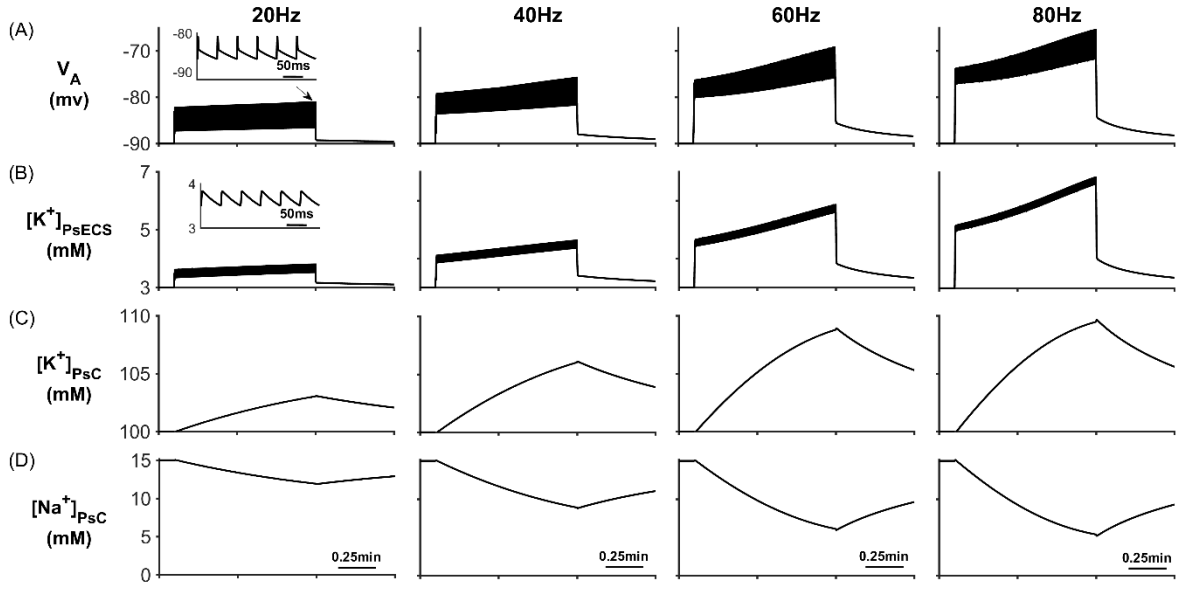

Fig 5.12. PsC membrane voltages and concentrations against time. (A) Astrocyte membrane voltage (V_A). (B) $[K^+]_{PsECS}$. (C) $[K^+]_{PsC.}$ transient. (D) $[Na^+]_{PsC}$ transient.

It can be observed in Fig 5.12 C-D that a K^+ microdomain is formed in the PsC and its magnitude increases with frequency while the magnitude of Na^+ reduces. This is due to the behaviour of the K^+ uptake by NKA dominating over the K^+ efflux pathways (See Fig 5.13).

5.4.2 Perisynaptic K^+ currents.

As stated above the astrocyte membrane voltage V_A oscillates (~7mV amplitude) as shown in Fig 5.12 A). This reversal is caused by the periodic reversal of the K_{ir} channel (See Fig 5.13A). The efflux of K^+ via the EAAT1/2 (Fig 5.13E) channel is caused by this reversal.

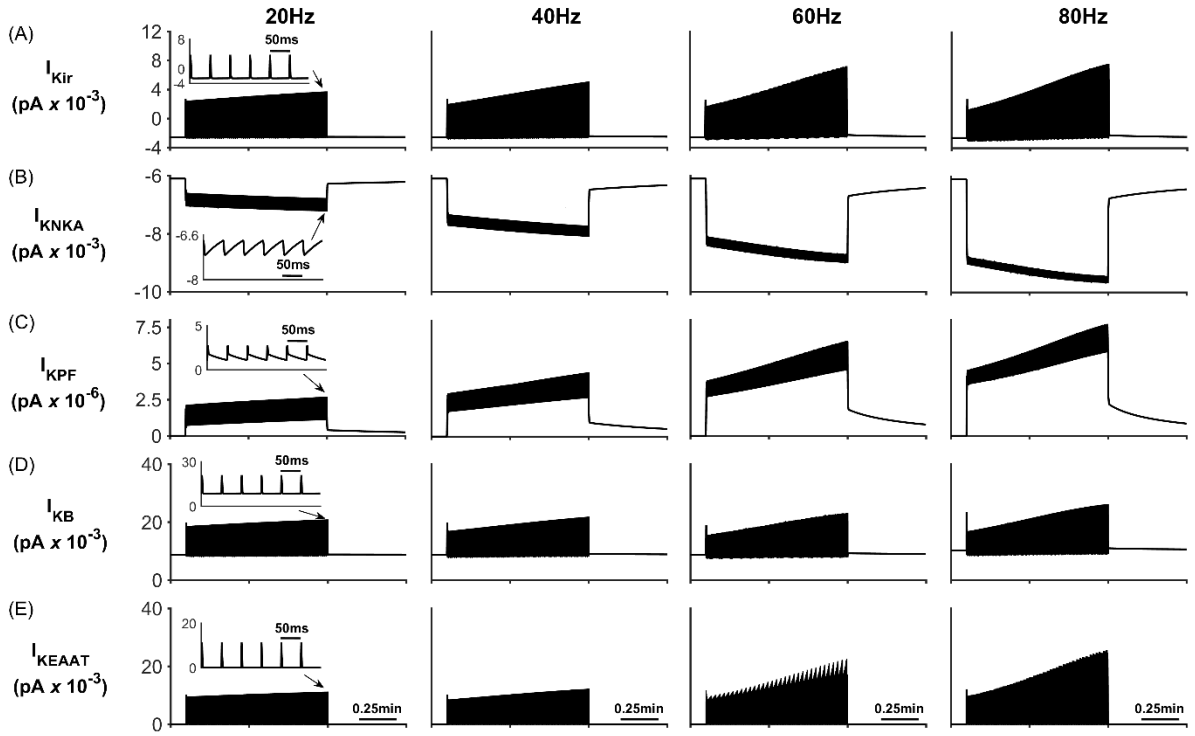

Fig 5.13. Perisynaptic K^+ currents. (A) K^+ K_{ir} current. (B) K^+ NKA current. (C) K^+ current along the process. (D) Background K^+ current. (E) K^+ EAAT current. Note: similar to the first simulation, as the neuron firing rate increases the magnitude of all currents also increase. The IKNA is orientated to drive an influx of K^+ and an efflux of Na^+ into the astrocyte soma, which is which due to its 3:2 Na^+ to K^+ stoichiometry is limited by the fixed Na^+ in the perisynaptic space.

5.5.3 K_{ir} Reversal (Neuron firing rate: 40Hz).

Moreover, the dynamic behaviour of the reversal potential of the K_{ir} and V_A continuously cause reversal of the overall polarity (Fig 5.14). This causes the K_{ir} channel to periodically reverse direction resulting in an efflux of K^+ into the ECS; this can be seen as oscillations in $[K^+]_{PsECS}$.

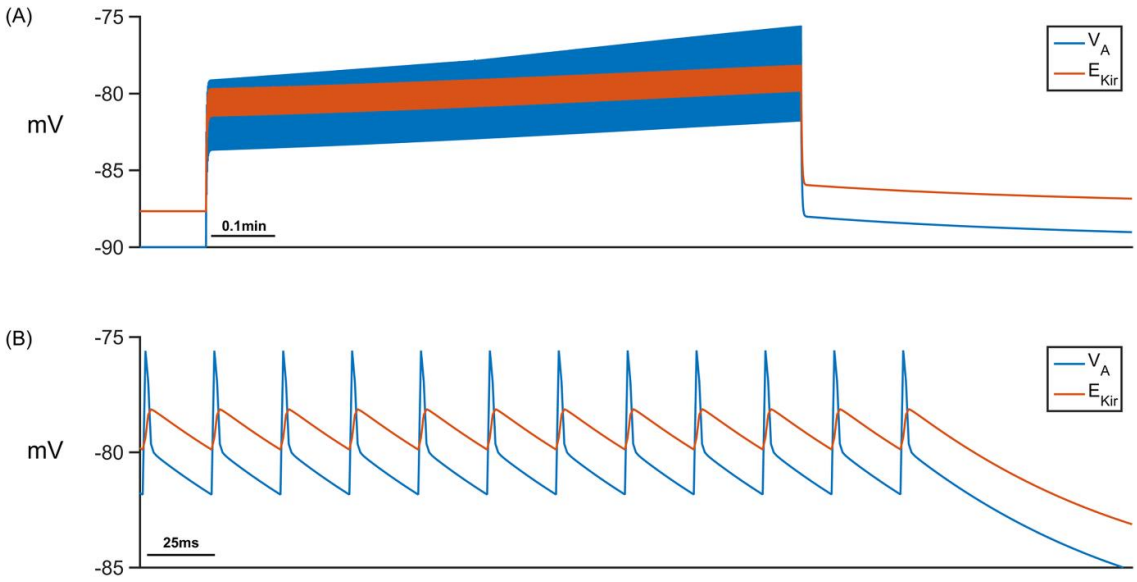

Figure 5.14. K_{ir} Reversal (Neuron firing rate: 40Hz). (A) The astrocyte membrane voltage (blue) and the K_{ir} reversal potential cross continually cross over during neuron stimulation. This results in periodic reversal of the K_{ir} channel. (B) Magnification of A for the last few hundred milliseconds of stimulation, time interval increased 240 times longer.

5.5.4 Perisynaptic Na^+ currents.

Fig 5.15 shows the Na^+ currents for the four different stimulus frequencies. As expected all Na^+ channels on the PsC membrane, except the NKA (Fig 5.15 B) which is aligned to transport Na^+ in the opposite direction in this membrane potential range, result in Na^+ influx to the PsC. I_{NaEAAT} has a large peak amplitude for a short duration (few milliseconds) due to the EAAT channel slowing down after removal of Glu from PsECS.

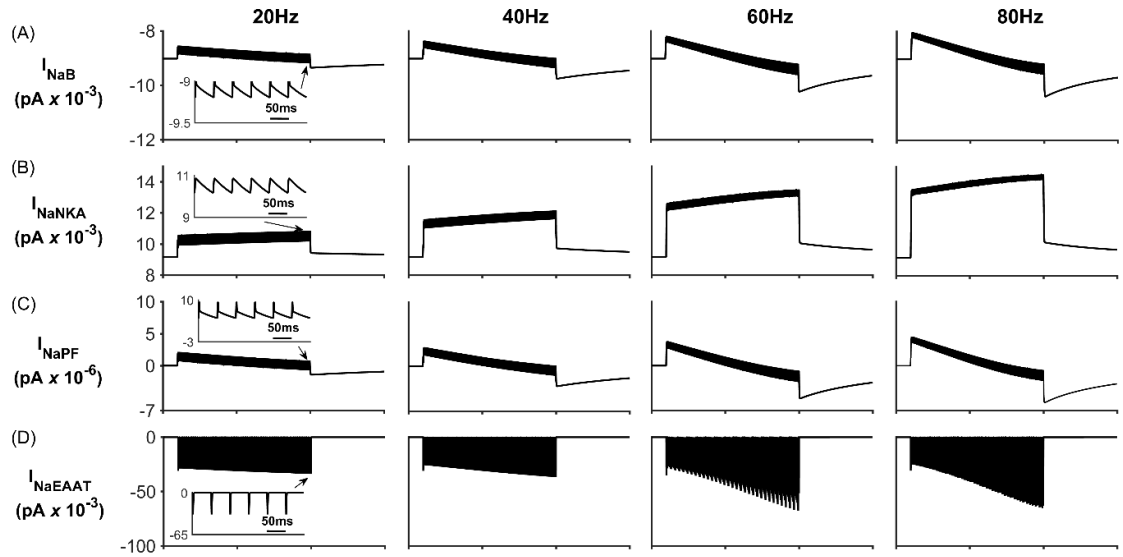

Fig 5.15 Perisynaptic Na^+ currents. (A) Background Na^+ current. (B) NKA current. (C) Na^+ current along the process. During neural activity, the NKA pumps Na^+ from the cell to allow for K^+ uptake, therefore there is a net decrease in $[Na^+]_{PsC}$. When the neuron stops firing, NKA slows down and there is a net uptake of Na^+ via the remaining channels.

5.5.1 Parameter sensitivity Analysis at 40Hz

Having analysed the formation of microdomains in the previous three simulations this thesis now explores the sensitivity of the model to its parameters. These parameters are PsC surface area, the maximum NKA pump rate, P_{max}, and the potential barrier to ion flow along the process, φ_w. In these simulations a neuronal firing rate of 40Hz was chosen.

A. Microdomain Sensitivity to PsC Surface Area (SA)

Three different values of PsC SA were chosen for this simulation; PsC SA × 0.75, PsC SA × 1 and PsC SA × 1.25. The results of these simulations are shown in Fig 5.16 where it is clearly shown that the amplitude of the K^+ microdomain increased with PsC SA with a corresponding drop in the concentration of Na^+. This is expected because more K^+ is being removed from the extracellular space as the area increases.

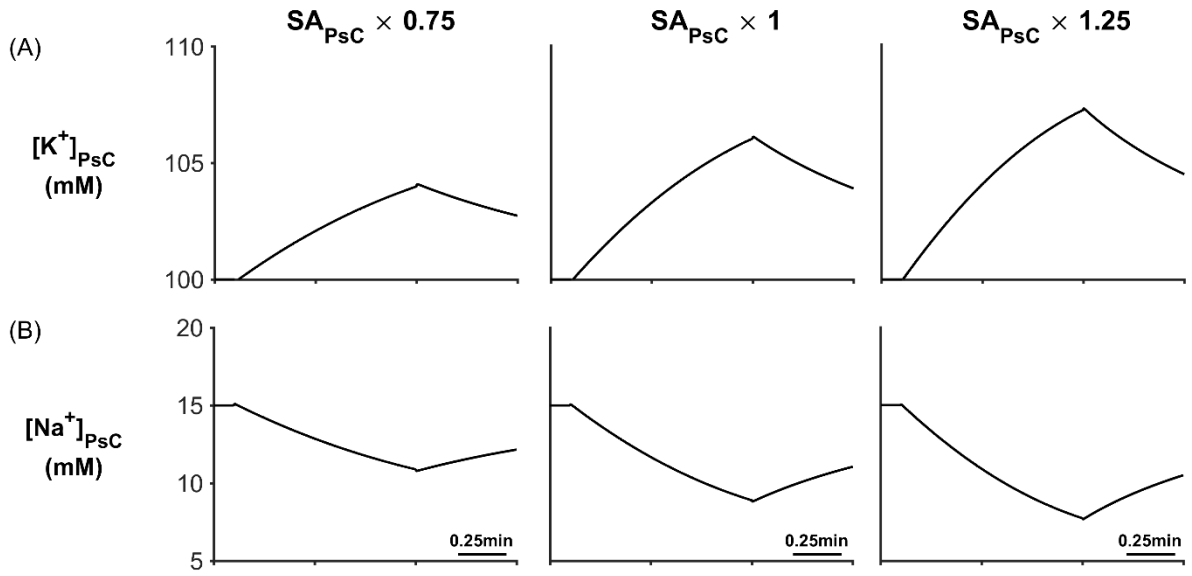

Fig 5.16. Microdomain formation for different PsC surface areas. (A) PsC K^+ concentration. (B) PsC Na^+ concentration. As the PsC surface area increases so the amplitude of the K^+ microdomain increases and the Na^+ microdomain amplitude decreases.

B. Microdomain Sensitivity to P_{max}

Four different values of P_{max} were chosen for this simulation; $P_{max} \times 0.2$, $P_{max} \times 0.5$, $P_{max} \times 1$ and $P_{max} \times 5$. The results of these simulations are shown in Fig 5.17 where it can clearly be seen that $[K^+]_{PsC}$ and $[Na^+]_{PsC}$ is strongly dependent on P_{max}.

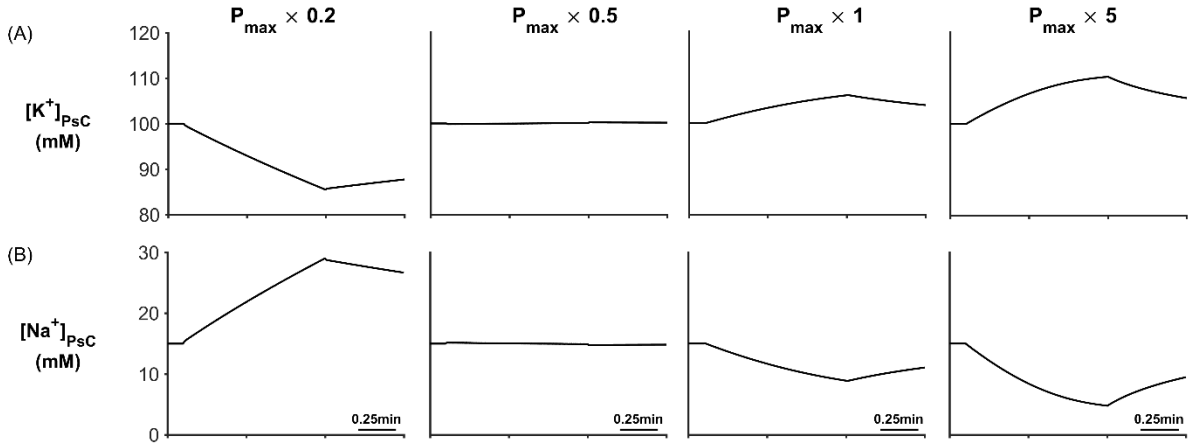

Fig 5.17. Microdomain formation for different values of NKA maximum pump rate: (A) $[K^+]_{PsC}$ as a function of Pmax and (B) $[Na^+]_{PsC}$ as a function of Pmax.

Using the P_{max} x 0.2 value causes $[K^+]_{PsC}$ to decrease and $[Na^+]_{PsC}$ to increases and as P_{max} increases, $[K^+]_{PsC}$ begins to form a microdomain with $[Na^+]_{PsC}$ steadily decreasing. From these simulations it can be concluded that when the NKA pump rate is low it is no longer the dominant co-transporter and both the EAAT co-transporter and K_{ir} channel dictate $[K^+]_{PsC}$ and $[Na^+]_{PsC}$ dynamics. The opposite is true when the pump rate is large.

C. Microdomain Sensitivity to φ_w

In this simulation φ_w was varied from 4 k_BT to 15 k_BT. Fig 5.14 shows the peak K^+ current along the process for the different values of φ_w. As φ_w is decreased, the peak current along the process increases exponentially. Therefore, with decreasing φ_w the formation of a microdomain becomes less likely as $I_{KPF,max}$ is increasing and eventually $I_{KPF,max}$ approaches an electro-diffusion limited model there is no likelihood of a microdomain forming at the PsC.

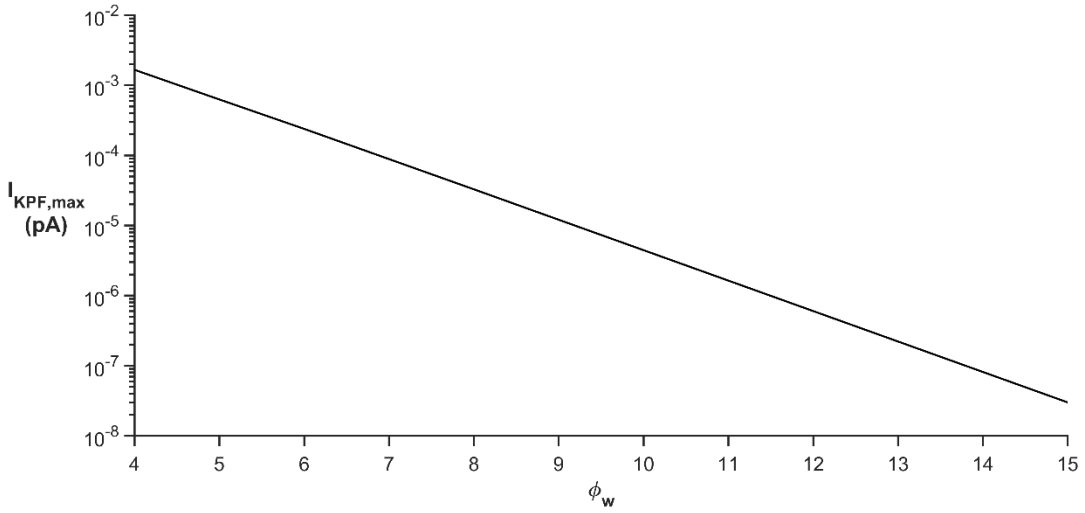

Fig 5.18. Peak K^+ current along the process for different values of φ_w.

These simulations add weight to our hypothesis as $I_{KPF,\max}$ decreases with increasing ϕ_w. It is also clear that the PsC SA can limit the maximum amplitude of the microdomain concentration. This is due to the increase/decrease of ion channel densities on the membrane of the PsC. Moreover, the NKA maximum pump rate also has an important role in the formation of microdomains whereby if the pump rate is low then K^+ clearance by NKA weakens; effectively these to ion transporters compete to move K^+ and Na^+ ion across the membrane but in opposite directions.

5.6 Discussion

In the previous chapter, it was proposed that ion retention within thin astrocyte processes can give rise to the formation of K^+ and Na^+ microdomains at the PsC. This localisation of astroglial ionic microdomains arises because in thin processes, surface conduction dominates over volume conduction, and because membrane lipids are negatively charged, deep potential wells form near the dipole heads restricting the flow of ions along the process. Therefore, ions must hop from well to well which restricts conduction along the membrane. This hopping effectively semi-isolates the PsC from the astrocytic main body allowing the formation of K^+ and Na^+ microdomains at the PsC under different conditions. Ionic responses of the PsC to the neuronal excitation were modelled and it resulted in an increase in K^+ concentration in the synaptic cleft. A series of simulations were carried out where glutamate in the cleft was held constant at the background level and, during neuronal excitation, K^+ was released into the PsECS leading to a depolarisation of the PsC membrane voltage due to ionic currents flowing through the PsC membrane. The simulations demonstrate that a K^+ microdomain formed at the PsC due to the restricted flow of these ions along the astrocyte process. It was further contemplated that the K^+ microdomain provides the driving force for the return of K^+ to the PsECS via background K^+ channels for uptake by the neuron via its NKA. Essentially, K^+ is transiently "stored" at the PsC during neuronal excitation where it decreases the electrochemical gradient of K^+, so reducing inward flow of K^+ through K_{ir}; this "stored Potassium" is then available to replenish neuronal K^+ levels when the excitation ceases, thereby preventing K^+ undershoot in the extracellular space (See Appendix 2).

The model also shows that the influx of Na^+ ions into the astrocyte process causes a Na^+ microdomain to form at the PsC where the decay rate of Na^+ is governed by the NKA. In this simulation, there is no neuronal excitation and the concentration of glutamate in the cleft was modulated using a Gaussian function and was taken up at the PsC by EAAT1/2. A slow decay of Na^+ was observed after the glutamate uptake ceased which is in strong agreement with experimental observations [39], [41]. Having simulated and analysed the formation of microdomains the sensitivity of the model to PsC surface area, maximum NKA pump rate, P_{max}, and the potential barrier to ion flow along the process, φ_w was investigated. From these simulations it is clear that the mechanism responsible for the formation of microdomains is the well formation along the process which effectively semi-isolate the PsC from the astrocyte soma when φ_w is 10 k_BT or greater. It is also clear that the PsC SA can limit the maximum amplitude of the microdomain concentration. This is due to the increase/decrease of ion

channel densities on the membrane of the PsC. Moreover, the NKA maximum pump rate also has an important role in the formation of microdomains whereby if the pump rate is low then K^+ clearance by NKA weakens; effectively these to ion transporters compete to move K^+ and Na^+ ion across the membrane but in opposite directions.

In summary, we accept the model for ion retention in thin astrocyte processes requires much more refinement. For example, the main challenge would be to account for the dynamic interaction between the fixed charge present in membrane proteins and the free ions in the astrocyte cytoplasm. Additionally, the dimensions of the astrocyte membrane are such that the membrane proteins are unlikely to be represented by point charges and a more atomistic view of the proteins would need to be found to create a map of the charge distribution at the atomic scale.

Also, any simulations would require a large number of atoms to be taken into account to obtain the electrostatic potential profile at the membrane-cytoplasm interface. Once the electrostatic potential in thin process is found and combined with the ion distribution, then the movement of ions can be modelled. Moreover, we have only considered K^+ and Na^+ ions in the model and therefore a more biophysical model would need to consider Ca^{2+} microdomains and Cl^- ion dynamics with the inclusion of the associated membrane transporters such as Sodium/Calcium exchanger and Sodium/Potassium/Chloride cotransporter.

An infinite Global Extracellular Space (GECS) has been assumed in this work, but this in reality this would not be the case. However, more biological data about the shape and size of extracellular spaces and morphology of the perisynaptic cradle is required. Despite this the model does however indicate that the morphological and biophysical properties of the astroglial perisynaptic processes facilitate emergence of Na^+ and K^+ microdomains that are essential for astroglial homeostatic support of synaptic transmission in the CNS, and also points to our new hypothesis and important implications for K^+ homeostasis during pathological activity such as seizures. Indeed, the model supports the existence of a mechanism that prevents local K^+ depletion during excessive neuronal firing and indicates a novel mechanism by which astrocytes maintain neuronal excitability during pathological activity.

In the next chapter we will build on the research presented in this chapter by investing the relationship between Na^+ and Ca^{2+} in the PsC.

6.

Ca^{2+} Microdomain Formation due to NCX Reversal.

6.1 Introduction

In the previous chapter and the accompanying paper [3] the issue of whether in thin (<100nm) astrocytic processes negatively charged ions dominate the flow of ions in PAP's was addressed. The results show that free cytosolic ion retention by traps, resulting from the negative fixed ions, can potentially explain the transient Na^+ and K^+ microdomains observed at perisynaptic complexes. This section aims to further develop this model with the inclusion of Ca^{2+} ions to test whether the reversal of the sodium/calcium exchanger (NCX) due to the Na^+ microdomain, leads to the formation of a Ca^{2+} microdomain in the perisynaptic compartment. Moreover, the Ca^{2+} microdomain is remote from any Endoplasmic Reticulum (ER) mediated Ca^{2+} release and we propose that this local source of Ca^{2+} may provide a previously under explored form of astrocyte Ca^{2+} signalling.

The synapse and PsC contain various ionic channels, exchangers and pumps to provide homeostasis and dynamic exchange of ions between the two cells and extracellular space and is described in Fig 6.1.

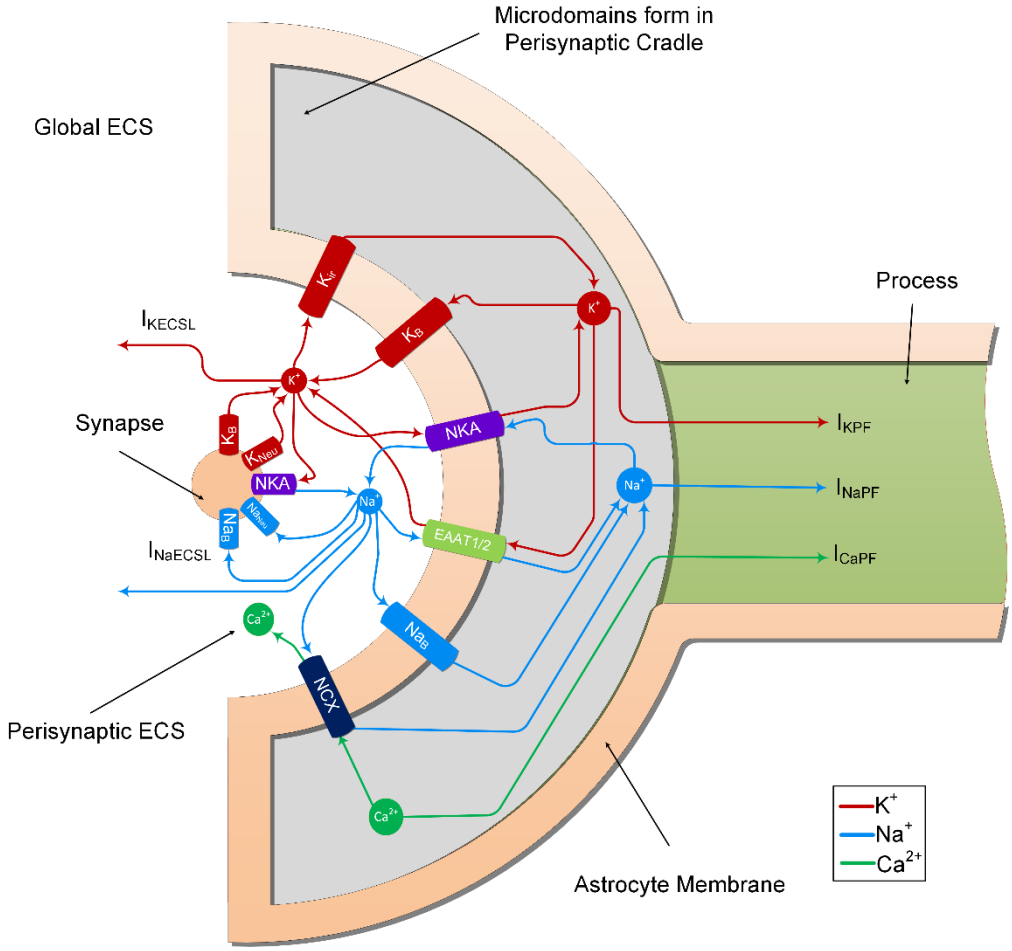

Fig 6.1 Ion transport machinery of the perisynaptic and synapse. It can be seen that the synapse and PsC contain various ionic channels, exchangers and pumps to provide homeostasis and dynamic exchange of ions between the two cells and extracellular space. The new complete model contains 11 transport mechanisms which move ions across the cellular membranes.

The neurone exchanges K^+ and Na^+ with the PsECS via a voltage-controlled potassium channel (K_{Neu}), voltage-controlled sodium channel (Na_{Neu}), a sodium potassium pump (NKA_{Neu}), a potassium background channel (KB on the synapse) and a sodium background channel (Na_B on the synapse). The astrocyte exchanges Na^+, K^+, and Ca^{2+} with the PsECS via a background sodium transport (Na_B on the astrocyte), potassium background transport (K_B on the astrocyte), potassium inwardly rectifying channel (K_{ir}), Na^+-K^+-ATPase (NKA), a glutamate-sodium-potassium cotransporter (EAAT1/2), and the NCX. In both the astrocyte and neurone models we define Na^+ and K^+ background channels; although modelled as a single transport channel for each ion, these background channels represent a lumped model for Na^+ and K^+ transport,

taking into account a multitude of astrocytic process to the soma. IK_{PF}, INa_{PF} and ICa_{PF} model the current flow of K^+, Na^+ and Ca^{2+} along the process to the soma. IK_{ECSL} and INa_{ECSL} models the K^+ and Na^+ currents generated by K^+ and Na^+ leaking from the Ps_{ECS} to the G_{ECS}. The mathematical descriptions of the ionic exchanges between a neurone and an astrocyte at the PsC are now presented.

In this section we carry out a series of simulations that demonstrate the formation of Ca^{2+} microdomain at the perisynaptic complex (PsC). The simulations will show that the Ca^{2+} microdomain is a direct results of ion retention along the thin astrocyte process. We have shown in the previous chapter and a recent paper [3] that ion retention underpins Na^+ and K^+ microdomain formation at the PsC during physiological neuronal excitation and in this chapter, we show that the uptake of Na^+, via EAAT channels during neuronal stimulus, creates the formation of a Na^+ microdomain in the PsC thereby causing the NCX to reverse. This in turn creates an uptake of Ca^{2+} via the NCX and a microdomain of Ca^{2+} is formed in the PSC.

6.2 NCX reversal under biophysical stimulus

To explore the reversal of the astrocyte NCX, a series of simulations with the presynaptic neuron stimulated using an external current to produce firing rates of 20Hz, 40Hz, 60Hz and 80Hz respectively were performed. The neural stimulus has a duration of ~1 minute where the first 0.1 minute allows the model to reach a steady state condition and the stimulus ceases after 1min. This long stimulus period allowed us to investigate what effect sustained neural activity would have on the intracellular/extracellular ionic concentrations. In these simulations PsECS Ca^{2+} is held constant, however K^+ is released and Na^+ is allowed to change via the neuron and astrocyte K^+ and Na^+ channels. Each time the neuron spikes, the PsECS Glu concentration is set to 1mM for 3ms and is then reset to baseline concentration. Furthermore, the astrocyte membrane voltage is held constant at ~ -80mV, this is widely accepted to be a common resting potential for astrocytes and interestingly is also very close to the reversal potential for the NCX. Therefore, during periods of homeostatic rest the NCX currents are virtually silent and there is no flow of Ca^{2+} or Na^+ across the membrane.

The results presented in Fig 6.2 A show that during periods of neural stimulus a K^+, builds up in the PsECS and is buffered away by the astrocyte which results in a K^+ microdomain formation at the PsC (Fig 6.2 B). At the start of the neural stimulation, there is a transient loss of Na^+ from the PsECS (Fig 6.2 C). This is caused by both the neuron and astrocyte removing

Na^+ from the PsECS. Furthermore, the transport of Na^+ across the astrocyte membrane via Na^+ background channels and EAAT channels results in a Na^+ microdomain formation (Fig 6.2 D).

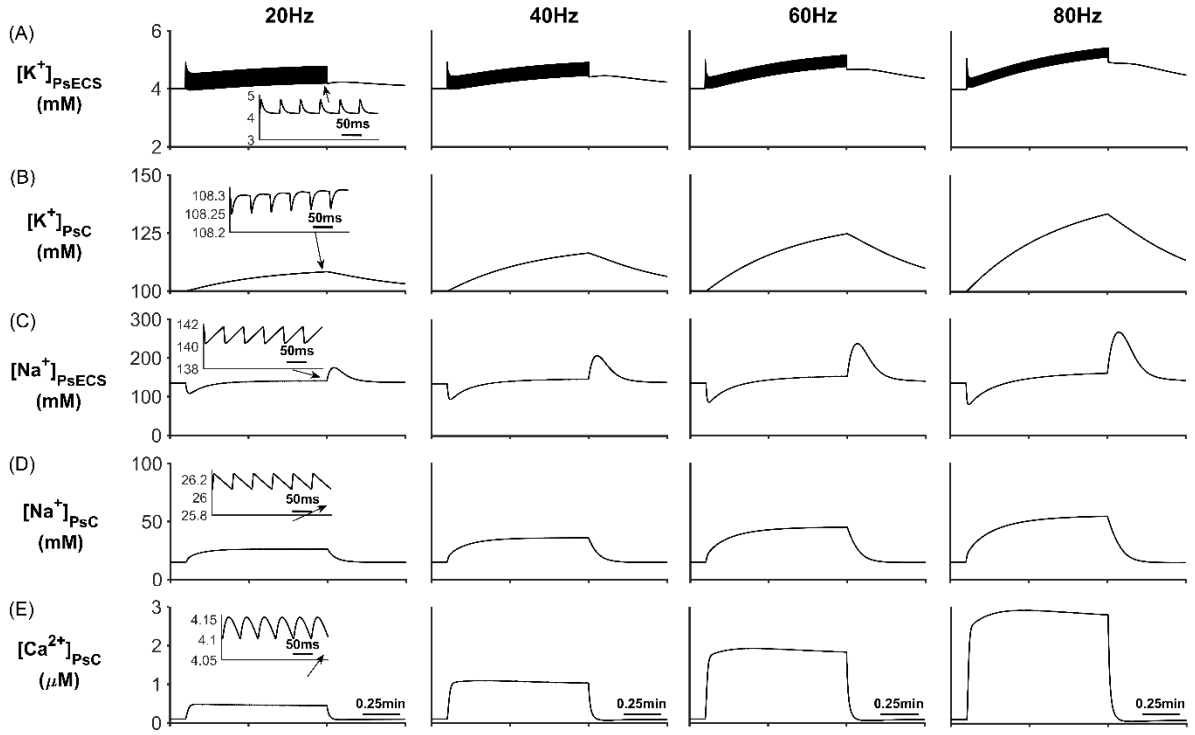

Fig 6.2. Astrocyte PSC and PsECS ion concentrations A) $[K^+]_{PsECS}$ B) $[K^+]_{PsC}$ C) $[Na^+]_{PsECS}$ D) $[Na^+]_{PsC}$ E) $[Ca^{2+}]_{PsC}$

In addition to Na^+ and K^+ microdomain formation, it is clear from Fig 6.2 E that a local PsC Ca^{2+} microdomain is also formed. This Ca^{2+} microdomain is formed even in the absence of an ER region which are widely believed to be essential for astrocyte calcium dynamics [189] [190]. The microdomain of Ca^{2+} is caused by the reversal of the NCX which causes Ca^{2+} influx in exchange for astrocytic Na^+ efflux. This can be seen in the INCX currents in Fig 6.3 C where the only Ca^{2+} influx pathway is via the NCX. The complete reversal of the NCX is due to the sudden changes in $[Na^+]_{PsEC}$ during neuronal stimulation onset as the astrocyte membrane is held constant as shown in Figure 6.2 D.

Fig 6.3 presents the Na^+ currents associated with the astrocyte. The main pathway for Na^+ efflux from the astrocyte is the NAK (Fig 6.3 A) and the Na^+ background channel (Fig 6.3 D), While the main pathway responsible for Na^+ uptake is the EAAT (Fig 6.3 B).

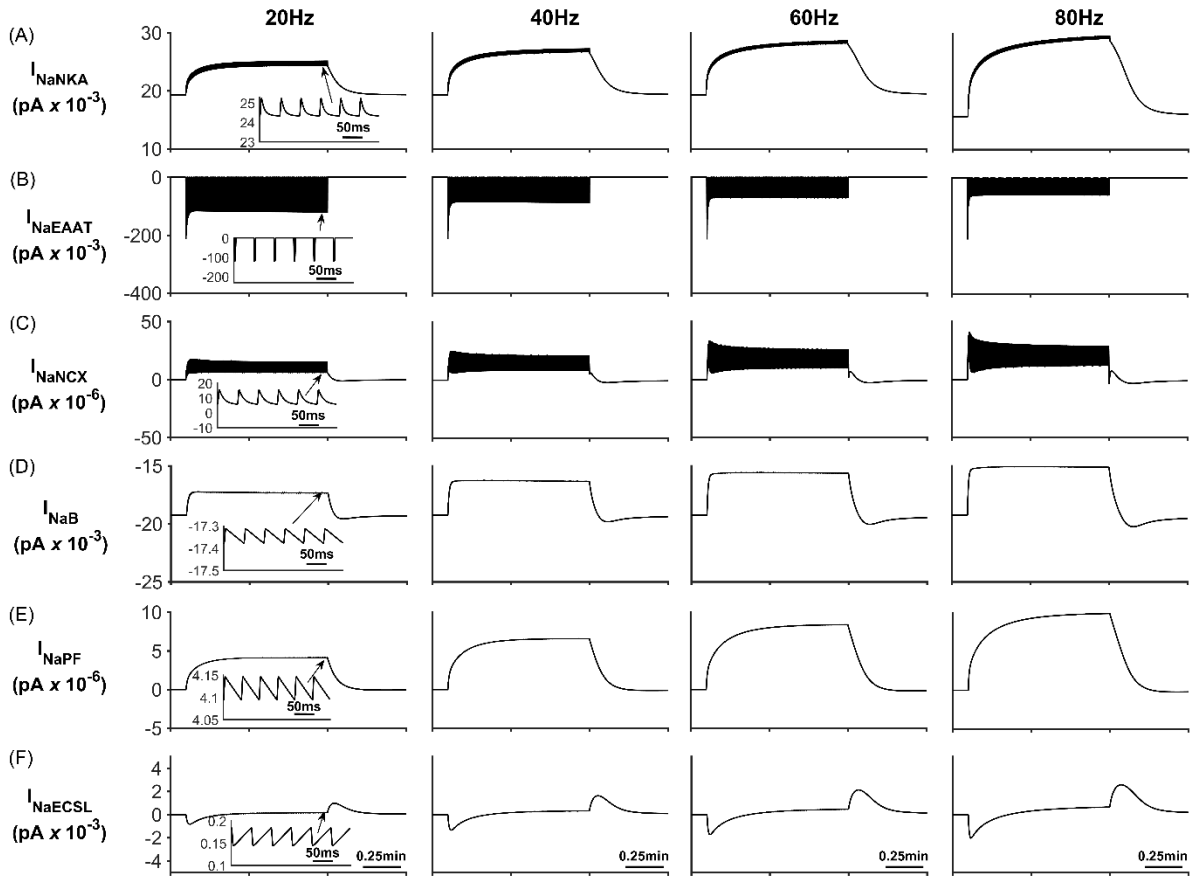

Fig 6.3. Astrocyte Na^+ currents. A) I_{NaNKA} B) I_{NaEAAT} C) I_{NaNCX} D) I_{NaB} E) I_{NaPF} F) I_{NaECSL}

The transient loss of Na^+, observed in the PsECS results in the previous set of graphs (Fig 6.2 C), is caused by the EAAT, which has a very fast initial rate (Fig 6.3 B). This fast initial EAAT Na^+ transport, compared to the slower NAK and NaB transport rates, tips the transport uptake/release balance in favour of inward transportation and starts the formation of a Na^+ microdomain. As the EAAT slows down and the NAK and NaB speeds up, due to the increased Na^+ concentration in the PsC, the influx/efflux Na^+ pathways once again reaches a state of equilibrium and the microdomain of Na^+ remains at a stable concentration. It is also noted that as Na^+ increases in the PSC, the NCX works in reverse mode to try and remove some of the Na^+ from the PsC. Fig 6.3 E-F show the Na^+ currents along the process and between PsECS and GECS respectively. Since the efflux of Na^+ via the process is several orders of magnitude smaller than the other Na^+ currents this is the main driving force for the creation of the Na^+ microdomain in the perisynaptic cradle. Moreover, as the PsECS Na^+ concentrations change the leak current (I_{NaECSL}) between the PsECS and GECS attempts to maintain the Na^+ levels in the PsECS.

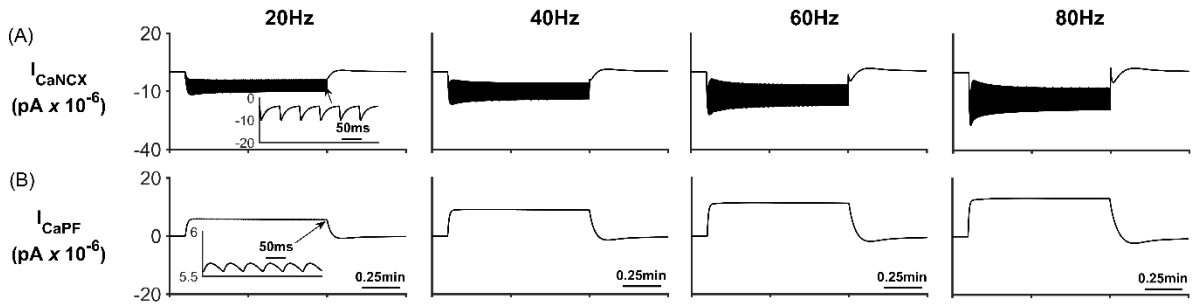

Fig 6.4. Astrocyte Ca^{2+} currents. A) NCX Ca^{2+} current B) Process Calcium Current due to Hopping Effect.

Fig 6.4 describes the astrocytic Ca^{2+} currents; again it can be seen that during neural stimulation, the influx of Na^{+} causes the NCX to work in reverse mode and therefore there is an influx of Ca^{2+} (Fig 6.4 A). The only efflux pathway for Ca^{2+} is via the thin astrocyte process which is also governed by the well hopping mechanism described earlier [3] (Fig 6.4 B). Therefore, the efflux pathway is weaker than the influx pathway which results in a microdomain of Ca^{2+} forming, as seen in Fig 6.2 E.

6.2.1 Astrocyte K^+ currents.

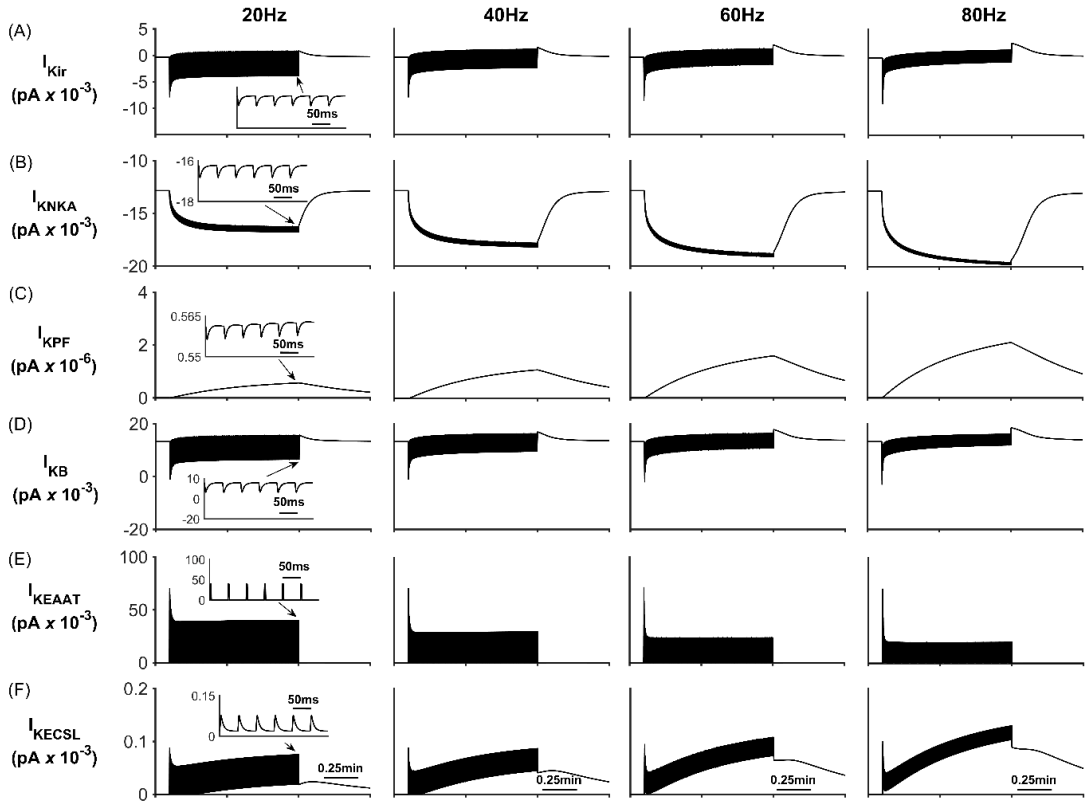

Fig 6.5. Astrocyte K^+ currents. (A) K^+ K_{ir} current. (B) K^+ NKA current. (C) K^+ current along the process. (D) Background K^+ current. (E) K^+ EAAT current. (F) ESC K^+ leak current

The K^+ currents behave in a similar manner as previously described in [3]. Again, the NKA is the main influx pathway with the K_{ir} in a constant state of transition between forward and reverse mode during neuronal stimulus. When neural stimulus ceases, the K_{ir} works in reverse mode (See Fig 6.5A) along with efflux of K^+ via the K^+ background channels to bring the PsC levels of K^+ back to the initial resting state.

6.2.2 Glutamate concentrations and currents.

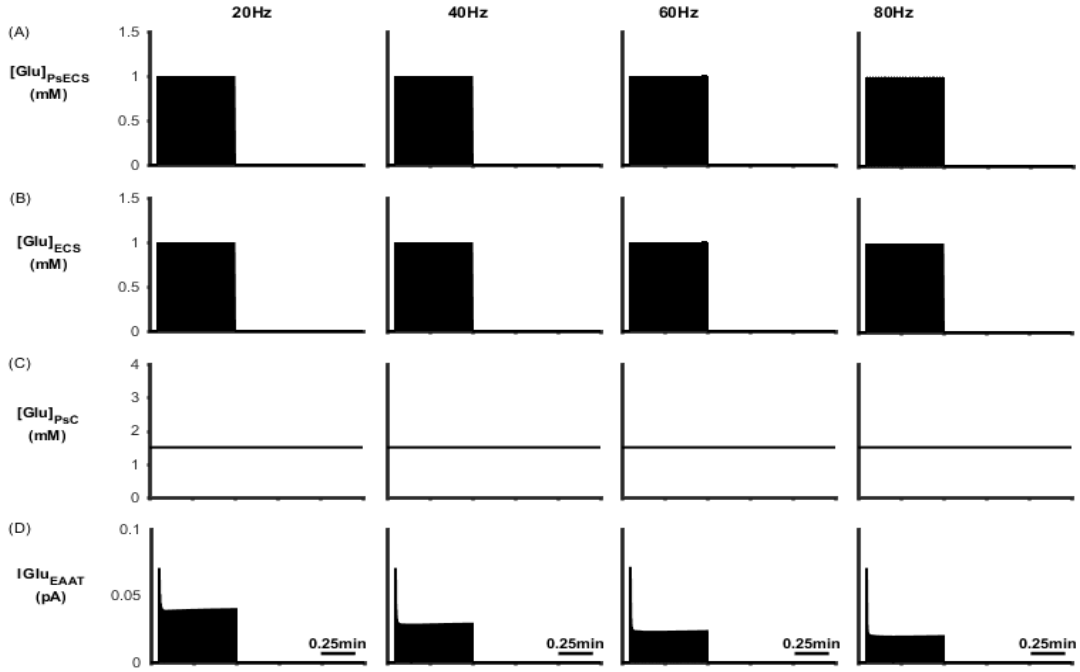

Figure 6.6 Glutamate concentrations and currents. (A) Glu Ps_{ECS} concentration. (B) Glu ECS concentration. (C) Glu concentration in the PsC. (D) Glu EAAT current.

Each time the neuron spikes, the PsECS glutamate concentration is set to 1mM for 3mins and is then reset to baseline concentration as demonstrated in Figure 6.6 A-B, this means that changes in the glutamate concentration in the process drive any change in glutamate concentration. Given that glutamate concentrations are higher on the inside of the process than in the ECS, there is a small decay in the rate of the EEAT uptake during the spike interval. This is due initially to the near 0 mV reversal potential for glutamate ions at the EAAT between the PsC and the process.

6.2.3 Process Reversal Potentials

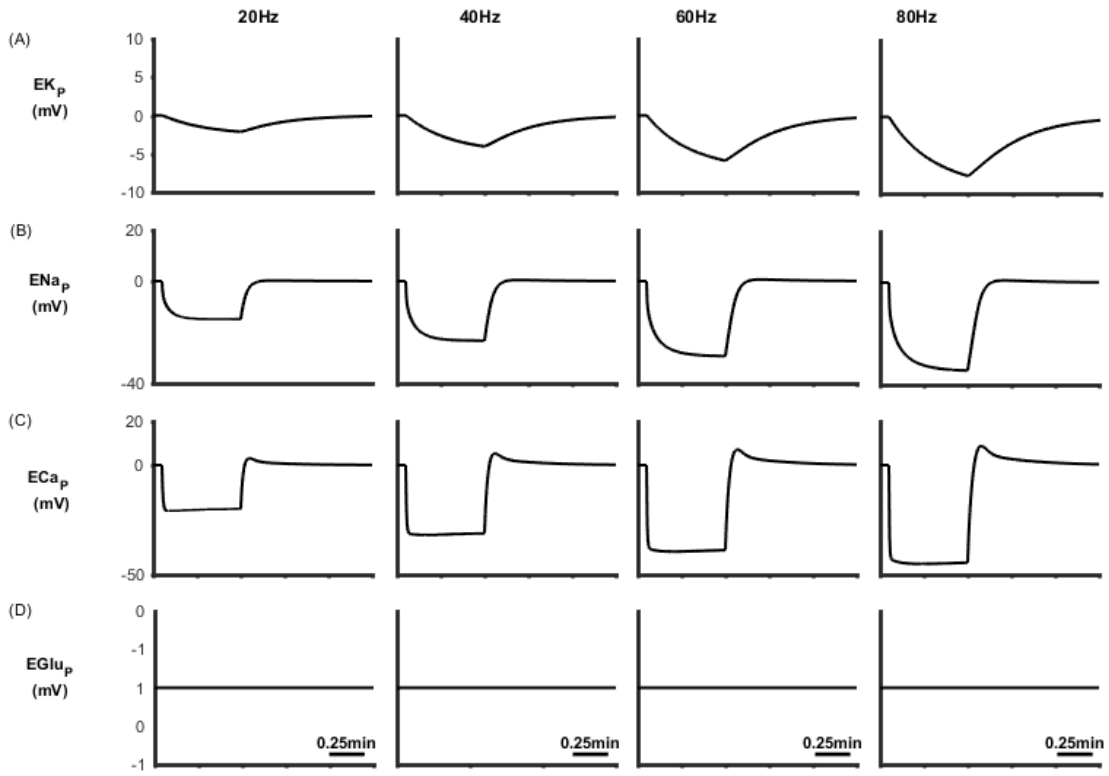

Figure 6.7 Process Reversal Potentials for K^+, Na^+, Ca^{2+} and glutamate at different frequencies: A) K^+, B) Na^+, C) Ca^{2+} and D) glutamate

Figure 6.7 shows the process reversal potentials for K^+, Na^+, Ca^{2+} and glutamate at different frequencies. Similar to that shown in Figure 5.7A, Figure 6.7A shows that the reversal potential for K^+, PRP_K, continually decreases with increasing presynaptic neuron activity, but under these conditions drops to approximately -8.0mV at 80Hz. This is due to the much stronger NKA current, which is changed because the Na^+ concentration in the PsECS is no longer held constant at the baseline level. Another reason is that additional Na^+ current flows are present in this model like the NCX and EAAT allowing a greater flow of Na^+ ions. As shown in Figure 5.7A before, Figure 6.7A similarly shows that when the presynaptic stimulus stops at 1 min PRP_K has reached this maximum and thereafter begins to return to a baseline level of zero. This reversal is because once again NKA is saturated and pumps K^+ from the PsECS to the PsC at a constant rate across all frequency ranges, affecting the strength of the K^+ microdomain. The effects of the stronger NKA current is also seen in the change of the process reversal potential for Na^+. NCX works in reverse mode to try and remove some of the Na^+ from the PsC

increasing Na^+ in the PSC as Fig 6.3 E and 6.3F show. At 80Hz the PRP_{Na} is saturated at approximately -35 mV due to the accumulation of $[Na^+]_{PsC}$ while the neuron is firing.
The process reversal potential for Ca^{2+} is governed by the NCX influx dominating over efflux via the astrocyte process. Gradually Ca^{2+} efflux when the NCX (Fig 6.4.A) operates in forward mode again as shown in (Fig 6.4.B).

6.2.4 Background Channel Reversal Potentials for K^+ and Na^+ at different frequencies

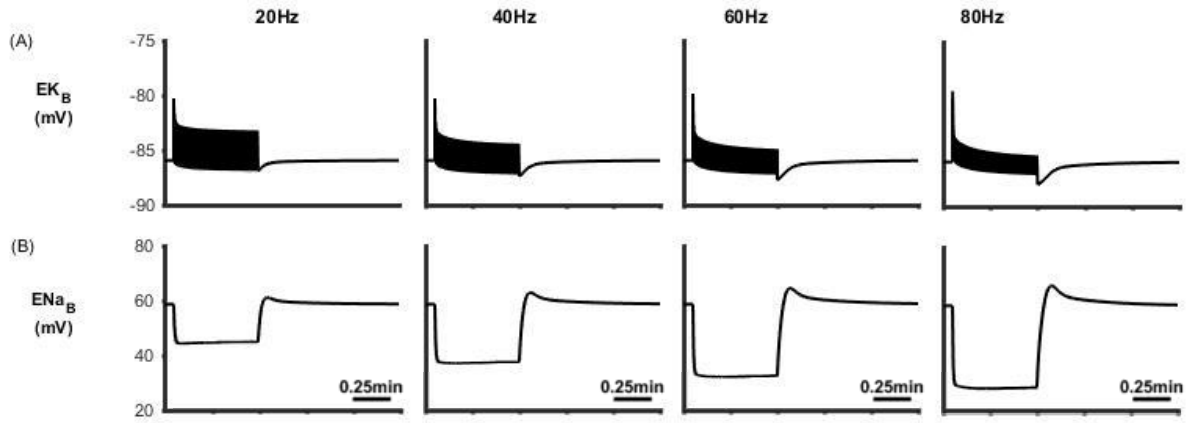

Fig 6.8 Background Channel Reversal Potentials for K^+ and Na^+ at different frequencies: A) K^+, B) Na^+

Figure 6.8 A) The shape of this reversal potential curve is driven by the background K^+ current which itself is driven by the K_{ir} channel being in a constant state of transition between forward and reverse mode during neuronal stimulus. This is shown in Figure 6.8 A. The background channel reversal potential for K^+ Efflux of K^+ via the K^+ background channels to bring the PsC levels of K^+ back to the initial resting state.

Figure 6.8 B) The shape of the reversal of the ENa_B potential is due to the INa_B being in competition for available Na^+ ions with EAAT. Initially EAAT Na^+ transport is faster than the Na_B transport rates and that tips the transport uptake/release balance in favour of inward transportation and a Na^+ microdomain forms as the EAAT current slows down and the Na_B current speeds up, due to having a higher Na^+ concentration in the PsC for a longer duration. When the influx/efflux Na^+ pathways once again reaches a state of equilibrium, the reversal potential returns close to its equilibrium value. The absence of Ca^{2+} and glutamate background channels means that the background reversal potential for these ions are zero.

6.3 Discussion

This chapter tested the concept that glutamate transporters and NCX working together are sufficient to create local Ca^{2+} microdomains in astroglial perisynaptic compartments.

The model demonstrates that stimulation of astrocytes with glutamate, mimicking neuronal activity generates substantial Na^{+} influx, which form a local microdomain due to the previously suggested mechanism of ion retention. In this situation cation retention in wells dominates over conventional electrochemical diffusion [3] [191]

Moreover, the generation of Ca^{2+} microdomains have previously been reported but the underlying ionic fluxes (and channels/transporters contributing to) have not been examined. This study has identified the molecular targets and their relative contributions to the formation of a Ca^{2+} microdomain in the absence of an ER region. Specifically, the Na^{+} microdomain switches the NCX into reverse mode, thus generating Ca^{2+} influx which is sufficient to produce relevant focal Ca^{2+} signals.

In essence only the EAAT, EKA and NCX are necessary and sufficient for the development of a Ca^{2+} microdomain: note that to avoid rapidly increasing Ca^{2+} concentrations within the cradle, with increasing neuronal frequency, this model would require a Ca^{2+} efflux pathway, and a likely candidate is the PMCA pump.

These mechanisms, which do not depend on intracellular sources for Ca^{2+} directly links neuronal activity and glutamate release to the formation of Na^{+} and Ca^{2+} microdomains in the perisynaptic astroglial processes, which are instrumental for generation of astroglial homeostatic response critical for maintenance of synaptic transmission.

7.

Conclusions

7.1 Summary of the Thesis

This thesis proposed that in thin astrocyte processes with large surface to volume ratio, fixed negative charges existing in inner process membrane will be the dominant ion conduction mechanism. Specifically, it was hypothesised that these negative charges give rise to potential wells and therefore ions must hop from well to well as they move along the thin astrocyte process. Consequently this low conductance pathway serves to semi-isolate the astrocytic perisynaptic cradle (PsC) from the astrocytic main body. This thesis showed, for the first time, that this low conductance pathway could explain the formation of K^+ and Na^+ microdomains at the PsC which points to a new theory for K^+ clearance. It has been widely reported [142] [53] that excitatory presynaptic neurons release K^+ into the extracellular space (ECS) which is subsequently cleared at the PsC and buffered away through diffusion to the main astrocyte body. However, this thesis proposed that the flow of K^+ away from the PsC is not volume diffusion limited, but rather is restricted due to the hopping effect along the process, and therefore a K^+ microdomain forms at the PsC during sustained presynaptic neuronal excitation: effectively the PsC acts as a K^+ store during neuronal excitation.

Chapter two reviewed existing biophysical studies on the structure and physiology of neurons and glia cells. Neurons are specialised for rapid communication in the body, while the smaller but more common neuroglial cells carry out a broad range of ancillary functions [62] [63] [64]. Among the neuroglial cells are astrocytes, which along with neurons form the presynaptic cradle which is of particular interest in this thesis: the cradle region is studied in the context of ionic homeostasis. The main focus was the effect of fixed negative charges in astrocyte processes where it is known that biological membranes consist of a continuous bilayer of lipid molecules and embedded membrane proteins. These bilayers are fluid with polar and non-polar portions in their structure are described as amphipathic. Fixed charges within the cell are due to phosphatidylserine (which carries a net negative charge) would have an impact on the diffusion rates of free cytosolic ions. This chapter also focuses on K^+ buffering and the role of volume changes in buffering.

Chapter three reviewed existing computational models of astrocytes, which is essential to the understanding of the interactions between transport processes within the brain and between cells. To-date available models are almost entirely focused on a single astrocyte, their interaction with neurons, volumetric changes within the astrocyte and detailed models of mitochondrial metabolism. Many of these computational models provided the physiological and structural data required to create the simulations used in this thesis as well as providing insights into biological realism.

Chapter four focuses on the development of a new model for ionic homeostatic at the PsC. The major contribution of this chapter focused on the derivation of models that support the hypothesis that fixed negative charge situated at, or close to, the inner side of the process membrane causes ionic hopping along the process in thin astrocytic processes. This is because these negative charges sets up potential wells along the process which traps ions momentarily thus causing ionic retention. To explore the effects of ionic retention in thin astrocytic process, a multi-compartmental model was developed consisting of a single synapse surrounded by an astrocytic perisynaptic complex (PsC). The new complete model contains 11 transport mechanisms which move ions across the cellular membranes. A neuronal model was also developed which exchanges K^+ and Na^+ with the PsECS via a voltage-controlled potassium channel (K_{Neu}), voltage-controlled sodium channel (Na_{Neu}), a sodium potassium pump (NKA_{Neu}), a potassium background channel (K_B on the synapse) and a sodium background

channel (Na_B on the synapse). The complete model facilitates a theoretical based investigation of ionic homeostatic at the PsC in the presence or neuronal firing, and these simulations were the subject of the following two chapters.

Chapter five provided simulation results, based on the models outlined in chapter 4, which support the hypothesis that ionic retention within astrocyte processes gives rise to K^+ and Na^+ microdomains at the PsC. These simulation results are supported by experimental data available in the literature and also pointed to a new theory for K^+ clearance, which strongly suggests that K^+ clearance is a locally restricted phenomenon. This finding challenges the orthodox view of the role of glial spatial potassium buffering during pathological activity. Indeed, the model supports the existence of a mechanism that prevents local K^+ depletion during excessive neuronal firing and indicates a novel mechanism by which astrocytes maintain neuronal excitability during pathological activity. Having simulated and analysed the formation of microdomains the sensitivity of the model to PsC surface area, maximum NKA pump rate, P_{max}, and the potential barrier to ion flow along the process, φ_w was investigated.

Chapter six builds on the research presented in chapter five by investigating the relationship between Na^+ and Ca^{2+} in the PsC. Simulation results presented in this chapter suggests that a local source for Ca^{2+} is provided by reversal of the NCX exchanger and that this reversal is caused by the formation of the Na^+ microdomain during sustained neuronal stimulus. Moreover, the generation of Ca^{2+} microdomains have previously been reported but the underlying ionic fluxes (and channels/transporters contributing to) have not been examined. This computational modelling study has identified the molecular targets and their relative contributions to the formation of a Ca^{2+} microdomain in the absence of an ER region. Specifically, the Na^+ microdomain switches the NCX into reversed mode, thus generating Ca^{2+} influx which is sufficient to produce relevant focal Ca^{2+} signals. This mechanism, which does not depend on intracellular sources for Ca^{2+} directly links neuronal activity and glutamate release to the formation of Na^+ and Ca^{2+} microdomains in the perisynaptic astroglial processes, which are instrumental for generation of astroglial homeostatic response critical for maintenance of synaptic transmission.

7.2 Contribution of the Thesis

The underlying hypothesis proposed in this thesis is that fixed negative charge in the membranes of long thin astrocyte processes results in a low conductance pathway between the perisynaptic cradle and the astrocyte soma. Using simulation throughout this thesis has shown that this hypothesis is credible in that microdomains of K^+, Na^+ and Ca^{2+} form at the PsC during sustained neuronal stimulation and these microdomains would not exist if conduction along the astrocyte processes was purely electro diffusion limited. Several significant contribution were made in this thesis.

- **Using a modified equation for ionic hopping as the core concept, this thesis developed a multi compartmental model of the PSC which included ionic hopping along thin astrocyte processes**

The ion hopping model draws on similar research in semiconductors devices to predict the restricted flow of ions within a thin astrocyte processes. The underlying mechanism for ionic retention in thin astrocyte processes is fixed negative charges, which exist in biological cell membranes. Experimental evidence [49] showed the presence of fixed negative charges within biological membranes including neurons and glial cells. Biological membranes consist of a continuous bilayer of lipid molecules with embedded membrane proteins. These bilayers are filled with polar and non-polar portions in their structure (amphipathic) [50]. They are also asymmetric in all eukaryotic membranes to allow two sides of the membrane with different biophysical properties to influence many key cellular processes including cell fusion and cell clearance [154]. Because both sides of its bilayer phospholipid membrane surface are negatively charged, and the ions in contract with the membrane surface are in deep potential wells near the dipole heads of that membrane, ions cannot slip along the membrane easily and must hop from well to well [6] [52]. Astrocyte processes are very thin and with all contact points of the membrane are in proximity, therefore this thesis put forward the hypothesis that these fixed charges will have a major effect in slowing down the diffusion of ions along the membrane.

- **This thesis showed that surface retention of ions can explain the existence of K^+ and Na^+ microdomains at the PsC.**

The multi compartmental model initially captured efflux/influx exchanges of K^+ and Na^+ ions between the astrocyte and the synaptic cleft and also efflux/influx of K^+ and Na^+ ions between a presynaptic neuron and the cleft**.** Capturing the molecular homeostatic control of ions at the perisynaptic cradle (PsC) is of fundamental importance for understanding the interplay between astroglial and neuronal compartments. The main conclusion is that the flow of K^+ ions by ion hopping is several orders of magnitude lower than the current carried by K_{ir} channels and therefore this slow leakage of K^+ away from the PsC appears to be a plausible explanation for the emergence of a K^+ microdomain. This localisation of astroglial ionic microdomains arises because in thin processes, surface conduction dominates over volume conduction, and because membrane lipids are negatively charged, deep potential wells form near the dipole heads restricting the flow of ions along the process. Therefore, ions must hop from well to well which restricts ionic conduction along the membrane. This hopping effectively semi-isolates the PsC from the astrocytic main body allowing the formation of K^+ and Na^+ microdomains at the PsC under different conditions. This work in this thesis challenged current thinking [184], where it was shown that the NKA is the dominant driving force for K^+ uptake while K_{ir} channels are much less so for K^+ clearance. Furthermore, clearance by K_{ir} diminishes over time because the changes in the associated reversal potential due to the $[K^+]$ PsC microdomain.

Our model also shows that the influx of Na^+ ions into the astrocyte process causes a Na^+ microdomain to form at the PsC where the decay rate of Na^+ is governed by the NKA. In this simulation, there is no neuronal excitation and the concentration of glutamate in the cleft was modulated using a Gaussian function and was taken up at the PsC by EAAT1/2. A slow decay of Na^+ was observed after the glutamate uptake ceased which is in strong agreement with experimental observations.

Having analysed the formation of microdomains and model behaviour the thesis set about exploring the sensitivity of the model to its main parameters. These parameters are PsC surface area, the maximum NKA pump rate, P_{max}, and the potential barrier to ion flow along the process, φ_w. It was found that as the PsC surface area increases so the amplitude of the K^+ microdomain increases and the Na^+ microdomain amplitude decreases. Also that when the NKA pump rate is low it was no longer the dominant co-transporter and both the EAAT co-transporter and K_{ir} channel dictate $[K^+]_{PsC}$ and $[Na^+]_{PsC}$ dynamics, and that the opposite is true when the pump rate is large. It was also found that the potential barrier to ion flow along the process, φ_w is 10 k_BT or greater, will effectively semi-isolate the PsC from the astrocyte soma.

It is also clear that the PsC surface area can limit the maximum amplitude of the microdomain concentration.

- **Several model predictions were in direct contrast to existing thinking around K^+ clearance and K^+ undershoot and also the model predicted the existence of a Ca^{2+} microdomain at the PsC.**

Our model challenges the orthodox view of the role of glial spatial potassium buffering during pathological activity. Simulation results point to a new theory where K^+ microdomain provides the driving force for the return of K^+ to the PsECS via background K^+ channels for uptake by the neuron via its NKA. Essentially, K^+ is transiently "stored" at the PsC during neuronal excitation where it decreases the electrochemical gradient of K^+, so reducing inward flow of potassium through K_{ir}; this "stored K^+" is then available to replenish neuronal K^+ levels when the excitation ceases, thereby preventing K^+ undershoot in the extracellular space. These observations are consistent with *in vivo* experimental data, and partly explain why inward rectifying K^+ channels may play a prominent role for K^+ uptake at large volume glial processes (e.g. terminal endfeet of retinal Muller cells) but not at low volume perisynaptic cradles. These results will also necessitate a reappraisal of the mechanisms and role of astrocytes in K^+ accumulation during seizure activity, especially given the observation that loss of function mutations in the gene encoding $K_{ir}4.1$ are associated with a human epilepsy syndrome and astrocyte $K_{ir}4.1$ expression is decreased in acquired epilepsy models. Moreover, other conditions that have been proposed to be due to abnormalities of K^+ homeostasis such as familial hemiplegic migraine are associated with mutations of the gene encoding the alpha2 subunit of NKA, which is predominantly expressed in astrocytes.

Our model also demonstrates that reversal of the NCX, instigated by an increase in the concentration of $[Na^+]$ at the PsC, is due to the activity of glutamate transport mediate Ca^{2+} influx which is sufficient to create a Ca^{2+} microdomain. This local source of Ca^{2+} may provide a previously underexplored form of Ca^{2+} signal. This computational modelling study has identified the molecular targets and their relative contributions to the formation of a Ca^{2+} microdomain in the absence of an ER region. Specifically, the generation of a Na^+ microdomain switches the NCX into reverse mode, which is sufficient to produce relevant focal Ca^{2+} signals. This mechanism, which does not depend on intracellular sources for Ca^{2+}, directly links neuronal activity and glutamate release to the formation of Na^+ and Ca^{2+} microdomains

in the perisynaptic astroglial processes, which are instrumental for generation of astroglial homeostatic response critical for maintenance of synaptic transmission.

7.3 Future Work

This thesis presented a new hypothesis, with supporting model simulations, to explain why microdomains of K^+ and Na^+ occurs at the PsC. The model also pointed to new theory regarding K^+ clearance from the synaptic cleft and showed that a Ca^{2+} microdomain is formed due to reversal of the NCX, which is driven by Na^+ accumulation at the PsC. However, while this thesis made significant progress around the understanding of ionic homeostasis at the PsC a number of other related issues where raised. In this section several suggestions for further research are outlined.

7.3.1 An atomic based model of ionic transport in thin processes

The thesis adapted an existing ion hopping model to capture the relationship between the flow of ions in thin processes in the presence of potential wells. While this model adequately predicted that ionic retention in these wells would impede the flow of ions within the process, a more atomic based approach is required to capture the dependency of ionic flow on process thickness, well spacing and variations of activation energy with distance [3]. This approach would relate electrostatic potential along the process to the exact location of the negative fixed charges: an atomistic view, as opposed to point charges, would be used to create a map of the charge distribution at the atomic scale. This could then be used to take account of the dynamic interaction between the charge present in membrane proteins and the charged ions in the astrocyte cytosol. The dominance of either a quasi-drift or a quasi-diffusion type transfer mechanism could be explored in order to determine an overall formulation that governs charge transport in thin astrocyte processes.

7.3.2 Morphology of the astrocyte process and cradle

The model presented in this thesis used a simplified compartmentalised approach where the cradle, synapse and astrocytic process assumed cylindrical like structures. However, to obtain a more biological realistic morphology our model could draw on research carried out elsewhere on large scale Monte Carlo simulator for cellular micro-physiology [160]. Also in the literature studied for the literature review there exist work that looked at tortuosity contribution to ionic diffusion from the process [5]. Recent detailed work outlined a methodology of recreating

astroglia in silico where firstly a “stem tree” representing the principal branch structure of the astrocyte needs to be constructed that reflects the main astrocyte branches readily identifiable on an optical microscope. Secondly software representing the cell anatomy and cell physiology as cylinder-compartment based shapes is run in the NEURON program, and physiology processes like diffusion and electrodiffusion is assigned to Monte Carlo simulation tests incorporated in the ASTRO program [192]. The final step was to populate the stem tree with randomly generated processes. Adjusting the diffusion and electrodiffusion part of ASTRO to incorporate fixed negative charges responsible for creating microdomains during ionic transport in astrocytes, would provide either a more robust confirmation of the fixed ion hypothesis of microdomains or perhaps an alternative explanation of the microdomain phenomenon [192]. As stated in the thesis already, one of the main challenges identified is accounting for the dynamic interaction between the charge present in membrane proteins and the charged ions in the astrocyte medium, this may help to overcome that.

7.3.3 Osmosis

An area not incorporated in the proposed model is osmosis. Osmosis can change the number of anions and cations at the PsC and the extracellular space, as well as the volumetric and membrane potential changes of both these regions via the transport of water by aquaporin channels and ion kinetics occurring due to ionic exchangers between cells and the extracellular space. Literature is available as a starting point which provides semi–phenomenological neuron–glia description of many aspects of the interplay between the neuron, astrocytes, and anion channels during spreading depolarizations accurately [145]. Also research is available which looks at cell osmosis not in the traditional context of the cell being semipermeable membrane where with osmotic pressure is converted to hydrostatic pressure at the membrane. Instead it represent it by making elastic energy stored in a swollen, cross-linked cytoskeleton become the critical variable to include when modelling cell volume regulation, rather than the potential energy in the cell cortex. Osmosis is an important phenomenon to consider because it could alter the morphology of narrow processes, their surrounding space and the PsC volume.

7.3.4 Different Neuron spiking Patterns

The model proposed in this thesis used a periodic spike train to stimulate the presynaptic neuron. However, the variability of neuronal responses is proportional to the mean in many brain areas, which suggests that neural responses might follow a Poisson distribution. Additionally, in the cortex, the timing of successive action potentials is highly irregular and the interpretation of this irregularity has led to two divergent views of cortical organization. Either they are due to stochastic forces, or that they are generated spikes which may result from precise coincidences of presynaptic events that may convey information. Consequently there is a need to investigate ionic homeostasis at the PsC using a more biologically realistic neuronal spike train stimulus. While there is undoubtable no biological evidence that neurons must follow a Poisson distribution there is evidence to suggest that this is a good assumption when modelling at the cellular level but when considering neuronal populations, their activity deviates from a Poisson type distribution. Nevertheless it is crucial that our model moves to a more non-linear type stimulus as this would allow a biologically realistic investigation of both the spatial and temporal dynamics of ions at the PsC.

References

[1] C. Ribrault, K. Sekimoto and A. Triller, "From the stochasticity of molecular processes to the variability of synaptic transmission," *Nat Rev.* , pp. 12: 375-387., 2011; .

[2] A. Derouiche and M. Frotscher, "Peripheral astrocyte processes: monitoring by selective immunostaining for the actin-binding ERM proteins.," *Glia.* , pp. 36: 330-341. , 2001;.

[3] K. Breslin, J. Wade, K. Wong-Lin, J. Harkin, B. Flanagan and e. al., "Potassium and sodium microdomains in thin astroglial processes: A computational model study.," *PLOS Comp Biol.,* vol. 14, no. 5, p. e1006151., 2018.

[4] J. J. Wade, K. Breslin, K. Wong-Lin, J. Harkin, B. Flanagan, H. V. Zalinge, S. Hall, M. Dallas, A. Bithell, A. Verkhratsky and L. McDaid, "Calcium Microdomain Formation at the Perisynaptic Cradle Due to NCX Reversal: A Computational Study," *Frontiers in Cellular Neuroscience,* vol. 13, no. 1, p. 185, 2019.

[5] G. Halnes, I. Østby, K. Pettersen, S. Omholt and G. Einevoll, "Electrodiffusive Model for Astrocytic and Neuronal Ion Concentration Dynamics.," *PLoS Computational Biology,,* 2013.

[6] M. Pekker and M. N. Shneider, "The surface charge of a cell lipid membrane," *Journal of Physical Chemistry & Biophysics,* vol. 5, no. 2, 2015.

[7] E. E. Ruppert, R. S. Fox and R. D. Barnes, ""Annelida".," in *Invertebrate Zoology (7 ed.).*, Thomson, Brooks/Cole, 2004, p. . 414–420..

[8] American Association of Neurological Surgeons., "A Neurosurgeon’s Overview the Brain's Anatomy.," Aans.org., 28 Jun 2006. [Online]. Available: https://www.aans.org/Patients/Neurosurgical-Conditions-and-Treatments/Anatomy-of-the-Brain. [Accessed 23 November 2018].

[9] H. Von Staden, in *Herophilus: The Art of Medicine in Early Alexandria*, H. Von Staden, Ed., Cambridge , Cambridge University Press, 1989, p. p. 140.

[10] C. Cajavilca, J. Varon and G. L. Sternbach, "Luigi Galvani and the foundations of electrophysiology," *Resuscitation,*, vol. 80, no. 2, pp. 159-162, 2009.

[11] A. Verkhratsky, Glial Neurobiology: A Textbook Paperback –, Wiley Publishing, 2007.

[12] J. A. D. Carlos and J. Borrell, "A historical reflection of the contributions of Cajal and Golgi to the foundations of neuroscience,," *Brain Research Reviews,*, vol. 55, no. 1, pp. 8-16, 2007.

[13] N. Swanson and L. W. Swanson., Histology of the nervous system of man and vertebrates. by S. Ramón y Cajal ; translated from the French by Neely Swanson and Larry W. Swanson., N. Swanson and L. W. Swanson., Eds., New York:: Oxford University Press., 1995.

[14] E. Vecino, F. Rodriguez, N. Ruzafa, X. Pereiro and S. C. Sharma, "Glia–neuron interactions in the mammalian retina," *Progress in Retinal and Eye Research,*, vol. 50, no. 1, pp. 1-40, 2016.

[15] H. Kettenmann and B. R. Ransom, "Neuroglia.," in *Neuroglia.*, B. Ransom, Ed., Oxford:, Oxford University Press,, 2013, p. 864.

[16] A. Verkhratsky and A. Butt, in *Glial Physiology and Pathophysiology.*, Chichester: , Wiley-Blackwell, 2013, p. 560..

[17] A. Verkhratsky and M. Nedergaard, "Physiology of astroglia.," *Physiological Reviews.* , in press: 2017.

[18] Oxford Dictionaries, "homeostasis | Definition of homeostasis in English by Oxford Dictionaries," 13 July 2005. [Online]. Available: https://en.oxforddictionaries.com/definition/homeostasis. [Accessed 14 April 2019].

[19] B. McEwen, "Chapter 5 - Central Role of the Brain in Stress and Adaptation: Allostasis, Biological Embedding, and Cumulative Change," in *Stress: Concepts, Cognition, Emotion, and Behavior: Handbook of Stress Series Volume 1*, Amsterdam, Elsevier Inc, 2016, pp. 39-55.

[20] P. Molenaar, "Systems Modeling," in *International encyclopedia of the social & behavioral sciences*, Oxford, Elsevier Science, 2002, pp. 15423-15428.

[21] M. Charvériat, C. Naus, L. Leybaert, J. Sáez and C. Giaume, "Connexin-Dependent Neuroglial Networking as a New Therapeutic Target.," *Front Cell Neurosci.* , vol. 11, p. 174., 2017.

[22] C. Giaume, A. Koulakoff, L. Roux, D. Holcman and N. Rouach, "Astroglial networks: a step further in neuroglial and gliovascular interactions.," *Nat Rev Neurosci.,* vol. 11, pp. 87-99., 2010.

[23] A. Verkhratsky, R. Reyes and V. Parpura, "TRP channels coordinate ion signalling in astroglia.," *Rev Physiol Biochem Pharmacol.* , vol. 166, pp. 1-22, 2014.

[24] M. Nedergaard and A. Verkhratsky, "Artifact versus reality - how astrocytes contribute to synaptic events.," *Glia.* , vol. 60: , pp. 1013-1023, 2012; .

[25] A. Verkhratsky and M. Nedergaard, "Astroglial cradle in the life of the synapse.," *Philos Trans R Soc Lond B Biol Sci.,* p. 369: 20130595., 2014.

[26] A. Verkhratsky and M. Nedergaard, "The homeostatic astroglia emerges from evolutionary specialization of neural cells.," *Philos Trans R Soc Lond B Biol Sci.,* p. 371: 20150428, 2016.

[27] P. Kofuji and E. Newman, "Potassium buffering in the central nervous system," *Neuroscience,* vol. 129, no. 4, pp. 1043-1054, 2004.

[28] B. Larsen, M. Assentoft, M. Cotrina, S. Hua, M. Nedergaard and K. Kaila, "Contributions of the Na^+/K^+-ATPase, NKCC1, and Kir4.1 to hippocampal K^+ clearance and volume responses.," *Glia,* pp. 62: 608-622, 2014;.

[29] B. Larsen and N. MacAulay, "Kir4.1-mediated spatial buffering of K^+: experimental challenges in determination of its temporal and quantitative contribution to K^+ clearance in the brain.," *Channels,* vol. 8, no. 6, pp. 544-550., 2014.

[30] K. Boddum, T. Jensen, V. Magloire, U. Kristiansen, D. Rusakov, I. Pavlov and e. al., " Astrocytic GABA transporter activity modulates excitatory neurotransmission.," *Nat Commun.* , Vols. 7, , p. 13572., 2016.

[31] D. Boison, J. Chen and B. Fredholm, "Adenosine signaling and function in glial cells.," *Cell Death Differ.* , vol. 17, pp. 1071-1082, 2010.

[32] L. Hertz, "The glutamate-glutamine (GABA) cycle: importance of late postnatal development and potential reciprocal interactions between biosynthesis and degradation.," *Front Endocrinol.,* vol. 4, p. 59, 2013.

[33] Y. Zhou and N. Danbolt, " GABA and glutamate transporters in brain.," *Front Endocrinology,* vol. 4, p. 165, 2013.

[34] L. Hertz, "Possible role of neuroglia: a potassium-mediated neuronal--neuroglial--neuronal impulse transmission system.," *Nature,* vol. 206:, pp. 1091-1094., 1965;.

[35] R. Orkand, J. Nicholls and S. Kuffler, "Effect of nerve impulses on the membrane potential of glial cells in the central nervous system of amphibia.," *J Neurophysiol. ,* vol. 29: , pp. 788-806., 1966; .

[36] L. Hertz and Y. Chen, "Importance of astrocytes for potassium ion (K^+) homeostasis in brain and glial effects of K^+ and its transporters on learning," *Neurosci Biobehav Rev.,* vol. 71, pp. 484-505, 2016.

[37] L. Hertz, D. Song, J. Xu, L. Peng and M. Gibbs, "Role of the astrocytic Na^+, K^+-ATPase in K^+ homeostasis in brain: K^+ uptake, signaling pathways and substrate utilization.," *Neurochem Res.,* vol. 40, pp. 2505-2516., 2015.

[38] S. Kirischuk, V. Parpura and A. Verkhratsky, " Sodium dynamics: another key to astroglial excitability?," *Trends Neurosci.,* pp. 35: 497-506., 2012;.

[39] C. Rose and A. Verkhratsky, "Principles of sodium homeostasis and sodium signalling in astroglial.," *Gia.,* p. 64: 1611–1627., 2016.

[40] J. Langer, N. Gerkau, A. Derouiche, C. Kleinhans, B. Moshrefi-Ravasdjani and M. e. a. t. Fredrich, "Rapid sodium signaling couples glutamate uptake to breakdown of ATP in perivascular astrocyte endfee," *Glia 2017,* vol. 65, pp. 293-308., 2017.

[41] S. Kirischuk, H. Kettenmann and A. Verkhratsky, "Membrane currents and cytoplasmic sodium transients generated by glutamate transport in Bergmann glial cells," *Pflug Arch Eur J Phy.,* vol. 454:, p. 245–252., 2007.

[42] R. Vandenberg and R. Ryan, "Mechanisms of glutamate transport.," *Physiol Rev.,* vol. 93, pp. 1621-1657, 2013.

[43] O. Palygin, U. Lalo, A. Verkhratsky and Y. Pankratov, "Ionotropic NMDA and P2X1/5 receptors mediate synaptically induced Ca^{2+} signalling in cortical astrocytes.," *Cell Calcium.,* vol. 48:, no. 2, pp. 25-231., 2010;.

[44] R. Reyes, A. Verkhratsky and V. Parpura, "RPC1-mediated Ca^{2+} and Na^+ signalling in astroglia: Differential filtering of extracellular cations," *Cell Calcium,* vol. 54, no. 2, pp. 120-125., 2013.

[45] A. Verkhratsky and F. Kirchhoff, "NMDA receptors in glia.," *Neuroscientist,* vol. 13, pp. 28-37, 2007;.

[46] A. Minelli, P. Castaldo, P. Gobbi, S. Salucci, S. Magi and S. Amoroso, "Cellular and subcellular localization of Na^{+}-Ca^{2+} exchanger protein isoforms, NCX1, NCX2, and NCX3 in cerebral cortex and hippocampus of adult rat.," *Cell Calcium.,* p. 41:221–34., 2007.

[47] V. Parpura, S. Kirischuk and A. Verkhratsky, "Sodium dynamics: another key to astroglial excitability.," *Trends Neurosi.,* vol. 35, no. 8, pp. 497-506., 2012;.

[48] J. Grosche, V. Matyash, T. Möller, A. Verkhratsky, A. Reichenbach and H. Kettenmann, "Microdomains for neuron–glia interaction: parallel fiber signaling to Bergmann glial cells.," *Nat Neurosci. ,* vol. 2, p. 139–143, 1999.

[49] R. Elul, "Fixed charge in the cell membrane.," *The Journal of Physiology.,* vol. 189, no. 3, pp. 351-365., 1967.

[50] B. Alberts, A. Johnson, J. Lewis, M. Raff, K. Roberts and P. Walter, "The Lipid Bilayer," in *Molecular Biology of the Cell. 4th edition.*, New York:, Garland Science;, 2002.

[51] B. Fadeel and D. Xue, "The ins and outs of phospholipid asymmetry in the plasma membrane: roles in health and disease.," *Crit Rev Biochem Mol Biol.,* vol. 44, no. 5, p. 264–277., 2009.

[52] L. H. Klausen, T. Fuhs and M. Dong, "Mapping surface charge density of lipid bilayers by quantitative surface conductivity microscopy," *Nature Communications,* vol. 7, 2016.

[53] A. Witthoft, J. A. Filosa, Karniadakis and G. Em, "Potassium Buffering in the Neurovascular Unit: Models and Sensitivity Analysis.," *Biophysical Journal,* vol. 105, no. 9, p. 2046–2054., 2013).

[54] R. D'Ambrosio, D. Gordon and H. Winn, "Differential role of KIR channel and Na^{+}/K^{+}-pump in the regulation of extracellular K^{+} in rat hippocampus.," *J Neurophysiol. 2001;,* vol. 87, no. 1, p. 87–102., 2001.

[55] H. Brew, P. Gray, P. Mobbs and D. Attwell, "Endfeet of retinal glial cells have higher densities of ion channels that mediate K^{+} buffering.," *Nature.,* vol. 324, no. 1, p. 466–468, 1986.

[56] G. V and B. BL., "Effects of astrocytic mechanisms on neuronal hyperexcitability.," *Conf Proc IEEE Eng Med Biol Soc.,* p. 4880–4883., 2014.

[57] M. Reichold, A. Zdebik, E. Lieberer, M. Rapedius, K. Schmidt, S. Bandulik and e. al., "KCNJ10 gene mutations causing EAST syndrome (epilepsy, ataxia, sensorineural deafness, and tubulopathy) disrupt channel function.," *Proc Natl Acad Sci U S A.*, vol. 107, no. 32, p. 14490–14495. pmid:20651251, 2010.

[58] S. Ivens, D. Kaufer, L. Flores, I. Bechmann, D. Zumsteg, O. Tomkins and e. al., "TGF-beta receptor-mediated albumin uptake into astrocytes is involved in neocortical epileptogenesis.," *Brain.*, vol. 130(pt2):, no. 1, p. 535–547., 2017;.

[59] M. D. Fusco, R. Marconi, L. Silvestri, L. Atorino, L. Rampoldi, L. Morgante and et al., "Haploinsufficiency of ATP1A2 encoding the Na^+/K^+ pump alpha2 subunit associated with familial hemiplegic migraine type 2.," *Nat Genet.*, vol. 33, no. 2, p. 192–196. pmid:12539047, 2003.

[60] A. Reichenbach, A. Derouiche and K. F, "Morphology and dynamics of perisynaptic glia.," *Brain Res Rev.*, vol. 63, no. 1-2, pp. 11-25, 2010.

[61] J. Langer and C. Rose, "Synaptically induced sodium signals in hippocampal astrocytes in situ.," *J Physiol.* , vol. 587: , p. 5859–5877., 2009.

[62] J. A. Kiernan and N. Rajakumar, in *Barr's the human nervous system: An anatomical viewpoint (10th ed.).*, P. W. K. Lippincott, Ed., Baltimore:, Lippincott Williams and Wilkins., 2013, pp. 13-33.

[63] R. A. Barker and F. Cicchetti, in *Neuroanatomy and Neuroscience at a Glance. 4th ed. At a Glance Series.*, Wiley-Blackwell, Ed., Chichester, West Sussex:, John Wiley & Sons, ©, 2012, pp. 32-35.

[64] C. Briar, Nervous System. Crash Course., 2 ed., London: Mosby Elsevier, 2003.

[65] G. Trébuchet and A. Giangrande, Glial Cells in Neural Development., Chichester. : In: eLS. John Wiley & Sons Ltd, , 2012.

[66] L. Heimar, The Human Brain and Spinal Cord, 2 ed., New York: Springer-Verlag, 1995.

[67] K. Young, J. Wise, P. DeSaix, D. Kruse, B. Poe, E. Johnson, J. Johnson, O. Korol, J. Betts and M. Womble, "Version 8.25 from the Textbook "OpenStax Anatomy and Physiology"," Wikipedia Commons, 18 May 2016. [Online]. Available: https://commons.wikimedia.org/wiki/File:1225_Chemical_Synapse.jpg. [Accessed 05 December 2018].

[68] D. Hebb, The Organization of Behavior., New York: : Wiley & Sons., 1949.

[69] C. F. Stevens and Y. Wang, " Facilitation and depression at single central synapses.," *Neuron,* vol. 14, no. 4, pp. 795-802, 1995.

[70] H. Markram and M. Tsodyks, "Redistribution of synaptic efficacy between neocortical pyramidal neurons," *Nature,* vol. 382, no. 6594, pp. 807-810., 1996.

[71] L. F. Abbott and G. R. Wade, "Synaptic Depression and Cortical Gain Control.," *Science,* vol. 275, no. 5297, pp. 221-224, 1997.

[72] R. S. Zucker and W. G. Regehr, "Short-Term Synaptic Plasticity.," *Annual Review of Physiology. ,* vol. 64, no. 1, pp. 355-405., 2002.

[73] L. F. Abbott and W. G. Regehr, "Synaptic computation.," *Nature. 431: ,* vol. 431, no. 7010, pp. 796-803, 2004.

[74] E. L. Bienenstock, L. N. Cooper and P. W. Munro, " Theory for the development of neuron selectivity: orientation specificity and binocular interaction in visual cortex.," *Journal of Neuroscience, ,* vol. 2:, p. 32–48., 1982.

[75] C. Glackin, L. Maguire, L. McDaid and H. Sayers, "Receptive field optimisation and supervision of a fuzzy spiking neural network," *Neural Networks,,* vol. 24, no. 3, pp. 247-256, 2011.

[76] J. Sjöström and W. Gerstner, "Spike-timing dependent plasticity.," *Scholarpedia,* vol. 5, no. 2, p. 1362., 2010.

[77] S. M. Bohte, J. N. Kok and H. La Poutré, "Error-backpropagation in temporally encoded networks of spiking neurons," *Neurocomputing,* vol. 48, pp. 17-37, 2002.

[78] S. M. Bohte, *Spiking Neural Networks. PhD thesis,* 2003.

[79] A. Belatreche, L. Maguire, M. McGinnity and Q. Wu, "A Method for Supervised Training of Spiking Neural Networks.," *Proc. IEEE Conf. Cybernetics Intelligence Challenges and Advances, CICA', Reading,,* p. 39–44., 2003.

[80] A. Belatreche, L. Maguire and T. Mcginnity, "Advances in Design and Application of Spiking Neural Networks.," *Soft Computing- A Fusion of Foundations, Methodologies and Applications,* vol. 11, no. 3, pp. 239-248., 2007.

[81] A. Gavrilov, V. Panchenko and O. Konstantin, "Methods of learning for spiking neural networks. A survey," *13th International Scientific-Technical Conference on Actual Problems of Electronics Instrument Engineering (APEIE),* vol. 1 p1, no. 1, pp. 455-460, 2016.

[82] B. Ruf and M. Schmitt, "Unsupervised learning in networks of spiking neurons using temporal coding.," *Gerstner W., Germond A., Hasler M., Nicoud JD. (eds) Artificial Neural Networks — ICANN'97. ICANN 1997. Lecture Notes in Computer Science,*, vol. 1327., 1997.

[83] R. Legenstein, C. Naeger and W. Maass, "What can a neuron learn with spike-timing-dependent plasticity?," *Neural Computation,* vol. 17, no. 11, pp. 2337-2382, 2005.

[84] F. Kasiński and A. Ponulak, "Experimental demonstration of learning properties of a new supervised learning method for the spiking neural networks," *In: Proc. 15-th Int. Conf. Artificial Neural Networks: Biological Inspirations, Lecture Notes in Computer Science. — Berlin :Springer,*, vol. 3696, no. 1, p. 145–153, 2005.

[85] P. D. Wasserman, Neural Computing: Theory and Practice, Scottsdale, Arizona: Coriolis Group C/O Publishing Resources Inc, 1989.

[86] R. J. Schalkoff, *Algorithms for a real-time automatic video tracking system (PhD Thesis),* Charlottesville, Virginia: University of Virginia 1979, 1979.

[87] W. McCulloch and W. Pitts, "A logical calculus of the ideas immanent in nervous activity," *Bulletin of Mathematical Biology,* vol. 5, no. 4, pp. 162-185, 1943.

[88] F. Rosenblatt, "The Perceptron: A Probabilistic Model for Information Storage and Organization in The Brain," *Psychology Review,* vol. 65, no. 6, pp. 386-408, 1985.

[89] B. Widrow and M. Hoff, "Adaptive switching circuits," *IRE WESCON Convention Record,* pp. 96-104, 1960.

[90] M. Minsky and S. Papert, Perceptrons: An Introduction To Computational Geometry (1st Edition), Cambridge, Massachusetts: MIT Press Cambridge, 1986.

[91] D. Rumelhart and J. McClelland, Parallel Distrubuted Processing: Explorations in the Microstructure of Cognition, Cambridge, Massachusetts: MIT Press Cambridge, 1986.

[92] I. Basheer and M. Hajmeer, "Artificial neural networks: fundamentals, computing, design, and application," *J Microbiol Methods. ,* vol. 43, no. 1, pp. 3-31., 2000.

[93] W. Maass and C. Bishop, "Pulsed Neural Networks.," in *MIT-Press*, 1998.

[94] T. Kohonen, "Self-organised formation of topologically correct feature maps," *Biological Cybernetics,* vol. 43, no. 1, pp. 59-69, 1982.

[95] A. Hodgkin and A. Huxley, "A quantitative description of membrane current and its application to conduction and excitation in nerve," .*J Physiol.* , vol. 117, no. 4, p. 500–544., 1952.

[96] T. Trappenberg, Fundamentals of Computational Neuroscience, Oxford: Oxford University Press, 2002.

[97] W. Gerstner and W. Kistler, Spiking Neuron Models - single neurons, populations, plasticity., Cambridge, UK: Cambridge University Press ISBN 0521890799, 2002.

[98] W. Gerstner and W. Kistler, Spiking Neuro Models: Single Neurons, Populations, Plasticity, Cambridge: Cambridge University Press, 2002.

[99] N. Kasabov and L. Benuskova, "Computational neurogenetics," *Journal of Computational and Theoretical Nanoscience*, vol. 1, no. 1, pp. 47-61, 2004.

[100] E. M. Izhikevich, "Which Model to Use for Cortical Spiking Neurons?," *IEEE TRANSACTIONS ON NEURAL NETWORKS, ,* vol. 15, no. 5, pp. 1063-1070, 2004.

[101] University of Sydney, " Izhikevich Neuron mode," University of Sydney, School of Physics, 6 Oct 2017. [Online]. Available: http://www.physics.usyd.edu.au/teach_res/mp/ns/doc/nsIzhikevich3.htm. [Accessed 23 November 2018].

[102] R. FitzHugh, "Impulses and physiological states in theoretical models of nerve membrane.," *Biophysical J.,* vol. 1, p. 445–466, 1961.

[103] J. Nagumo, S. Arimoto and S. Yoshizawa, "An active pulse transmission line simulating nerve axon.," *Proc. IEEE. ,* vol. 50, no. 1, p. 2061–2070, 1962.

[104] C. Koch, Biophysics of Computation: Information Processing in Single Neurons., Oxford: Oxford University Press, 1999.

[105] E. M. Izhikevich and R. FitzHugh, "FitzHugh-Nagumo model.," *Scholarpedia, ,* vol. 1, no. 9, p. 1349., 2006.

[106] Encyclopædia Britannica., "oligodendrocyte," 15 June 2012. [Online]. Available: https://www.britannica.com/science/oligodendrocyte. [Accessed 09 July 2017].

[107] Y.-J. Son and W. J. Thompson, "Schwann Cell Processes Guide Regeneration of Peripheral Axons," *Neuron, Vol. 14,*, pp. 125-132, 09, July 1995.

[108] M. Hanani, "Satellite glial cells in sympathetic and parasympathetic ganglia: in search of function," *Brain Res Rev. 64 (2): ,* p. 304–27., 2010.

[109] N. Bowery, D. Brown and S. Marsh, "gamma-Aminobutyric acid efflux from sympathetic glial cells: effect of 'depolarizing' agents," *J. Physiol. (Lond.).*, p. 293: 75–101., 1979.

[110] A. Bacci, C. Verderio, E. Pravettoni and M. Matteoli, "“The Role of Glial Cells in Synaptic Function,”," *Philosophical Transactions of the Royal Society of London. Series B, Biological Sciences,* vol. 354, no. 1381, pp. 403-409, 1999.

[111] P. Kurosinski and J. Gotz, "“Glial Cells Under Physiologic and Pathologic Conditions,”," *Archives of neurology, ,* vol. 59, no. 10, pp. 1524-1528, 2002.

[112] E. B. Alger, "“Retrograde Signaling in the Regulation of Synaptic Transmission: Focus on Endocannabinoids,”," *Prog. Neurobiol., ,* vol. 68, pp. 247-286, 2002.

[113] M. Navarrete and A. Araque, "“Endocannabinoids Potentiate Synaptic Transmission Through Stimulation of Astrocytes,"," *Neuron,* vol. 68, no. 1, pp. 113-126, 2010.

[114] A. Araque, V. Parpura, R. P. Sanzgiri and P. G. Haydon, " “Tripartite Synapses: Glia, the Unacknowledged Partner,”," *Trends in Neurosci.*, vol. 22, no. 5, pp. 208-215, 1999.

[115] M. Naeem, L. J. McDaid, J. Harkin, J. J. Wade and J. Marsland., "On the role of astroglial syncytia in self-repairing spiking neural networks," *IEEE Transactions on Neural Networks and Learning Systems, ,* vol. 26, no. 10, pp. 2370-80, 2015.

[116] J. T. Porter and K. D. McCarthy, "“Hippocampal Astrocytes in Situ Respond to Glutamate Released from Synaptic Terminals,”," *J. Neurosci.*, vol. 16, no. 16, pp. 5073-5081, 1999.

[117] C. Agulhon, J. Petravicz, A. B. McMullen, E. J. Sweger, S. K. Minton, S. R. Taves, K. B. Casper, T. A. Fiacco and K. D. McCarthy, "“What is the Role of Astrocyte Calcium in Neurophysiology?”," *Neuron,* vol. 59, pp. 932-946, 2008.

[118] S. Weerth, L. Holtzclaw and J. Russell, "“Signaling Proteins in Raft-Like Microdomains are Essential for Ca^{2+} Wave Propagation in Glial Cells”," *Cell Calcium,,* vol. 41, pp. 155-167, 2007.

[119] R. Rizzuto and T. Pozzan, "“Microdomains of Intracellular Ca^{2+}: Molecular Determinants and Functional Consequences,”," *Physiol. Rev.*, vol. 86, pp. 369-408, 2006.

[120] L. Pasti, A. Volterra, T. Pozzan and G. Carmignoto, "“Intracellular calcium oscillations in astrocytes: a highly plastic, bidirectional form of communication between neurons and astrocytes in situ,”," *J. Neurosci.,* vol. 17, p. 7817–7830, 1997.

[121] A. Volterra and J. Meldolesi, "Astrocytes, from brain glue to communication elements: the revolution continues," *Nature Reviews Neuroscience 6,* pp. 626-640 , 2005.

[122] M. V. Sofroniew and H. V. Vinters, "Astrocytes: biology and pathology," *Acta Neuropathol* , p. 119:7–35, 2010.

[123] D. A. Rusakov, K. Zheng and C. Henneberger, "Astrocytes as Regulators of Synaptic Function: A Quest for the Ca^{2+} Master Key," *UK Neuroscientist.,* vol. 17, no. 5, p. 513–523., 2011.

[124] R. Ventura and K. Harris, "Three-dimensional relationships between hippocampal synapses and astrocytes.," *J Neurosci.,* vol. 19:, p. 6897–906., 1999; .

[125] K. Lehre and D. Rusakov., "Asymmetry of glia near central synapses favors presynaptically directed glutamate escape.," *Biophys J.,* p. 83:125–34., 2002;.

[126] M. Witcher, S. Kirov and K. Harris, "Plasticity of perisynaptic astroglia during synaptogenesis in the mature rat hippocampus.," *Glia,* vol. 55, no. 1, pp. 13-23, Jan 2007.

[127] I. Lushnikova, G. Skibo, D. Muller and I. Nikonenko, "Synaptic potentiation induces increased glial coverage of excitatory synapses in CA1 hippocampus.," *Hippocampus.,* vol. 19, no. 8, pp. 753-62., 2009.

[128] M. Krzisch, S. Temprana, L. Mongiat, J. Armida, V. Schmutz, M. Virtanen, J. Kocher-Braissant, R. Kraftsik, L. Vutskits, K. Conzelmann, M. Bergami, F. Gage, A. Schinder and N. Toni, "Pre-existing astrocytes form functional perisynaptic processes on neurons generated in the adult hippocampus.," *Brain Struct Funct.,* vol. 220(4):, no. 4, pp. 2027-42, 2015.

[129] G. Ghézali, G. Dallérac and N. Rouach, "Perisynaptic astroglial processes: dynamic processors of neuronal information," *Brain Struct Funct,* Vols. 221,, no. 5, p. 2427, 2016.

[130] I. Patrushev, N. Gavrilov, V. Turlapov and A. Semyanov, "Subcellular location of astrocytic calcium stores favors extrasynaptic neuron-astrocyte communication.," *Cell Calcium.,* vol. 54, no. 5, pp. 343-9, 2013.

[131] I. Østby, L. Øyehaug, G. Einevoll, E. Nagelhus and E. Plahte, "Supporting Text S1: Astrocytic mechanisms explaining neuralactivity-induced shrinkage of extraneuronal space," *PLoS Comput Biol 5(1),* p. e1000272, 2009.

[132] F. Gabbiani and S. Cox, "Mathematics for Neuroscientists," Amsterdam Boston:, Elsevier Academic Press., 2010, pp. 193-222.

[133] D. Noble and A. Herchuelz., "Role of Na/Ca exchange and the plasma membrane Ca^{2+}-ATPase in cell function.," *Conference on Na/Ca Exchange. EMBO Reports.,* vol. 8, no. 3, pp. 228-232, 2007.

[134] Encyclopædia Britannica, ""sodium-potassium pump". .," 2015. [Online]. Available: Encyclopædia Britannica Online.. [Accessed 16 December 2015].

[135] C. Gillen, S. Brill, J. Payne and B. Forbush, ""Molecular cloning and functional expression of the K-Cl cotransporter from rabbit, rat, and human. A new member of the cation-chloride cotransporter family," *J. Biol. Chem.,* vol. 271, no. 27, p. 16237–44. , 1996.

[136] K. Higashi, A. Fujita, A. Inanobe, M. Tanemoto, K. Doi, T. Kubo and Y. Kurachi, "An inwardly rectifying K^+ channel, Kir4.1, expressed in astrocytes surrounds synapses and blood vessels in brain.," *American Journal of Physiology-Cell Physiology,* vol. 281, no. 3, pp. C922-C931, 2001.

[137] Y. Kubo, T. J. Baldwin, Y. N. Jan and L. Y. Jan, "Primary structure and functional expression of a mouse inward rectifier potassium channel," *Nature volume* , vol. 362, p. 127–133, 1993.

[138] T. Takumi, T. Ishii, Y. Horio, K.-I. Morishige, N. Takahashi, M. Yamada, T. Yamashita, H. Kiyama, K. Sohmiya, S. Nakanishi and Y. Kurachi, "A Novel ATP-dependent Inward Rectifier Potassium Channel Expressed Predominantly in Glial Cells," *The Journal of Biological Chemistry,* vol. 270, no. 1, pp. 16339-16346., 1995.

[139] P. Kofuji, B. Biedermann, V. Siddharthan, M. Raap, I. Iandiev, I. Milenkovic, A. Thomzig, R. W. Veh, A. Bringmann and A. Reichenbach, "Kir potassium channel subunit expression in retinal glial cells: Implications for spatial buffering (PDF Download Available).," *GLIA 39(3),* pp. 292-303, OCTOBER 2002.

[140] W. Waltz, ""“Role of astrocytes in the clearance of excess extracellular potassium,”," *Neurochemistry International,* vol. 36, no. 4–5, pp. 291–300,, 2000.

[141] M. Goldberg, M. D. Pittà, V. Volman, H. Berry, E. Ben-Jacob and e. al., "“Nonlinear Gap Junctions Enable Long-Distance Propagation of Pulsating Calcium Waves in Astrocyte Networks,”," *PLoS Computational Biology,,* August 2010.

[142] P. Kofuji, E. Newman and E. Newman, "Potassium buffering in the central nervous system," *Neuroscience,* vol. 129, no. 4, pp. 1043-1054, 2004.

[143] J. Nahy and J. Rash, " Connexins and gap junctions of astrocytes and oligodendrocytes in the CNS.," *Brain Res Rev. ,* vol. 32, no. 1, pp. 29-44., 2000.

[144] N. Rouach, E. Avignone, W. Même, A. Koulakoff, L. Venance, F. Blomstrand and e. al., "Gap junctions and connexin expression in the normal and pathological central nervous system.," *Biol Cell.,* vol. 94, no. 7-8, pp. 457-75., 2002; .

[145] S. Murakami and Y. Kurachi, "Mechanisms of astrocytic K^+ clearance and swelling under high extracellular K^+ concentrations," *The Physiological Society of Japan and Springer Japan,* vol. 66:, p. 127–142, 2016.

[146] B.-J. Jin, H. Zhang, D. K. Binder and A. Verkman, "Aquaporin-4–dependent K^+ and water transport modeled in brain extracellular space following neuroexcitation," *The Journal of General Physiology,* vol. 141, no. 1, pp. 119-32, 2013.

[147] D. Binder, X. Yao, Z. Zador, T. Sick, A. Verkman and G. Manley., "Increased seizure duration and slowed potassium kinetics in mice lacking aquaporin-4 water channels.," *Glia.,* vol. 53, p. 631–636, 2006.

[148] P. Padmawar, X. Yao, O. Bloch, G. Manley and A. Verkman., "K^+ waves in brain cortex visualized using a long-wavelength," *Nat. Methods.,* vol. 2, p. 825–827, 2005.

[149] S. Strohschein, K. Hüttmann, S. Gabriel, D. Binder, U. Heinemann and C. Steinhäuser, "Impact of Aquaporin-4 Channels on K^+ Buffering and Gap Junction Coupling in the Hippocampus," *Glia,* vol. 59:, p. 973–980, 2011.

[150] T. Eid, T. Lee, M. Thomas, M. A.-M. L. Bjørnsen, D. Spencer, P. Agre, O. Ottersen and a. N. d. Lanerolle, "Loss of perivascular aquaporin-4 may underlie deficient water and K^+ homeostasis in the human epileptogenic hippocampus," *Proc. Natl. Acad. Sci. USA.,* vol. 102, no. 1, p. 1193–1198., 2005.

[151] E. A. Nagelhus, Y. Horio, A. Inanobe, A. Fujita, F.-M. Haug, S. Nielsen, Y. Kurachi and O. P. Ottersen, "Immunogold evidence suggests that coupling of K^+ siphoning and

water transport in rat retinal Muller cells is mediated by a coenrichment of Kir4.1 and AQP4 in specific membrane domains," *Glia,* vol. 26, p. 47–54, 1999.

[152] H. Zhang and A. Verkman, "Aquaporin-4 independent Kir4.1 K^+ channel function in brain glial cells.," *Molecular and Cellular Neuroscience,* vol. 37, no. 1, pp. 1-10, 2008.

[153] J. Ruiz-Ederra, H. Zhang and A. S. Verkman, "Evidence against Functional Interaction between Aquaporin-4 Water Channels and Kir4.1 Potassium Channels in Retinal Müller Cells," *Biol. Chem. ,* vol. 282, p. 21866–21872, 2007.

[154] D. Xue and B. Fadeel, "The ins and outs of phospholipid asymmetry in the plasma membrane: roles in health and disease," *Crit Rev Biochem Mol Biol.,* vol. 44, no. 5, p. 264–277., 2009.

[155] F. Calderon and H.-Y. Kim, "Detection of intracellular phosphatidylserine in living cells," *Journal of Neurochemistry,* vol. 104, no. 1, p. 1271–1279, 2008.

[156] A. Abe and J. A. Shayman, "The role of negatively charged lipids in lysosomal phospholipase A2 function," *J Lipid Res. ,* vol. 50, no. 10, p. 2027–2035., 2009 .

[157] C. R. Rose and C. Karus, "Two sides of the same coin: Sodium homeostasis and signaling in astrocytes under physiological and pathophysiological conditions," *Glia,* vol. 61, no. 8, pp. 1191-1205, 2013.

[158] G. Halnes, I. Østby, K. H. Pettersen, S. W. Omholt and S. W. Omholt, "Electrodiffusive model for astrocytic and neuronal ion concentration dynamics.," *PLoS Comput Biol,* vol. 9, 2013.

[159] C. L. Lopreore, T. M. Bartol, J. S. Coggan, D. X. Keller, G. E. Sosinsky, M. H. Ellisman and T. J. Sejnowsk, "Computational Modeling of Three-Dimensional Electrodiffusion in Biological Systems: Application to the Node of Ranvier," *Biophysical Journal.,* Vols. 95, , no. 6, pp. 2624–2635,, 2013.

[160] V. Volman, M. Bazhenov and T. Sejnowski, "Computational models of neurons and astrocytes," *Front Comput Neurosci.,* vol. 6, no. 58, 2012.

[161] L. Pasti, A. Volterra, T. Pozzan and G. Carmignoto, "Intracellular Calcium Oscillations in Astrocytes: A Highly Plastic, Bidirectional Form of Communication between Neurons and Astrocytes In Situ," *The Journal of Neuroscience,,* vol. 17, no. 20, pp. 7817-7830;, 15 October 1997,.

[162] P. M. Kekenes-Huskey, Y. Cheng, J. E. Hake, F. B. Sachse, J. H. Bridge, M. J. Holst, J. A. McCammon, A. D. McCulloch and A. P. Michailova, "Modeling Effects of L-Type Ca^{2+} Current and Na^{+}-Ca^{2+} Exchanger on Ca^{2+} Trigger Flux in Rabbit Myocytes with Realistic T-Tubule GeometriesMyocytes with Realistic T-Tubule Geometrie," *Front Physiol,* vol. 3, p. 351, 2012.

[163] H. Anwar, C. J. Roome, H. Nedelescu, W. Chen, B. Kuhn and E. De Schutter, "Dendritic diameters affect the spatial variability of intracellular calcium dynamics in computer models.," *Frontiers in Cellular Neuroscience,*, Vols. 8,, p. 168., 2014.

[164] J. J. Wade, L. J. McDaid, J. Harkin, V. Crunelli and J. A. S. Kelso, "Bidirectional Coupling between Astrocytes and Neurons Mediates Learning and Dynamic Coordination in the Brain: A Multiple Modeling Approach," *PLoS ONE,* , vol. 6, no. 12, 2011..

[165] J. Wade, L. McDaid, J. Harkin, V. Crunelli and S. Kelso, "Self-repair in a bidirectionally coupled astrocyte-neuron (AN) system based on retrograde signaling," *Frontiers in Computational Neuroscience,* , vol. 6 , no. 76, 2012..

[166] M. Naeem, L. McDaid, J. Harkin, J. Wade and J. Marsland, "“On The Role of Astroglial Syncytia in Self-Repairing Spiking Neural Networks”," *IEEE Trans. Neural Net. & Learning Sys, (In press),* 2015..

[167] I. Østby, L. Øyehaug, G. Einevoll, E. Nagelhus and E. Plahte, "Astrocytic Mechanisms Explaining Neural-Activity-Induced Shrinkage of Extraneuronal Space.," *PLOS Computational Biology* , vol. 5, no. 1, p. e1000272, 2009.

[168] D. Goldman, "Potential, impedance, and rectification in membranes.," *J. Gen. Physiol.* , vol. 27, no. 1, p. 37–60. , 1943..

[169] A. Hodgkin and B. Katz, ". The effect of sodium ions on the electrical activity of giant axon of the squid.," *J. Physiol.*, vol. 108:, no. 1, p. 37–77, 1949.

[170] O. Alvarez and R. Latorre, "The enduring legacy of the “constant-field equation”," *The Journal of General Physiology,* vol. 149, no. 10, pp. :911-920., 2017.

[171] C. O. Diekman, C. P. Fall, J. D. Lechleiter and D. Terman, "Modeling the Neuroprotective Role of Enhanced Astrocyte Mitochondrial," *Biophysical Journal V,* vol. 104 , p. 1752–1763, April 2013.

[172] S. Cortassa, M. A. Aon, E. Marbán, R. L. Winslow and B. O'Rourke, "An Integrated Model of Cardiac Mitochondrial Energy Metabolism and Calcium Dynamics.," *Biophysical Journal.,* vol. 84, no. 4, pp. 2734-2755., 2003;.

[173] S. Cortassa, M. Aon, B. O'Rourke, R. Jacques, H. Tseng, E. Marbán and R. Winslow, "A computational model integrating electrophysiology, contraction, and mitochondrial bioenergetics in the ventricular myocyte.," *Biophysical Journal* , vol. 91, no. 1, p. 1564–1589, 2006.

[174] S. Kirischuk, H. Kettenmann and A. Verkhratsky, "Membrane currents and cytoplasmic sodium transients generated by glutamate transport in Bergmann glial cells.," *Pflugers Arch,* vol. 454 , pp. 245-252., 2007.

[175] A. Abe and J. A. Shayman., "The role of negatively charged lipids in lysosomal phospholipase A2 function," *Journal of Lipid Research,,* vol. 50, no. 10, p. 2027–2035., 2009.

[176] J. Frenkel, "On pre-breakdown phenomena in insulators and electronic semi-conductors.," *Phys Rev.,* vol. 54:, pp. 647-648., 1938;.

[177] I. Patrushev, N. Nikolay Gavrilov, V. Turlapov and A. Semyanov, "Subcellular location of astrocytic calcium stores favors extrasynaptic neuron–astrocyte communication.," *Cell Calcium.,* vol. 54:, p. 343– 349., 2013;.

[178] M. Xu-Friedman, K. Harris and W. Regehr, "Three-dimensional comparison of ultrastructural characteristics at depressing and facilitating synapses onto cerebellar Purkinje cells.," *J Neurosci.,* vol. 21, no. (17):, p. 6666–6672., 2001;.

[179] D. Sterratt, B. Graham, A. Gillies and D. Willshaw, Principles of computational modelling in neuroscience., Cambridge University Press; , 2011.

[180] C. Grewer, A. Gameiro and T. Rauen, "SLC1 glutamate transporters.," *Pflug Arch Eur J Phy.,* vol. 466(, no. 1, p. 3–24., 2014;.

[181] C. Murphy-Royal, J. D. JP, J. Varela, A. Panatier and B. Pinson, "Surface diffusion of astrocytic glutamate transporters shapes synaptic transmission.," *Nat Neurosci.*, vol. 18:, no. 1, pp. 219-226., 2015. .

[182] T. Otis and M. Kavanaugh, "Isolation of current components and partial reaction cycles in the glial glutamate transporter EAAT2.," *J Neurosci. ,* vol. 20, no. 1, pp. 2749-2757., 2000.

[183] S. Blanchard, S. Saillet, A. Ivanov, P. Benquet, C.-G. Bénar, M. Pélégrini-Issac and e. al., "A New computational model for neuro-glio-vascular coupling: astrocyte activation can explain cerebral blood flow nonlinear response to interictal events.," *Plos One.*, vol. 11, no. 2, p. 1, 2016.

[184] M. Butt and A. Kalsi, "Inwardly rectifying potassium channels (Kir) in central nervous system glia: a special role for Kir4.1 in glia functions.," *J Cell Mol Med.*, vol. 10, no. 1, pp. 33-44., 2006.

[185] G. Jeffs, B. Meloni, A. Bakker and N. Knuckey, "The role of Na^{+}/Ca^{2+} exchanger (NCX) in neurons following ischemia.," *J Clinical Neurosci*, vol. 14, no. 6, pp. 507 - 514, 2007.

[186] F. Gabbiani and S. J. Cox, "CHAPTER 13 - Neuronal Calcium Signaling*, Pages," in *Mathematics for Neuroscientists*, Elsevier Inc., 2010 , pp. 193-222.

[187] J. McHugh and J. Kenyon, "An Excel-based model of Ca^{2+} diffusion and fura 2 measurements in a spherical cell," *Am J Physiol Cell Physiol.*, vol. 286, no. 2, pp. C342-8, 2004.

[188] A. Schousboe, S. Scafidi, L. Bak, H. Waagepetersen and M. McKenna, "Glutamate metabolisim in the brain focusing on astrocytes," *Adv Neurobiol.*, vol. 11:, pp. 13-30., 2014.

[189] Y. Bernardinelli, M. D. and I. Nikonenko, "Astrocyte-Synapse Structural Plasticity," *Neural Plasticity,*, vol. 2014, no. 1, p. 232105., 2014,.

[190] A. Peters, P. S. and H. Webster, in *The Fine Structure of the Nervous System: Neurons and Their Supporting Cells*, New York, NY, USA, Oxford University Press; , 1991..

[191] W. J, M. D. L. Breslin K, F. B, H. J and W.-L. K, ""Cation Retention in Membrane Potential Wells: Ionic Microdomain Formation at the Perisynaptic Cradle"," in *11th FENS (Federation of European Neuroscience Societies) Forum of Neuroscience*, Berlin, Germany, 20018.

[192] L. P. Savtchenko, L. Bard, T. P. Jensen, J. P. Reynolds, I. Kraev and N. Medvedev, "Disentangling astroglial physiology with a realistic cell model in silico," *Nature Communications*, vol. 9, no. 1, p. Article no. 3554., 2018.

[193] M. Samoilova, K. Wentlandt, Y. Adamchik, A. Velumian and P. Carlen, "Connexin 43 mimetic peptides inhibit spontaneous epileptiform activity in organotypic hippocampal slice cultures.," *Exp Neurol.*, vol. 210, no. 2, pp. 762-775., 2008.

[194] N. Rouach, A. Koulakoff, V. Abudara, K. Willecke and C. Giaume, "Astroglial metabolic networks sustain hippocampal synaptic transmission.," *Science.,* vol. 322, no. 5907, pp. 1551-1555, 2008.

[195] A. Wallraff, R. Köhling, U. Heinemann, M. Theis, K. Willecke and C. Steinhäuser, "The impact of astrocytic gap junctional coupling on potassium buffering in the hippocampus.," *J Neurosci. ,* vol. 26: , pp. 5438-5447., 2006 .

[196] M. Samoilova, K. Wentlandt, Y. Adamchik, A. Velumian and P. Carlen., "Connexin 43 mimetic peptides inhibit spontaneous epileptiform activity in organotypic hippocampal slice cultures.," *Exp Neurol.,* vol. 210, no. 2, pp. 762-775., 2008.

[197] N. Rouach, A. Koulakoff, V. A. V, K. Willecke and C. Giaume., "Astroglial metabolic networks sustain hippocampal synaptic transmission.," *Science.,* vol. 322, no. 5907, pp. 1551-1555, 2008.

[198] W. Wolfgang, "“Role of astrocytes in the clearance of excess extracellular potassium,”," *Neurochemistry International,* vol. 36, no. 4–5, pp. 291–300,, 2000.

[199] P. Haydon and G. Carmignoto, "Astrocyte control of synaptic transmission and neurovascular coupling.," *Physiol Rev.,* vol. 86:, p. 1009–1031, 2006.

[200] M. Angulo, A. Kozlov, S. Charpak and E. Audinat, "Glutamate released from glial cells synchronizes neuronal activity in the hippocampus.," *J Neurosci.,* vol. 24, p. 6920–6927., 2004;.

[201] N. Hamilton and D. Attwell, "Do astrocytes really exocytose neurotransmitters?," *Nat Rev Neurosci.,* vol. 11: , p. 227–238., 2010;.

[202] J. Langer, J. Stephan, M. Theis and C. Rose, "Gap junctions mediate intercellular spread of sodium between hippocampal astrocytes in situ.," *Glia,* vol. 60, pp. 239-252, 2012.

[203] V. Volman, E. Ben-Jacob and H. Levine, "The astrocyte as a gatekeeper of synaptic information transfer," *Neural Comput.,* vol. 19, p. 303–326., 2007;.

[204] S. Nadkarni and P. Jung, "Dressed neurons: modeling neural-glial interactions.," *Phys Biol.,* vol. 1, p. 35–41., 2004; .

[205] S. Nadkarni and P. Jung, "Modeling synaptic transmission of the tripartite synapse.," *Phys Biol.,* pp. 4: 1-9., 2007.

[206] M. De Pittà, M. Goldberg, V. Volman, H. Berry and E. Ben-Jacob, "Glutamate regulation of calcium IP3 oscillating and pulsating dynamics in astrocytes.," *J Biol Phys. 2009;* , p. 35: 383–411., 2009; .

[207] M. De Pitta, V. Volman, H. Levine and E. Ben-Jacob, " Multimodal encoding in a simplified model of intracellular calcium signaling.," *Cogn Process.* , p. 10 Suppl 1: 55., 2009; .

[208] S. Nadkarni, T. Bartol, T. Sejnowski and H. Levine, "Modelling vesicular release at hippocampal synapses.," *PLoS Comp Biol.*, vol. 6, no. 11, 2010;.

[209] J. Grosche, V. Matyash, T. Möller, V. A, A. Reichenbach and H. Kettenmann, "Microdomains for neuron–glia interaction: parallel fiber signaling to Bergmann glial cells.," *Nat Neurosci.*, vol. 2, p. 139–143., 1999;.

[210] M. Blaustein, M. Juhaszova, V. Golovina, P. Church and E. Stanley, "Na/Ca exchanger and PMCA localization in neurons and astrocytes: functional implications.," *Ann N Y Acad Sci*, vol. 976: , p. 356–366., 2002.

[211] S. Owe, P. Marcaggi and D. Attwell, "The ionic stoichiometry of the GLAST glutamate transporter in salamander retinal glia.," *J Physiol.* , pp. 591–599., 577:, 2006;.

[212] N. Zerangue and M. Kavanaugh, "Flux coupling in a neuronal glutamate transporter.," *Nature.*, vol. 383: , p. 634–637., 1996;.

[213] N. Burnashev, A. Khodorova, P. Jonas, P. Helm, W. Wisden, H. Monyer and e. al., "Calcium-permeable AMPA-kainate receptors in fusiform cerebellar glial cells.," *Science.*, vol. 256: , p. 1566–1570., 1992;.

[214] T. Muller, T. Moller, T. Berger, J. Schnitzer and H. Kettenmann, "Calcium entry through kainate receptors and resulting potassium-channel blockade in Bergmann glial cells.," *Science.*, vol. 256, no. 5063:, p. 1563–1566., 1992;.

[215] S. Sze and K. Ng, " Physics of semiconductor devices," in *Physics of semiconductor devices, 2nd edition,.*, Hoboken, N.J.: , Wiley-Interscience. , 1981.

[216] G. T. Balls, S. B. Baden, T. Kispersky, T. M. Bartol and T. J. Sejnowski, "A large scale Monte Carlo simulator for cellular microphysiology," Santa Fe, NM, USA, , 2004, .

[217] L. Vargová and E. Syková, "Astrocytes and extracellular matrix in extrasynaptic volume transmission," *Philos Trans R Soc Lond B Biol Sci.* , vol. 369, no. 1654, p. 20130608., 2014 .

[218] F. Sachs and M. V. Sivaselvan, "Cell volume control in three dimensions: Water movement without solute movement," *The Journal of General Physiology* , vol. 145, no. 5, pp. 373-380, 2015.

[219] M. Potokar, J. Jorgačevski and R. Zorec, "Astrocyte Aquaporin Dynamics in Health and Disease," *Int J Mol Sci.,* vol. 17, no. 7, p. 1121, 2016 .

[220] G. Halnes, K. H. Pettersen, L. Øyehaug, M. E. Rognes, H. P. Langtangen and G. T. Einevoll, "Astrocytic Ion Dynamics: Implications for Potassium Buffering," *arXiv Quantitative Biology Cell Behavior.,* vol. 12, 2016.

[221] N. Rouach, K. D. Duc, J. Sibille and D. Holcman, "Dynamics of Ion Fluxes between Neurons, Astrocytes and the Extracellular Space during Neurotransmission," *Opera Medica et Physiologica,* vol. 4, no. 1, pp. 1-18, 2018.

[222] C. Wilson and A. Mongin, "The signalling role for chloride in the bidirectional communication between neurons and astrocytes.," *Neuroscie Lett.,* vol. 18, no. 30012-0., pp. S0304-3940, 2018.

[223] M. N. Shadlen and W. T. Newsome, "Is there a signal in the noise?," *Current Biology,,* vol. 5, p. 248–250, 1995.

[224] C. Allen and C. F. Stevens, "An evaluation of causes for unreliability of synaptic transmission.," *Proc.Natl. Acad. Sci.,,* vol. 91, no. 1, p. 10380–10383, 1994.

[225] B. Liebeskind, D. Hillis and H. Zakon, "Evolution of sodium channels predates the origin of nervous systems in animals," *Proc Natl Acad Sci U S A.,* vol. 108, no. 22, pp. 9154-9., 2011.

[226] V. A. Andrushko and J. W. Verano, " Prehistoric trepanation in the Cuzco region of Peru: A view into an ancient Andean practice," *American Journal of Physical Anthropology.* , vol. 137 (, no. 1, p. 4–13., 2008.

[227] H. M. Atta, ""Edwin Smith Surgical Papyrus: The Oldest Known Surgical Treatise," *American Surgeon.* , vol. 65 , no. 12, p. 1190–1192., 1999.

[228] F. Rose, "Cerebral Localization in Antiquity," *Journal of the History of the Neurosciences.* , vol. 18, no. 3, p. 239–247., 2009.

[229] R. S. Tubbs, S. Riech, K. Verma, J. Chern, M. Mortazavi and A. A. Cohen-Gadol, ""China's first surgeon: Hua Tuo (c. 108-208 AD)," *Child's Nervous System*, vol. 27, no. 9, p. 1357–1360, 2011.

[230] N. R. Al-Rodhan and J. L. .. Fox, ""Al-Zahrawi and Arabian neurosurgery, 936-1013 AD"," *Surgical Neurology.* , vol. 26, no. 1, p. 92–95., 1986.

[231] A. Aciduman, B. Arda, F. G. Ozaktürk and U. F. Telatar, ". "What does Al-Qanun Fi Al-Tibb (the Canon of Medicine) say on head injuries?"," *Neurosurgical Review.*, vol. 32, no. 3, pp. 255–263, discussion 263., 2009.

[232] P. Lutgendorf, "Monkey in the Middle," in *Hanuman's Tale: The Messages of a Divine Monkey*, Oxford University Press. , 2007, p. 348.

[233] P. Tessman and J. Suarez, "Influence of Early Printmaking on the Development of Neuroanatomy and Neurology.," *Arch Neurol.*, vol. 59, no. 12, p. 1964–1969., 2002.

[234] A. Pestronk, ""The first neurology book. De Cerebri Morbis...(1549) by Jason Pratensis".," *Archives of Neurology.* , vol. 45, no. 3, p. 341–344. , 1988.

[235] A. Neher, ""Christopher Wren, Thomas Willis and the Depiction of the Brain and Nerves," *Journal of Medical Humanities.* , vol. 30, no. 3, p. 191–200. , 2009.

[236] S. Haykin, "Neural Networks and learning Machines," in *Neural Networks and learning Machines 3e ed*, Upper Saddle River, New Jersey, United States, Prentice-Hall, 2009, p. 939.

[237] J. J. Hopfield, "Neural networks and physical systems with emergent collective computational abilities," *Proceedings of the National Academy of Sciences of the USA,*, vol. 79, no. 8, p. 2554–2558, 1982.

[238] J. Hopfield and D. Tank, " "Neural" computation of decisions in optimization problems.," *Biological Cybernetics.* , vol. 52, no. 1, pp. 141-52. , 1984.

[239] S. Lowel and W. Singer, "Selection of intrinsic horizontal connections in the visual cortex by correlated neuronal activity," *Science,* vol. 255 , no. 1, pp. 209-212, 1992.

[240] M. H. Sazli, "A brief review of feed-forward neural networks," *Commun. Fac. Sci. Univ. Ank. Series A2-A3,* vol. 50, no. 1, pp. 11-17, 2006.

[241] R. Chandradevan, "Radial Basis Functions Neural Networks — All we need to know.," Towards Data Science, Medium.com, 18 August 2017. [Online]. Available: https://towardsdatascience.com/radial-basis-functions-neural-networks-all-we-need-to-know-9a88cc053448 . [Accessed 23 November 2018].

[242] P. Wallisch, M. E. Lusignan, M. D. Benayoun, T. I. Baker, A. S. Dickey and N. G. Hatsopoulos, MATLAB® FOR NEUROSCIENTISTS, 2nd Edition, Amsterdam ,

Boston, Heidelberg, London, New York, Oxford, Paris, San Diego, San Francisco, Singapore, Sydney, Tokyo : Academic Press, Elsevier, 2014.

[243] S. Haykin., “Neural Networks, A Comprehensive foundation”, 2nd edition., New Jersey, United States: Prentice Hall, 1998.

[244] T. Pivneva, B. Haas, D. Reyes-Haro and H. Kettenmann, "Store-operated Ca^{2+} entry in astrocytes: Different spatial arrangement of endoplasmic reticulum explains functional diversity in vitro and in situ.," *Cell Calcium.,* vol. 43, no. 6, pp. 591-601., 2008;.

[245] S. Murakami and Y. Kurachi., "Mechanisms of astrocytic K^+ clearance and swelling under high extracellular K^+ concentrations," *The Journal of Physiological Science,* vol. 66, no. 2, p. 127–142, 2015.

Appendices

Appendix 1: Nernst Potential and Goldman Equation

The Nernst equation calculate the potential of an ion of charge *z* across a membrane. This potential is determined using the concentration of the ion (X in this case) both inside and outside the cell:

$$E_x \cong \frac{RT}{zF} \ln\left(\frac{[X_o]}{[X_i]}\right) \quad \text{(A.1)}$$

In this equation: R is the ideal gas constant, T is the temperature and F is the Faraday's constant, E_x is the Nerst Potential, the potential across the cell membrane that exactly opposes net diffusion of a particular ion through the membrane. [64]

When there is no net flux of ions, the membrane is in thermodynamic equilibrium so the membrane potential must be equal to the Nernst potential. In situations where the cell is not in equilibrium such as due to active ion pumps, the Goldman equation determines the resting potential. The Goldman Equation is given by

$$E_m = \frac{RT}{F} \ln\left(\frac{\sum_i^n P_{M_i^+} [M_i^+]_{out} + \sum_j^m P_{A_j^-} [A_j^-]_{in}}{\sum_i^n P_{M_i^+} [M_i^+]_{in} + \sum_j^m P_{A_j^-} [A_j^-]_{out}}\right) \quad \text{(A.2)}$$

In this equation: M represents monovalent positive ionic species, A represents negative ion species and n and m represent the total number of each type respectively. E_m is the resting membrane potential, P_{ion} is the permeability for that ion, $[ion]_{in}$ is the intracellular concentration of that ion and $[ion]_{out}$ is the extracellular concentration of that ion. For a transporter than transfers potassium, sodium and chloride, the Goldman equation for that transporter is:

$$E_m = \frac{RT}{F} \ln\left(\frac{P_{K^+}[K^+]_{out} + P_{Na^+}[Na^+]_{out} + P_{Cl^-}[Cl^-]_{in}}{P_{K^+}[K^+]_{in} + P_{Na^+}[Na^+]_{in} + P_{Cl^-}[Cl^-]_{out}}\right) \quad \text{(A.3)}$$

Appendix 2: The NKCC Pump

The NKCC pumps Na^+, K^+ and Cl^- into the cell and has a stoichiometry of 1:1:2. Since there are two positively charge ions transported for every two negatively charged ions, the NKCC is considered electrically neutral. The Na^+ current of the pump is given by [53]:

$$I_{NaNKCC} = PNKCC_{max} log\left[\frac{[K^+]_{PsECS}}{[K^+]_{PsC}}\frac{[Na^+]_{PsECS}}{[Na^+]_{PsC}}\left(\frac{[Cl^-]_{PsECS}}{[Cl^-]_{PsC}}\right)^2\right] SA_{PsC}F \quad (A.4)$$

where $PNKCC_{max}$ is the maximum pump rate of the NKCC. The K^+ current component of the pump is given by:

$$I_{KNKCC} = I_{NaNKCC} \quad (A.5)$$